EVALUATION AND COMPARISON OF MECHANICAL AND HYDRAULIC BEHAVIOUR OF TWO ENGINEERED CLAY SEALING MATERIALS

By

David Eric Sakari Anderson

A Thesis
Submitted to the Faculty of Graduate Studies
In Partial Fulfillment of the Requirements for the Degree of

Master of Science

Department of Civil Engineering
University of Manitoba
Winnipeg, Manitoba

May, 2003

THE UNIVERSITY OF MANITOBA

FACULTY OF GRADUATE STUDIES

*****

COPYRIGHT PERMISSION

Evaluation and Comparison of Mechanical and Hydraulic Behaviour of Two Engineered Clay Sealing Materials

BY

David Eric Sakari Anderson

A Thesis/Practicum submitted to the Faculty of Graduate Studies of The University of Manitoba in partial fulfillment of the requirement of the degree

Of

Master of Science

ABSTRACT

This thesis examines and compares the mechanical and hydraulic characteristics of two compacted buffers. Three experimental testing programs have been conducted to evaluate the characteristics of these unsaturated materials.

The first program evaluated the influence of suction on the volume change behaviour of both buffers. A series of specimens were subjected to selected relative humidity environments, which induced suction increases, under zero external pressure. The resulting volume changes were measured. The results have been interpreted and a simple model for determining the suction as a function of measured water contents is presented.

The second experimental program examined the behaviour of the buffers when subjected to generalized stress paths (in the triaxial stress state), including isotropic and shear conditions. A new, fully automated stress path control and data acquisition system is discussed, along with results of tests conducted using the equipment. The measurements from the experimental program are interpreted using an elastic-plastic constitutive framework.

The third experimental series used one type of buffer to investigate the hydraulic characteristics of buffer. After subjecting the specimens to known intervals of increased suction the water content distributions are measured. Estimates of hydraulic conductivity are made based on these measurements to assess the movements of water in the unsaturated buffer.

ACKNOWLEDGEMENTS

I would like to thank Dr. James Blatz, P.Eng for his patience and guidance during this research program. His endless encouragement and support helped me grow both academically and professionally. I look forward to a continued collaboration both professionally and personally.

Special thanks to Dr. Jim Graham, Dr. Bruce Kjartanson, Dr. Neil Chandler, and Dr. David Dixon with whom I had many fruitful discussions, from which a great deal of light was shone on this research topic.

I would also like to thank the graduate students who helped me through discussions on my research and their friendship; Nelson Ferriera, Greg Siemens, Blair Garinger, Grant Ferguson, Kate Franklin, Vivek Bhardawj, Lee Peters, Yadav Pathak and Alex Man. Also, I would like to thank the support and work done by the summer student Ritchie Armstrong.

I would like to acknowledge the financial support provided by the Natural Sciences and Research Council of Canada, Atomic Energy of Canada Limited, Ontario Power Generation, the Department of Civil Engineering at the University of Manitoba, the Canadian Geotechnical Society, and the friends and colleagues of Neil Burgess.

Finally, I would like to thank my parents Eric and Henna for their endless love, support, and patience throughout these past years. Also thanks to, my cousin J.P. for his help and taking my mind off my research once and a while, my cousin Cathy for the inspirational thesis title of "Dirt with David", and my W.C.C. church family whose prayer and support has been greatly appreciated.

TABLE OF CONTENTS

LIST OF SYMBOLS AND ABBREVIATIONS

AECL Atomic Energy of Canada Limited

c' cohesion intercept of the soil

Δp change in total mean stress

ΔS change in total suction

Δt length of time in desiccator

E Young's Modulus

$E_{1\%}$ Secant Young's Modulus at one percent strain

$E_{50\%}$ Secant Young's Modulus at 50% of peak deviator stress

ε_s shear strain

HITEP high temperature high pressure

I_p Plasticity index

κ_i initial load index under first time loading during isotropic compression

κ_u unload index under unloading during isotropic compression

χ Bishop's Chi factor

λ plastic hardening load index during isotropic compression

LSY load suction yield line

LVDT linear variable displacement transformer

LY load yield line

M slope of q,p failure envelope

M^b slope of the q,S failure envelope

N slope of $(q / p)_f$ for ellipse tops in constant suction yield model

OCR overconsolidation ratio

p	total mean stress
p'	effective mean stress
p_c	total maximum mean stress during isotropic compression
p_{cs}	total mean stress at critical state
p_{eot}	total mean stress at end of triaxial shear test
p_{peak}	total maximum mean stress during triaxial shear
p_{ul}	total mean stress after isotropic unloading
p_y	interpreted initial yield during isotropic compression
p_{yield}	total yield mean stress during triaxial shear
ϕ^b	friction angle with respect to suction changes
ϕ'	internal angle of friction between soil particles
q	deviator stress
q_{cs}	deviator stress at critical state
q_{eot}	deviator stress at end of triaxial shear test
q_{peak}	maximum deviator stress during triaxial shear
q_{yield}	yield deviator stress during triaxial shearing
q/p	ratio of deviator stress to mean stress
RBM	reference buffer material
S	total suction
S_{eot}	total suction at the end of triaxial shearing
S_f	total suction in desiccator and specimen after equilibration
S_i	total initial suction in desiccator
S_{is}	total suction at the start of triaxial shearing

S_{peak} total suction at peak shear load

S_r degree of saturation

S_{target} desired total suction to be applied to specimens

SWCC soil water characteristic curve

SY suction yield line

S_y total suction at the interpreted shear load yield

T tensile strength of buffer material

u_a pore air pressure

u_w pore water pressure

V specific volume

V_w water specific volume

w_L liquid limit

w_P plastic limit

w water content

w_i water content in specimen after removal from desiccator

LIST OF TABLES

LIST OF FIGURES

1.0 INTRODUCTION

1.1 General Overview

In engineering practice, it is common to treat soil as a two-phase system, either being completely dry (solid particles and air) or completely saturated (solid particles and water). This is a historic simplification in soil mechanics that is still used in engineering practice today. More recently, the behaviour of "unsaturated" soil has been examined in research and engineering practice. Unsaturated soil is a three-phase system comprising of solid particles, liquid and gas. Application of the principles of unsaturated soil mechanics (in cases where the soil is neither completely dry nor completely saturated) has led to better predictions of soil behaviour where the traditional simplified soil mechanics theories are not fully representative.

Many engineering applications influence soil near or at the ground surface. In semi-arid areas of the world unsaturated soil is abundant (Fredlund and Rahardjo 1993). A key component of unsaturated soil behaviour is the negative pore-water pressures or suctions that are present in the soil. These negative pressures in the soil are not permanent and are greatly affected by the environmental conditions occurring at the ground surface. Conditions, which result in wetting of the soil, result in the reduction of these negative pressures, and conversely drying of the soil results in an increase of negative pressures in the soil. It is due to the transient nature of environmental conditions (and their affect on soil suctions) that unsaturated soils have been found recently to greatly affect analysis in geotechnical engineering applications (Ferreira *et al.* 2001).

One area of considerable interest in the mechanics of unsaturated soil is the development and calibration of constitutive models that can be implemented in numerical modeling tools for analysis purposes. Advancements in laboratory testing have provided new insights into understanding the influence of suction on strength, deformation and hydraulic flow characteristics. While the behaviour of unsaturated soil is becoming better understood, more information is required to define failure and yielding under application of isotropic and shear loading conditions for more advanced elastic-plastic constitutive frameworks.

Storage of waste materials in deep geologic repositories is one example of an engineered system where the behaviour of unsaturated soil is of utmost importance. In Atomic Energy of Canada Limited's (AECL) deep geologic repository concept, a sand-bentonite mixture (referred to as buffer) will be used as a seal to transmit heat from containers to the surrounding rock and form a barrier to inhibit groundwater flow and radionuclide transport. Since heat and moisture flow are coupled processes, temperature gradients in the buffer will cause drying near the container and wetting near the rock.

Since, the buffer will be placed in an unsaturated state, suctions will be present in the buffer upon placement in the deep geologic repositories. The processes of wetting and drying affect the hydro-mechanical characteristics of the buffer material significantly (Graham *et al.* 1997). Understanding the unsaturated behaviour of buffer is important for understanding the changes in suction in the vault configuration and the associated behaviour of proposed sealing systems.

Varying suctions, which are directly related to changes in water content in the material, cause differences in material behaviour. With the possibility that different deposits of bentonite may be used in combination with sand to produce buffer, it seems evident that behaviour will also be affected by the mineralogy and dominant exchangeable cation of the bentonite that is selected. Bentonite products can differ significantly in terms of their composition (Dixon 1994), which can lead to differences in mechanical behaviour. Understanding the behavior of different bentonite materials and their engineering properties is important to ensure the most appropriate mixture is selected for the proposed engineered sealing system.

Research for AECL at the University of Manitoba was originally directed at examining the stress-strain behaviour of saturated buffer at combinations of total stresses and pore water pressures up to 10 MPa (Saadat 1989) and temperatures up to 100°C (Lingnau 1993, Lingnau *et al.* 1996, Tanaka 1995). Following these initial studies, the experimental programs expanded to examine the properties of unsaturated buffer (Graham *et al.* 1995) including development of more fundamental concepts regarding the behaviour of unsaturated soils (Delage and Graham 1995). The latest work has included development of new technologies for suction control and measurement (Wan *et al.* 1995, Tang *et al.* 1997, Blatz and Graham 2003). These have included the construction of an automated triaxial apparatus for examining generalized stress paths.

The research conducted to date has used mixtures of Saskatchewan bentonite (Avonlea bentonite) and sand. In this research program Saskatchewan

bentonite was used to further understand the behaviour of the Saskatchewan buffer, which is a mixture of sand and bentonite, at high suctions. Also, Wyoming bentonite was used in combination with sand (Wyoming buffer) to understand its behaviour when subjected to the same stress conditions as Saskatchewan buffer. The two different bentonites have been used to compare and contrast their performance in the proposed sealing application and to examine the influence of bentonite properties on buffer behaviour.

1.2 Hypothesis and Objectives

Hypothesis:

The different physical properties of Wyoming buffer as compared to Saskatchewan buffer will result in different mechanical behaviour at similar suction levels.

***Objectives of Testing Program*:**

1. To undertake laboratory tests that examine the effects of drying (increased suction) on the behaviour of two unsaturated buffers.
2. To evaluate and compare the mechanical behaviour of two different sand-bentonite buffers.
3. To undertake laboratory tests that examine the movement of liquid and/or vapour in unsaturated soils when subjected to drying environments.

1.3 Organization of Thesis

The thesis is organized as follows: Chapter 2 presents a literature review of past work and theories important to understanding work described in this

thesis. Chapter 3 describes the materials and procedures used to prepare buffer for the testing programs. Chapter 4 discusses the equipment used in the testing. Chapter 5 presents results and a comparison of the initial drying behaviour of each of the buffers. Chapter 6 presents results from isotropic compression and triaxial shear tests on both materials and a comparison of these results. Chapter 7 presents water content distributions at defined times during drying of larger specimens. Chapter 8 discusses the results from all of the testing and the similarities with past research on buffer. Chapter 9 presents conclusions and recommendations for future work.

2.0 LITERATURE REVIEW

2.1 Introduction

The purpose of this research is to examine the mechanical and hydraulic behaviour of two unsaturated high-plastic sand-bentonite mixtures. Understanding the mechanical behaviour of these materials requires an understanding of concepts of clay structure and mineralogy, unsaturated soil mechanics, and constitutive modeling. The work presented in this thesis is an additional component of a larger research program on unsaturated soil mechanics at the University of Manitoba. It builds on the understanding and knowledge that has been presented previously by Wan (1996), Wiebe (1996), Tang (1999) and Blatz (2000). In addition to the Saskatchewan sand-bentonite mixture studied by previous researchers, a second sand-bentonite mixture using Wyoming bentonite has been evaluated in this thesis.

Lambe (1958) presented the concept of unsaturated soils as a three-phase system containing soil particles (solid minerals), gas (air or vapour), and liquid (usually water). With a third phase (saturated and fully dry soils are two-phase systems) in unsaturated soils, the measurement of volume state must include a measure of water content, w, or degree of saturation, S_r, of the soil along with specific volume. As with volume state parameters, the number of parameters required to define the stress state of unsaturated soil also increases. With two-phase soils in the triaxial state, the stress state variables are total mean stress (p) and deviator stress (q). The other independent stress state variable required to fully define the stress state of an unsaturated soil is suction, S.

Suction is an internal stress in the soil structure that acts to make the soil stiffer and stronger and is associated with the water potential of the soil.

Wheeler and Sivakumar (1995) proposed that with the three stress state variables, the volume state variable (specific volume), and with the water specific volume, V_w, the behaviour of unsaturated soils may be described using a flow rule. In this research a five state variable approach using p, q, S, V and either S_r or w has been adopted to describe the unsaturated behaviour of soils (Wheeler and Sivakumar 1993).

2.2 Past Research at the University of Manitoba

Since this thesis is a further step in a series of research projects on unsaturated soil mechanics at the University of Manitoba (Wan 1996, Wiebe 1996, Tang 1999 and Blatz 2000), theories previously presented by these researchers will only be briefly introduced. This section provides a synopsis of previous research at the University of Manitoba.

2.2.1 Soil Mineralogy and Structure

Interpretation of experimental results has focused on the mineralogy and structure of compacted sand-bentonite buffer. An in-depth presentation of the mineralogy and structure of the buffer material and its constituents can be found in **Wan (1996)**. While this material is a mixture of sand and bentonite it is the bentonite that dominates the response to changes in suction (water content). The sand component is angular quartz sand (described in Chapter 3), which is chemically inert, while the bentonite (also described in Chapter 3) is a clay mineral that possesses a net negative charge on the mineral surfaces. These

mineral surfaces vary depending on the clay mineral. For example, the surface area of Saskatchewan bentonite is 520 – 630 m^2/g, while Wyoming bentonite has a surface area of 750 – 800 m^2/g (Dixon and Miller 1995). The negative charge on the mineral surface exerts electrostatic forces on water and other nearby cations.

The pore size distribution of compacted buffer has been found to be generally bimodal (Wan *et al.* 1990). The bimodal distribution of the buffer results from a micro- and macrostructure in the soil structure. The microstructure consists of the pore spaces between clay platelets that form in aggregates (peds) of clay mineral particles. The macrostructure is the framework of these peds and the pore spaces between them. The molding water content affects the size of the micropores and the compactive effort determines the size of the macropores (Wan *et al.* 1990). The pore distribution affects the development of suction in buffer and the movement of water and air during external load application. Since the pore distribution has an effect on the performance of the compacted materials, reference parameters defined by AECL were used to make consistent specimens in this research and in previous research. The reference parameters included a water content of 19.4% and a dry density of 1.67 Mg/m^3 (Dixon and Gray 1985), which resulted in a degree of saturation of 85%.

2.2.2 Soil Suction

The suction generated in soil is defined by Richards (1974) as the water potential in a soil-water system. Richards (1974) lists three components of suction in unsaturated soils, namely capillarity, adsorption of water on the surface

of the clay minerals, and osmotic phenomena. Only two components are generally considered in engineering studies, matric and osmotic suctions. Matric suction is generated by capillarity and the osmotic suction is generated by pore fluid chemistry and water adsorption (Wan *et al.* 1995). Matric suction is generally considered the dominant component of total suction in soil. Osmotic suction is insensitive to changes in water content (as long as pore fluid chemistry remains constant). Therefore changes in total suction in unsaturated soils can generally be attributed to changes in matric suction (Fredlund and Rahardjo 1993). In this research, 'suction' refers to total suction. Changes in suction reflect changes in matric suction since the pore fluid chemistry was maintained constant in all testing.

2.2.2.1 Soil Water Characteristic Curve

The relationship between water content and suction is called the soil water characteristic curve (SWCC) (Fredlund and Rahardjo 1993). Since the behaviour of unsaturated soil is a function of suction, the SWCC is a very important relationship to define unsaturated soil behaviour. The range of possible water contents and suction states is bounded by two curves that represent the outer limits of the suction-water content relationship (Tang *et al.* 1998). One bounding curve is measured by drying a soil from a fully saturated condition, while the other bounding curve is measured by wetting a soil from completely dry conditions to saturation. Hysteresis in the SWCC is observed as a family of curves that connect to the two bounding SWCC curves that represent individual drying or wetting paths. Drying / wetting paths conducted on compacted soils by

Tang *et al.* (1998) and Blatz (2000) have shown that suction in compacted soils is a function of the hydrating water content used to prepare the specimen, the current water content of the specimen, and the drying / wetting history of the specimen. This is important for determining suction by direct measurement of water content.

2.2.2.2 Generating Suctions in the Laboratory

Environments of various relative humidities can be created in sealed desiccators using acid or salt solutions. A water exchange between the liquid and vapour phases occurs in the desiccator headspace until equilibrium between the two phases is achieved. This creates a partial vapour pressure in the desiccator that is a function of the concentration of the solution. Partial vapour pressures of common chemical systems can be found in Stokes and Robinson (1948) and Young (1967). Suctions are produced in soil specimens by the water exchange between the specimen and the vapour in the headspace of a desiccator. Tang (1999) demonstrated that equilibrium in 50 mm diameter specimens is reached after 30 days in the desiccator.

When drying specimens, concentrations of the acid solutions change because the system is a constant mass environment. The mass of water in the solution increases as water is removed from specimens and taken up by the solution. This increase in the mass of water results in a change in the concentration of the solution and must be accounted for when drying specimens and determining the final suction after equilibration.

2.2.3 Shear Strength of Unsaturated Soils

Bishop (1959) recognized that Terzaghi's effective stress equation (Terzaghi 1936) was not able to represent the effective stress of an unsaturated soil since there was an observed higher strength in unsaturated soils as compared to saturated soils. Terzaghi's effective stress equation describes effective stress in terms of total stress and pore water pressure and does not account for pore air pressure that is present in unsaturated soils. To account for the difference, Bishop included the pore air pressure, u_a, along with the pore water pressure, u_w, and also a term to account for the degree of saturation of the soil called Bishop's Chi factor χ.

$$\sigma'_n = (\sigma - u_a) + \chi(u_a - u_w)$$

The traditional definition of the saturated shear strength of soils is written as a function of the material parameters ϕ' (internal angle of friction between soil particles) and c' (cohesion intercept of the soil). The Mohr-Coulomb formulation follows:

$$\tau = c' + \sigma'_n \tan(\phi')$$

Using the Mohr-Coulomb formulation of shear strength along with the equation for effective stress, the shear strength of unsaturated soils can be determined. However, the use of Bishop's Chi factor for a value greater than unity showed that this formulation was inconsistent in predicting the behaviour of unsaturated soils. This is because the χ parameter is a material property and as such, should not be included in the stress state definition. The use of the Chi parameter results in the effective stress equation having the form of a constitutive

model instead of a natural stress state definition. State variables are defined as "a limited set of dynamical variables of the system, such as pressure, temperature, volume, etc., which are sufficient to describe the state of the system completely for the considerations at hand" (Michel 1961), and must be independent of the physical properties of the material (Fredlund and Rahardjo 1993). The χ parameter is acting as a means of relating one state variable

$(u_a - u_w)$ to another state variable $(\sigma - u_a)$, and is not independent of the physical properties of the material.

To resolve this problem, the stress state variables for unsaturated soils had to be dealt with independently (Jennings and Burland 1962 and Coleman 1962). It was shown by Fredlund and Morgenstern (1977) that the independent stress variables $(u_a - u_w)$ and $(\sigma - u_a)$ could be used to define the shear strength and volume change behaviour of unsaturated soils. With this knowledge, the shear strength of unsaturated soils was defined as an extended form of the original Mohr-Coulomb equation (Fredlund *et al.* 1978) as:

$$\tau = c' + (\sigma - u_a) \cdot \tan\phi' + (u_a - u_w) \cdot \tan\phi^b$$

where $(\sigma - u_a)$ is the net total stress, $(u_a - u_w)$ is the suction, and ϕ^b is the friction angle with respect to changes in suction. Originally it was thought that ϕ^b was constant. Fredlund *et al.* (1987) showed that it was in fact curved, which means that ϕ^b is not constant but varies with suction.

Research into the shear strength of buffer material at the University of Manitoba has shown good agreement with the hypothesis that ϕ^b is curved

(Wiebe *et al.* 1998). These results however must be considered carefully, since molding water content was modified to generate different initial suctions in the specimens. As stated earlier, the molding water content affects the pore distribution of the material and therefore the SWCC for the material. The results presented by Wiebe *et al.* (1998) are valuable for determining the effect of molding water content on strength but interpretation of suction characteristics is limited. This problem was addressed in research conducted by Blatz (2000). All specimens were made to the reference buffer material parameters and a range of suctions generated using drying environments. As expected, this research showed suctions produced in specimens using two different techniques (varying molding water content and drying environments) affected the measured shear strength.

2.2.4 Constitutive Modeling of Soil Behaviour

As has just been presented for the shear strength formulation, generally theories for unsaturated soil mechanics have been derived as extensions to formulations that exist for saturated soils. This sounds counter-intuitive because unsaturated theories are more generalized forms of constitutive models. For example in the unsaturated shear strength equation (presented earlier) when the suction component drops out (u_a = 0) the simplified saturated shear strength equation remains. The saturated case needs to be viewed as a bounding condition for unsaturated soil mechanics instead of vice versa.

To account for the coupled relationship between strength and deformation of soils, elastic-plastic models have been used to describe soil behaviour. With

this type of model the behaviour of the soil is separated into two components, the elastic and plastic components. The elastic component models recoverable soil behaviour at pressures lower than the yield stress. Elastic deformations are recovered upon removal of the load. This portion of the model can be described by many relationships such as linear, hyperbolic, or non-linear stress-strain behaviour. The second component is the non-recoverable component, which consists of both elastic and plastic deformations. These deformations occur when soil experiences a load higher than its yield stress. Plastic deformations that occur are not fully recoverable if load is removed and these represent permanent change to soil structure that has been rearranged to equilibrate with the applied load. Elastic-plastic models have been modified to include and represent additional features of soil behaviour such as the effects of temperature (Tanaka 1995), creep (Yin and Graham 1999), anisotropy (Graham and Houlsby 1983), and unsaturation (Delage and Graham 1995).

2.2.4.1 An Elastic-Plastic Model for Soils

The most widely accepted elastic-plastic model that describes soil behaviour is the Modified Cam Clay model (Roscoe and Burland 1968). As powerful as this model is for predicting the elastic-plastic behaviour of saturated soft clays the assumptions that are made in applying this model are its major hindrances; the soil is assumed to be isotropic, have a constant shear modulus, and semi-logarithmic elasticity.

The definition of the state variables for saturated soils are described with three variables p', q (stress state) and V (volume state) and these variables form

the orthogonal axes of the model. Figure 2.1 shows the state boundary surface for the Modified Cam Clay model. The surface shown separates the region of elastic behaviour inside the state boundary surface from plastic behaviour on the state boundary surface. Yield loci are normally taken in the form of ellipses for isotropic soils. The elastic parameters of Young's Modulus and Poisson's ratio (or the bulk and shear moduli) define the stress-strain behaviour of the soil within the elastic region. When the soil is stressed to a point on the yield surface, plastic strains begin to accumulate following yielding. With continued stressing in shear, the soil may "move" towards critical state, which defines steady-state large strain loading conditions, formally defined as (Wood 1990):

$$\frac{\partial p'}{\partial \varepsilon_s} = \frac{\partial q}{\partial \varepsilon_s} = \frac{\partial u_w}{\partial \varepsilon_s} = \frac{\partial \varepsilon_v}{\partial \varepsilon_s} = 0$$

2.2.4.2 Constitutive Models for Unsaturated Soils

Many general models for unsaturated soils have been conceptualized using elastic-plastic behaviour (Alonso *et al.* 1990, Gens and Alonso 1992, Wheeler and Sivakumar 1995, Toll 1990, and Delage and Graham 1995). The main differences between these conceptual models arise because of a lack of physical laboratory data to show the response of volume change to changes in suction when external stress is applied. The common bond between each of these models is that each of them is based on an elastic-plastic framework related to the saturated Cam-Clay framework.

As mentioned earlier, to properly describe the behaviour of unsaturated soils, five state variables are required: p, q, S, V and either water content or degree of saturation. With the use of these five variables, the model can be

visualized as two three-dimensional surfaces and a SWCC to relate suction to degree of saturation or water content. The three-dimensional surfaces used by Blatz and Graham (2003) to define the elastic-plastic behaviour of unsaturated soil are shown in Figure 2.2. Figure 2.2 (a) shows the p-q-S stress surface and Figure 2.2 (b) shows the p-S-V volume change surface. Under plastic hardening and softening the elastic region within the p-q-S space expands and compresses respectively.

Compacted unsaturated high-plastic clays have been shown to have both micro- and macrostructures, which contribute to their observed behaviour. To be able to capture the complete range of behaviour of unsaturated soils, the behaviour of both the micro- and macrostructure must be modeled. First work on the behaviour of the microstructure was initiated by soil scientists and developed by engineering geologists. Microstructural features, such as cementation bonds, have been related to mechanical features such as compressibility, strength, and sensitivity (Delage and Graham 1995 and Garinger 2002). These microstructural features are related to the mineralogy and physico-chemistry at the level of the elementary interactions between clay particles and clay-water interfaces.

Delage and Graham (1995) posed the question, "When yielding is observed upon loading, upon suction increase, and sometimes upon wetting, are these mechanisms independent or inter-related?" Alonso *et al.* (1987), Josa *et al.* (1987), and Wheeler and Sivakumar (1995) suggest that they are in fact related to fundamentally similar changes in the soil microstructure. While there has been a great effort defining the effects of the microstructure on the

behaviour of unsaturated soils, relationships linking microstructural phenomena to the macrostructural behaviour have remained difficult to assess (Gens and Alonso 1992).

2.2.4.3 Constant Suction Yielding Model

Before a model can be used to describe the behaviour of unsaturated soil, the initial state of the soil must be defined in terms of its external stress, suction, and specific volume. The greater part of modeling of elastic-plastic behaviour of unsaturated soil has been concentrated on results from tests done at constant suction. Wheeler and Sivakumar (1995) have proposed that the yield loci in p-q-S space are represented by ellipses, as shown in Figure 2.2. This represents their conceptualized state boundary surface for isotropic unsaturated soils. Asymmetric loci however would better represent natural and compacted unsaturated soils (Graham and Houlsby 1983 and Moulin 1989), which are rarely isotropic (Delage and Graham 1995 and Cui and Delage 1996).

Figure 2.3 (a) shows a trace of a yield locus in p-S space as defined by Alonso *et al.* (1990). The load yield (LY) line represents when yielding is first observed under increasing isotropic loading at different suction levels. The figure also defines a line that represents where yielding would first be observed under increased suction loading called the suction yield (SY) line. Enlargement of the elastic region occurs when soil is subjected to stresses beyond its initial yield and contraction of the elastic region for strain softening. This enlargement can occur by either increase in suction or pressure, as shown in Figure 2.3 (b). Alonso *et al.* (1990) suggested that there is coupling between the load and

suction yield, an increase in the load yield would result in an increase in the suction yield and vice versa. There is a very distinct discontinuity in Figure 2.3 where the LY and SY lines meet. Since a sharp discontinuity would not be expected to occur in natural materials, Delage and Graham (1995) proposed that a curved line should represent the elastic region as one combined LSY locus (Figure 2.4). The LSY locus combines the load and suction yield lines into one smooth line. It must be remembered that when a material is in the elastic region and subjected to pressure or suction changes the material will initially behave elastically and will undergo elastic volume strains until yielding is reached. It is this fact that may account for the differences in shape between Alonso *et al.* (1990) and Ho *et al.* (1992), where the LSY locus does not lie on a constant volume plane.

2.3 Conclusions and Potential Questions to Answer

Some of the key findings from past research at the University of Manitoba are:

1. Suction is a function of the current water content, the water content at the time of hydration, and drying / wetting history (Wan 1996, Tang 1999, and Blatz 2000).
2. Undrained behaviour (both liquid and vapour) of compacted high-plastic clay subjected to suction loading is affected by soil suction and changes in density associated with changing suction (Blatz 2000).

3. The constant suction model can be used to reliably predict behaviour of unsaturated high-plastic clay for stress ranges presented in Blatz (2000), but Tang and Graham (2002) presented a different model for predicting behaviour of unsaturated high-plastic clays.

Questions that remain to be answered include:

1. What is the dominant component of resistance in unsaturated soils, suction or effective stress?
2. How will the buffer behave under cycled suction loading?
3. Are the effects of suction consistent during isotropic and shear stress loading above 8 MPa total suction (the limit in the research by Blatz 2000)?
4. What impacts will different bentonite minerals have on the behaviour of buffer?
5. How is the hydraulic behaviour of buffer affected by changes in suction?

The research reported in the remainder of this thesis document attempts to answer these questions.

2.4 Justification of Research

All of the work to date at the University of Manitoba has used sand-bentonite mixtures of Saskatchewan bentonite (formally called Avonlea bentonite) with sand. In this research program Saskatchewan bentonite is used once again, to further increase the understanding of the behaviour of the

Saskatchewan buffer material. Also included in this program is the use of Wyoming bentonite in combination with sand. This testing program also examined the behaviour of buffer material when subjected to varying stress paths. This helps to better define the yielding behaviour in p-q-S space of compacted high-plastic clays at higher suctions than have previously been used to define yielding. The results provide new experimental measurements of buffer behaviour required for understanding the behaviour of the engineered seal in the AECL disposal application. Also provided is experimental data required to further our understanding of the fundamental physics of unsaturated clay soils.

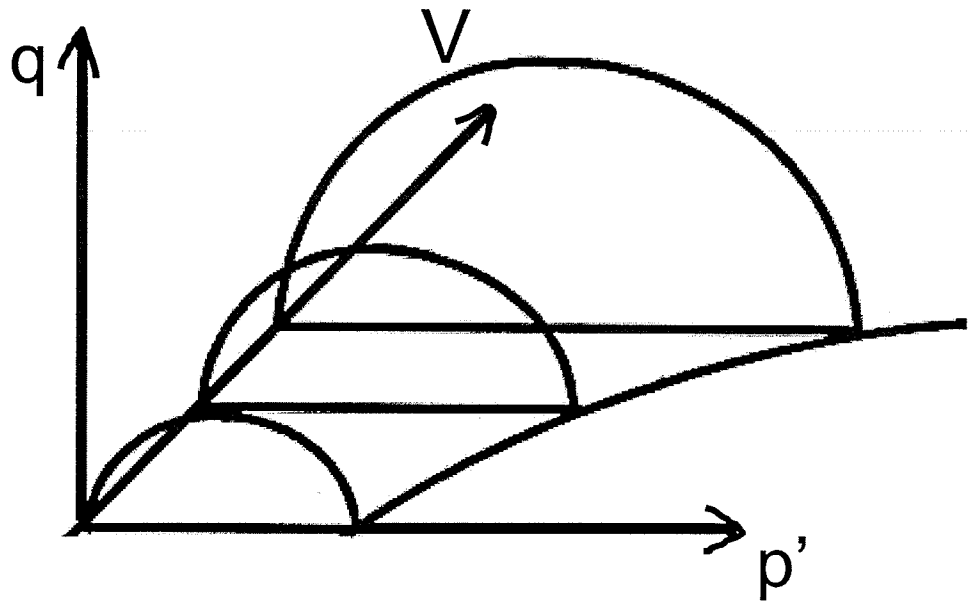

Figure 2.1 Modified Cam Clay model

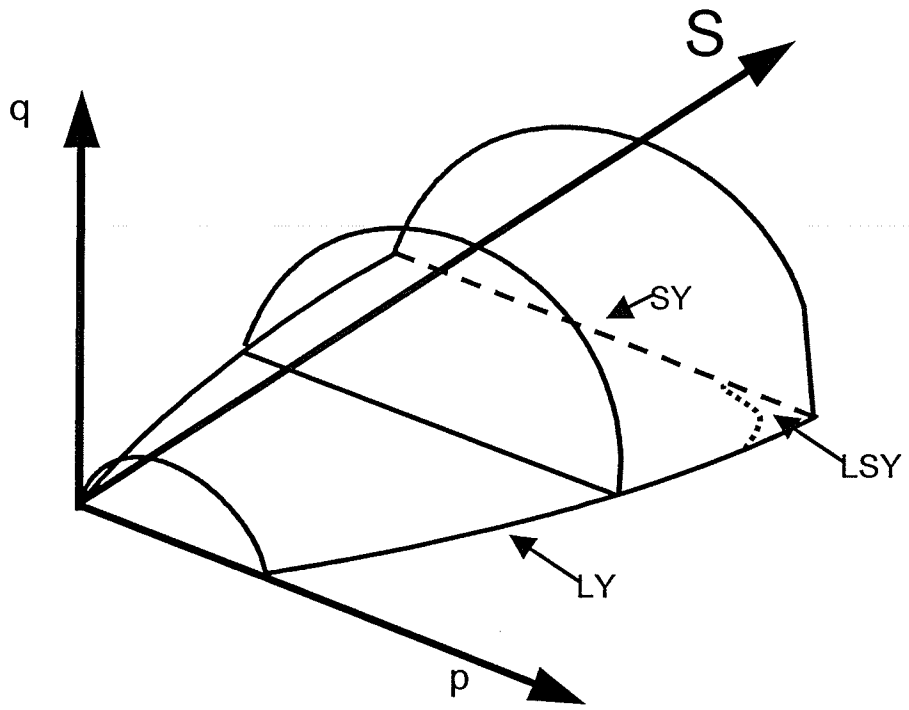

Figure 2.2 (a) Three-dimensional visualization of the unsaturated stress surface (after Blatz and Graham 2003)

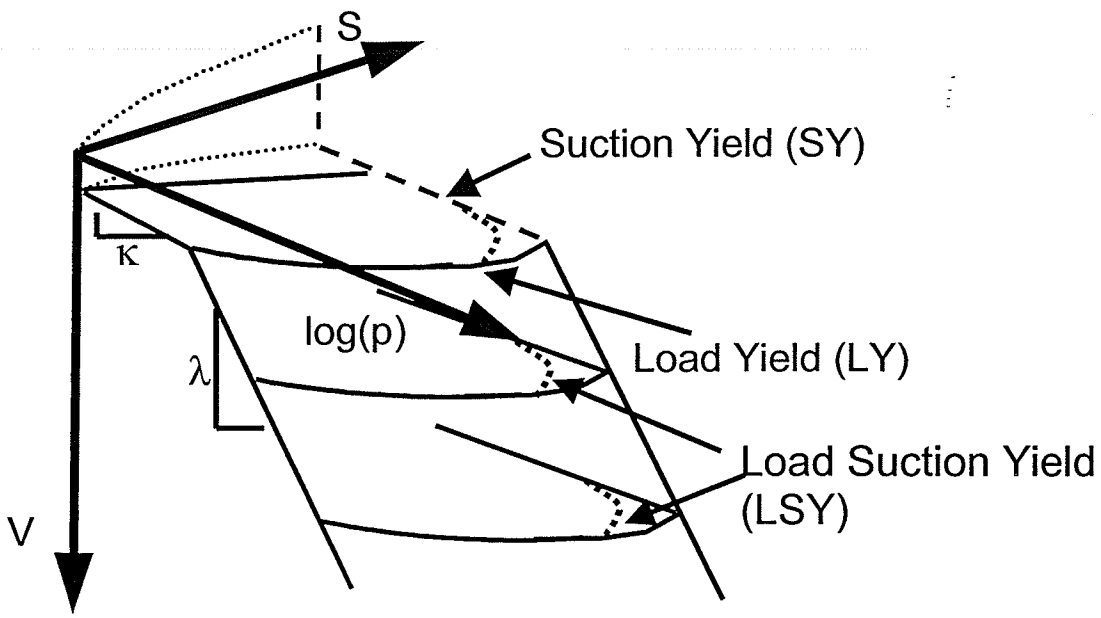

Figure 2.2 (b) Three-dimensional visualization of volume state surface (after **Blatz and Graham 2003**)

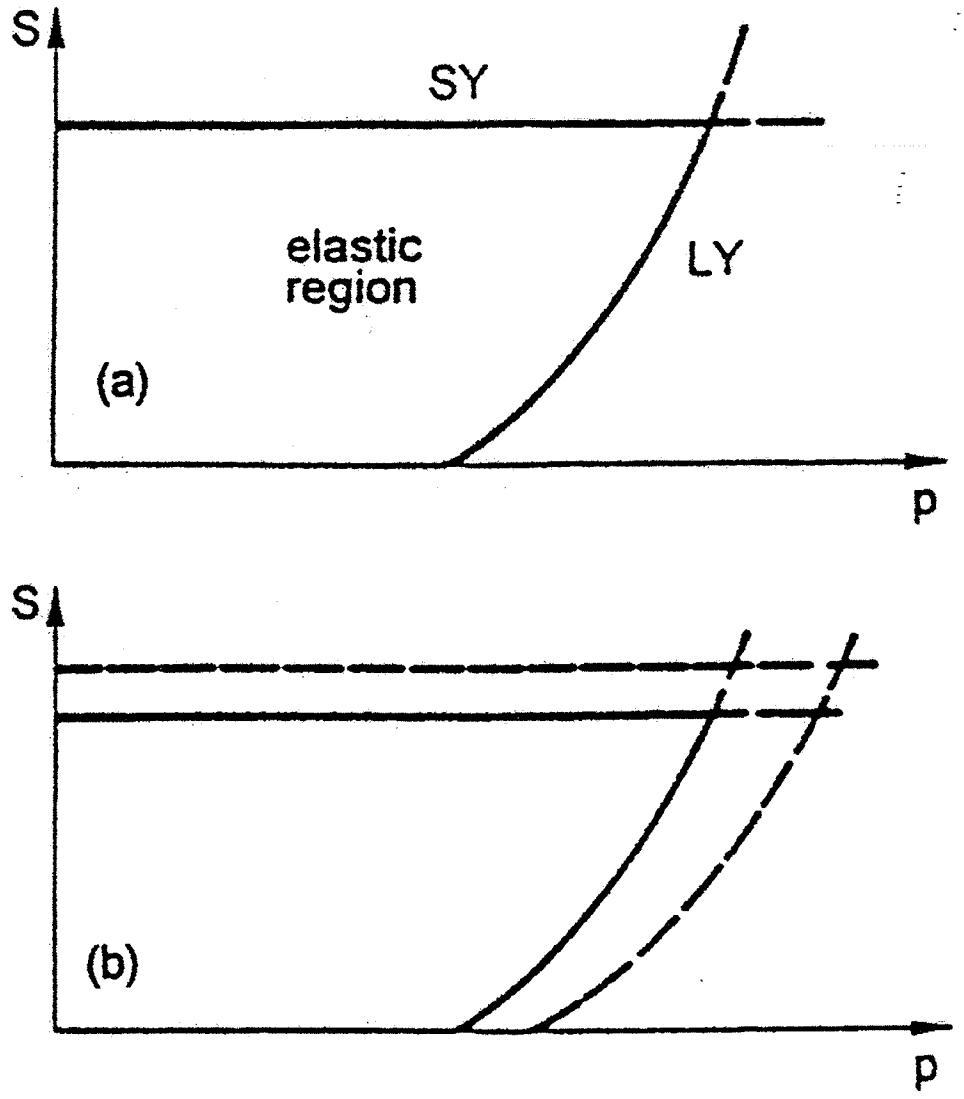

Figure 2.3 p-S yielding as proposed by **Alonso *et al.* (1990)**

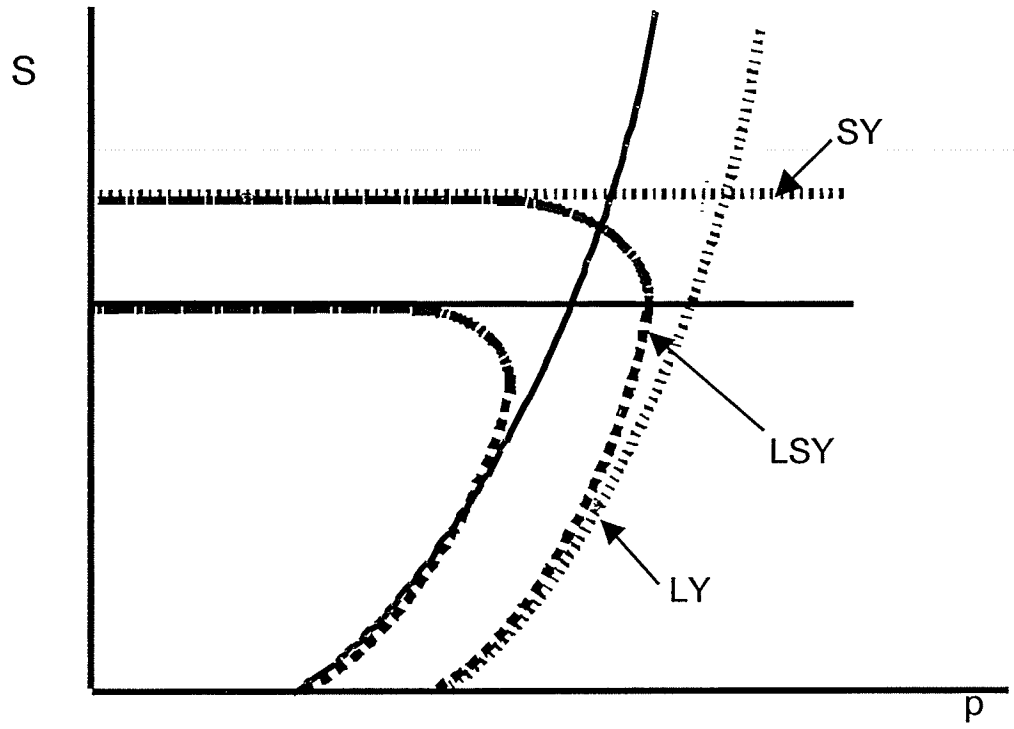

Figure 2.4 Proposed LSY loci by **Delage and Graham (1995)**

3.0 MATERIALS, SPECIMEN PREPARATION AND EXPERIMENTAL PROGRAM

3.1 Introduction

This chapter describes the materials used in the testing programs, details of how specimens were prepared, and details of the experimental program. This chapter serves to document the procedures used in this testing program so that subsequent researchers may use the same techniques, confirm the results, and extend the knowledge of materials tested. The processes of preparation and compaction of unsaturated buffer material has been covered by other researchers in considerable detail. This chapter documents the procedures used in this research program and focuses on differences from past programs.

3.2 Reference Buffer Material (RBM)

Consistent specimens of reference buffer material (RBM) were prepared by mixing, curing and then statically compacting 50:50 mixtures by dry mass of bentonite and sand with deaired, deionized water. Specified target properties for the buffer materials are water content = 19.4% and dry density = 1.67 Mg/m^3. These produce a degree of saturation of approximately 85%.

3.2.1 Saskatchewan and Wyoming Bentonite

There were two separate buffers used in this program. Both buffers were mixed to the specified target parameters. The only difference between the two buffers was the constituent bentonite. The first type of bentonite used was Saskatchewan bentonite that has been used in past research at the University of Manitoba. Atterberg Limits showed a liquid limit w_L = 222% and a plasticity index

I_p = 176%. This is consistent with Atterberg limits reported by past researchers at the University of Manitoba and close to the values specified by Dixon and Gray (1985). The second type of bentonite used was Wyoming bentonite. Wyoming bentonite showed an average liquid limit w_L = 605% and an average plasticity index I_p = 561%. All Atterberg Limit testing was conducted using distilled water. Table 3.1 below summarizes the results of Atterberg Limit testing conducted on both supplies of bentonite provided by AECL to the University of Manitoba Geotechnical Laboratory.

Sample	Wyoming Bentonite	Wyoming Bentonite	Wyoming Bentonite	Saskatchewan Bentonite
w_L	585	607	589	222
w_P	41	48	40	46
I_P	544	559	549	176

Table 3.1 Atterberg Limits for Saskatchewan and Wyoming bentonite

The principal difference between the two bentonites lies in their physico-chemical composition and the surface area of the clay minerals (presented in Chapter 2). The Saskatchewan and Wyoming bentonites are similar in mineralogical structure (Dixon and Miller 1995). The mineralogical composition of Saskatchewan bentonite is 80% montmorillonite and Wyoming bentonite has 75% montmorillonite. The remaining 20% and 25% respectively are composed of quartz, feldspars and other non-smectitic minerals (Oscarson and Dixon 1989, Baumgartner 2000 and Karnland 1997). In Wyoming bentonite, the predominant exchangeable cation that satisfies the net negative charge in the diffuse double

layer is sodium (Pusch 1994); while in Saskatchewan bentonite there is a mixture of calcium and sodium cations (Dixon et al. 1999). These two factors affect the overall net negative charge of the minerals and therefore the behaviour of each material.

3.2.2 "Frac" Sand

The sand component of the buffer is a crushed, medium, sub-angular, uniform, silica sand. The "Frac" sand provided by AECL, was combined according to the specifications presented by Dixon et al. (1994), with the gradation of the sand being within the specified tolerances at all times as shown in Figure 3.1. Also included in the figure is the gradation of the sand used by Blatz (2000). While both gradations are within the specifications, there are slight differences between the two sand mixtures used in the programs. This is an important note that is discussed in later sections.

3.2.3 Distilled Deaired Water

To ensure that the pore fluid chemistry and hence the osmotic suction remained constant, distilled deaired water was used for preparing all specimens. The distilled water produced in the University of Manitoba Geotechnical Laboratory. It was deaired for 24 hours using a vacuum pump prior to preparing specimens.

3.3 Specimen Preparation and Compaction

3.3.1 Mixing Buffer Specimens

Prior to mixing specimens, the bentonite and sand were stored in an oven at 104°C for a minimum of 48 and 24 hours respectively. After removing the

materials from the oven, the containers were sealed with plastic wrap and a rubber band to ensure moisture was not pulled from the air into the materials. The materials were allowed to equilibrate with room temperature for 90 minutes before measurements and mixing commenced.

The required dry weights of the constituent bentonite clay, silica sand, and distilled deaired water for buffer specimens were determined using a spreadsheet, which calculates the masses, based on the specified target properties (water content = 19.4% and dry density = 1.67 Mg/m^3). The spreadsheet calculations were verified with hand calculations for specimens used for quality control.

The distilled deaired water was first added to the dry mass of sand in a steel-mixing bowl. The required dry mass of bentonite clay was then measured in a separate glass container. Each batch had a wet mass of approximately 550 g, which included the bentonite, sand, and water. The mixing bowl with sand and water and the glass container with the bentonite were covered after measurements were complete. All the materials were then transported to a cool 4C environmental chamber where the mixing process was performed.

The bentonite clay was added to the sand / water mixture and slowly worked together using a mixing tool. After two minutes, the top of the mixture was packed down lightly to create a flat surface. The surface was then broken up by crushing and grinding the material along the sides of the bowl. After all the material had been broken up, the mixing continued for a total time of eight minutes after adding the clay to the sand / water mixture. Mixing was performed

in a uniform manner ensuring that large clumps were crushed against the bowl. Packing and grinding were then repeated.

This process tended to distribute the water more efficiently than simply mixing. The change in consistency of the mixture before and after the packing / breaking process was notable. After repetition of the packing and break up, mixing continued for a total time of 16 minutes. The mixture was then sealed in a sample bag, which was placed in a second sampling bag. The specimen was labeled and allowed to equilibrate for a 48-hour period as specified by Graham et al. (1995). Water content measurements were taken 48 hours after the mixing process to evaluate the actual water content of the material in the bag. This water content was then used in the spreadsheet calculations to determine the wet soil mass required in the compaction procedure to meet the water content and density requirements. These procedures were followed for both types of buffer.

3.3.2 Specimen Compaction

Specimens were compacted with the pre-existing rigid, one-dimensional static compaction ram and mould at the University of Manitoba shown in Blatz (2000). Procedures developed by Yarechewski (1993) for preparing triaxial specimens of sand-bentonite were followed. All specimens (both Saskatchewan and Wyoming buffer) were compacted to RBM parameters described in section 3.2.

3.3.2.1 High Pressure Triaxial Specimens

All triaxial specimens were compacted to a nominal height of 100 mm and diameter of 50 mm. Specimens were compacted in five equal lifts using the constant lift height (20 mm) criterion as described by Wiebe (1996) and Yarechewski (1993). The constant lift height criterion was adopted in this work as it was believed that specimen consistency with past research was important because this program was building on and adding to past programs related to the overall research efforts at the University of Manitoba on unsaturated soil mechanics. Moreover, this technique produces samples with minimal water content and density variations as documented by Yarechewski (1993).

3.3.2.2 Hydraulic Characteristic Specimens

The one main difference with the compaction of the specimens for the hydraulic characteristics tests is that the dimensions of the specimens used in this part of the research were 100 mm in diameter by 100 mm in height. They were compacted to RBM parameters as presented in section 3.2. Only Saskatchewan buffer was used in the hydraulic characteristics test. Compaction of these larger specimens required that the existing static compaction ram had to be modified and a new larger mould had to be used. This is shown in Figure 3.2.

3.4 Experimental Program

3.4.1 Shrinkage Tests

Immediately following compaction, the mass and dimensions of all specimens were recorded before placing them in the relative humidity (suction)

environments. The ionic solutions were contained in sealed glass desiccators where a perforated plate was located above the ionic solution (Figure 3.3). For this study five different target suction levels were selected (10, 20, 40, 80, and 160 MPa). During drying in the suction environments, water was drawn from the specimens to the vapour environment where it was then transferred to the ionic solution. With the increase in water content in the ionic solution, the concentration of the solution was reduced, thereby reducing the applied suction. A formula was developed to recalculate the final suction in the desiccator to take into account this mass balance consideration. Following removal of the specimens after equilibration (30 days) in the desiccators (Tang 1999), the mass and dimensions were measured again prior to placement in the triaxial cell.

3.4.2 High Pressure Triaxial Tests

Specimens were placed immediately into the high pressure, high temperature (HITEP) triaxial cell following manual measurements of the dimensions and mass after equilibration in the desiccators. Stress paths that included external isotropic and shear loading were undertaken to evaluate the compressibility, strength and yield characteristics for buffer at target suction levels of 10, 20, 40, 80, and 160 MPa. Once placed in the HITEP cell, specimens were separated from the cell fluid (silicon oil) by two membranes that were held in place in the cell by 7 O-rings, 4 at the bottom pedestal and 3 at the top-loading cap. These procedures are similar to those described by Tang (1999) and Blatz (2000).

Specimens were initially compressed using specified cell pressure increments up to a maximum value of 5 MPa. During the initial stages of the testing program three specimens were compressed to 6 MPa after which the maximum pressure in all tests was reduced to 5 MPa. The initial tests to 6 MPa were used to determine what maximum pressure level would be appropriate to ensure all specimens showed yielding and plastic deformations. The initial tests showed that 5 MPa as a maximum pressure was more than adequate to show yielding and plastic strain hardening. The cell pressure increments were applied every 24 hours to ensure suction and volume change equilibration between increments (Blatz 2000). During compression, the axial and radial displacements were measured using linear variable displacement transducers (LVDT's) mounted on the top of the specimen and at two locations at the specimen mid-height. No drainage of air or moisture was permitted from specimens during compression. The tests are therefore referred to as 'constant mass' tests. Although no drainage is permitted, there is a change in suction associated with isotropic compression. The change in suction follows the approximate slope of $\Delta S/\Delta p = -0.83$, where ΔS = change in suction and Δp = change in total mean stress, as shown in Tang et al. (1997) and Blatz and Graham (2003). Volume strains were inferred from the point measurements of axial and radial displacement taken by the LVDT's. All instrumentation was monitored using a Campbell Scientific CR7 data acquisition system until the implementation of a new fully automated data acquisition and stress path control system in the spring of 2001. Both systems are described in Chapter 4.

Following compression, specimens were unloaded to a cell pressure corresponding to half the maximum isotropic stress value achieved during initial loading. This corresponds to the approximate mid-point of a yield ellipse (OCR equal to 2.0) in the elastic space of the state boundary surface (halfway between the maximum mean stress ever achieved and the tensile strength at the current suction (Tang and Graham 2000)). From this known stress state, evaluation of yielding in shear was conducted by shearing the samples along various predetermined shearing stress paths.

Following isotropic unloading to the midway point in the elastic region, specimens were allowed to equilibrate for 24 hours before shearing commenced. Three target stress paths were selected to examine the yield envelopes along approximately constant suction traces in q-p space. The three shearing stress paths corresponded to constant-p, q/p ratio of 1:1 and q/p ratio of 3:-1. The specimens were sheared at a constant strain rate of 0.0139 mm/min (20 mm over 24 hours) to ensure suction equilibrium during the shearing phase (Blatz *et al.* 1999). Instrumentation was monitored using a Campbell Scientific CR7 data acquisition system until commissioning of a new, fully automated data acquisition and stress path control system in spring 2001. After shearing was completed, specimens were removed from the cell and their mass and dimensions were recorded. Final water contents were also taken for all specimens.

3.4.3 Hydraulic Characteristic Testing

Following compaction, specimens were placed into a desiccator at known target suction levels (40, 80 and 160 MPa). Multiple specimens were placed in the different suction environments and removed at various times (5 days, 15 days, and 30 days) with an understanding that the specimens were not in equilibrium with the suction environment (Tang 1999). This allowed for the spatial distribution of water content to be measured after a known time interval under specified suction conditions. Knowing the distribution of local water contents of each specimen allowed for the suction distribution to be inferred from the soil water characteristic curve. Figure 3.4 is a photograph of one of the large specimens used in this test program after 30 days in a 160 MPa target suction desiccator.

Once removed, specimens were carefully broken into defined regions using a cutting template machined at the University of Manitoba. This allowed for the spatial distribution of water content to be accurately measured in both the axial and radial directions. The cutting template and shoe are shown in Figure 3.5. These tests, done under 'unconfined' conditions, represent a simplification of the real application where confinement will be provided by the host rock and the container. However for shrinkage paths, such as in the drying tests reported in this thesis, confinement is not a critical issue. Since during drying tests the specimens are shrinking and they would shrink away from any confinement provided.

3.5 Quality Control

To ensure specimens were uniform and the laboratory procedures were consistent with previous researchers, a series of quality control tests were performed. The mass of water used during the mixing process was altered in three quality control specimens (DA-001 to DA-003), to ensure consistency with respect to the target water content (19.4%). Figure 3.6 shows the water content and the dry density for all triaxial specimens used during testing. Figure 3.7 shows the quality control for the water content distributions of one of the larger specimens. This specimen was used to ensure that the compaction process provided a uniform water content distribution prior to placement of specimens in the desiccators and also to help modify the compaction and breaking process so to yield consistent specimens using the modified ram, mould, and cutting tool.

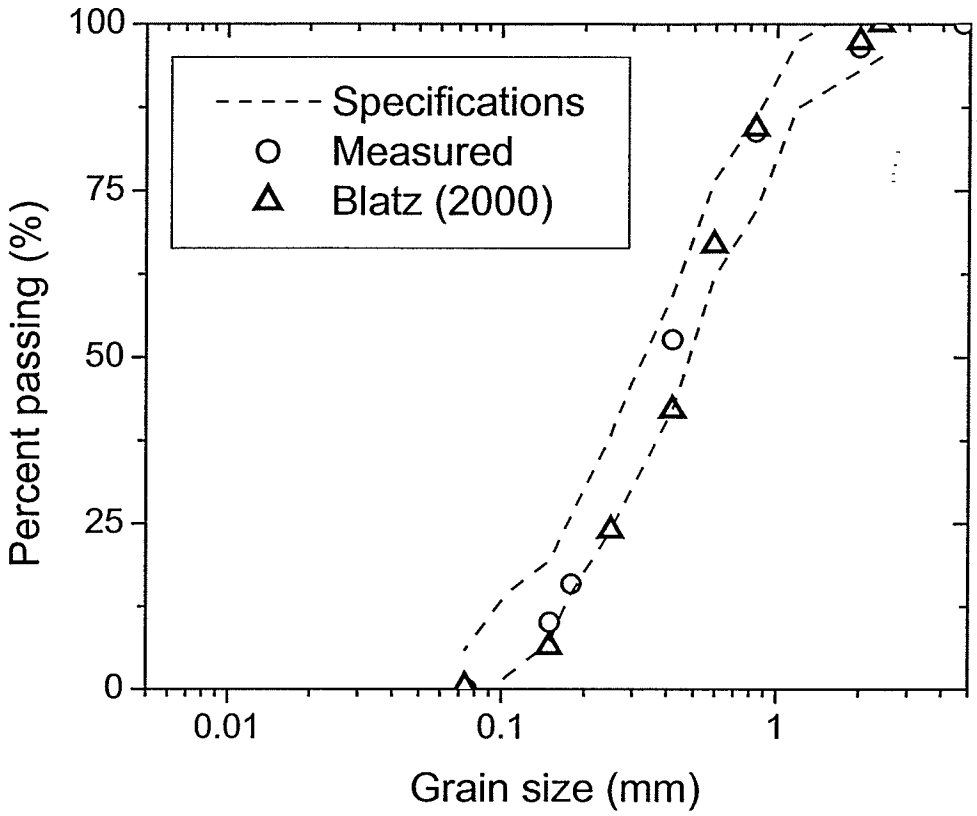

Figure 3.1 Frac sand sieve results compared with the specifications from Dixon et al. 1994

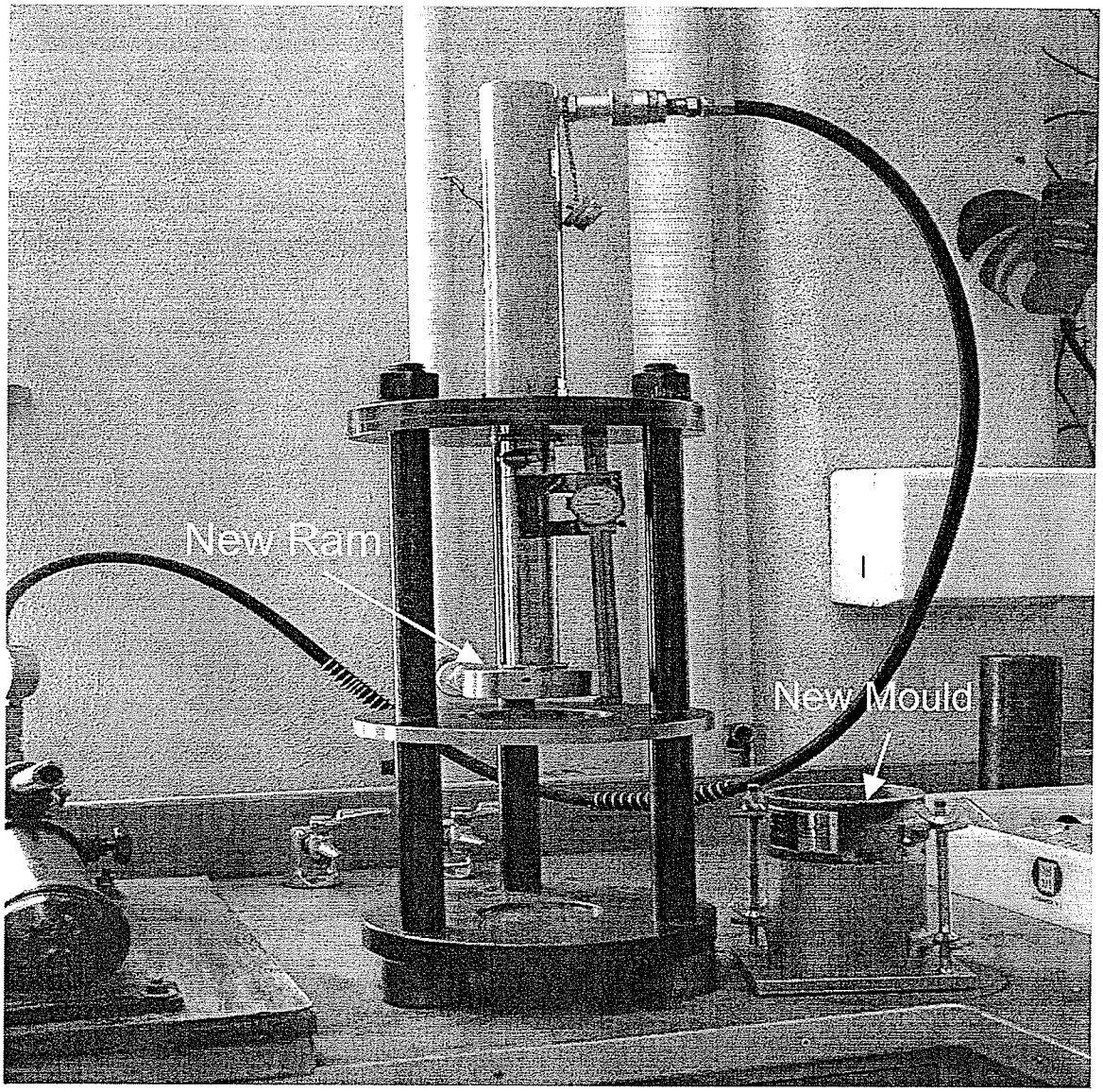

Figure 3.2 New static compaction equipment

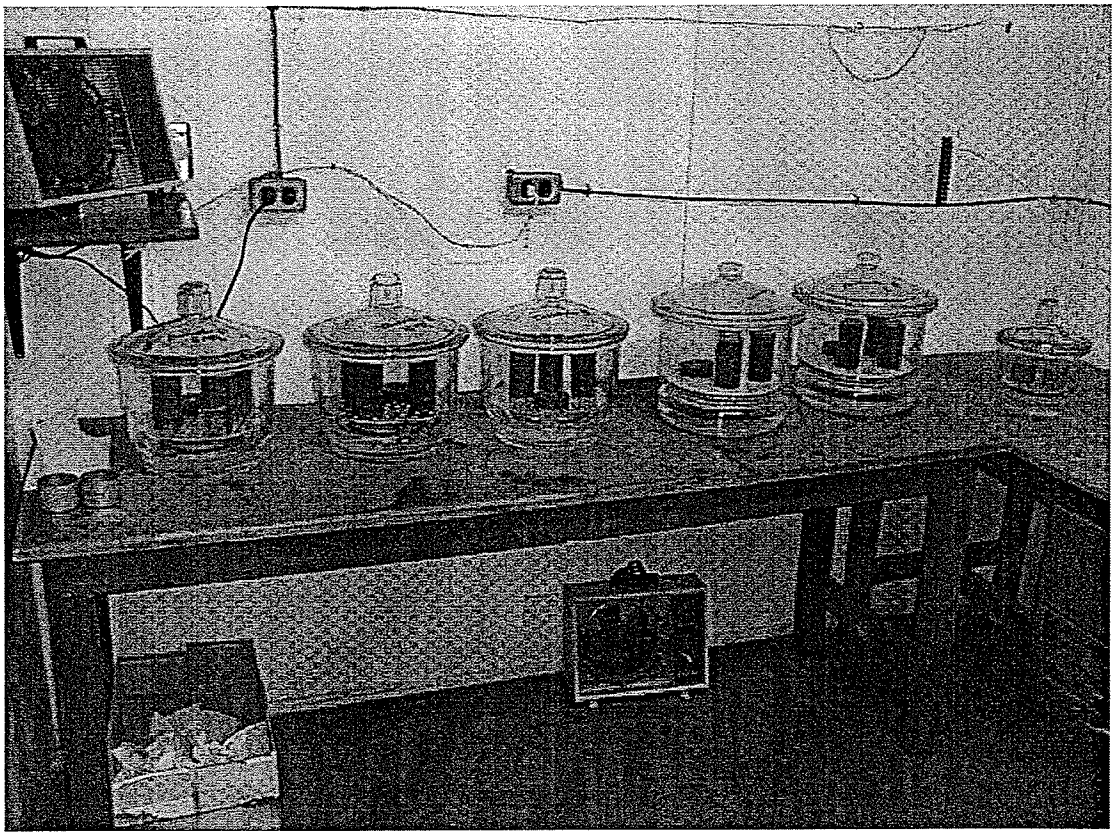

Figure 3.3 Relative humidity desiccators

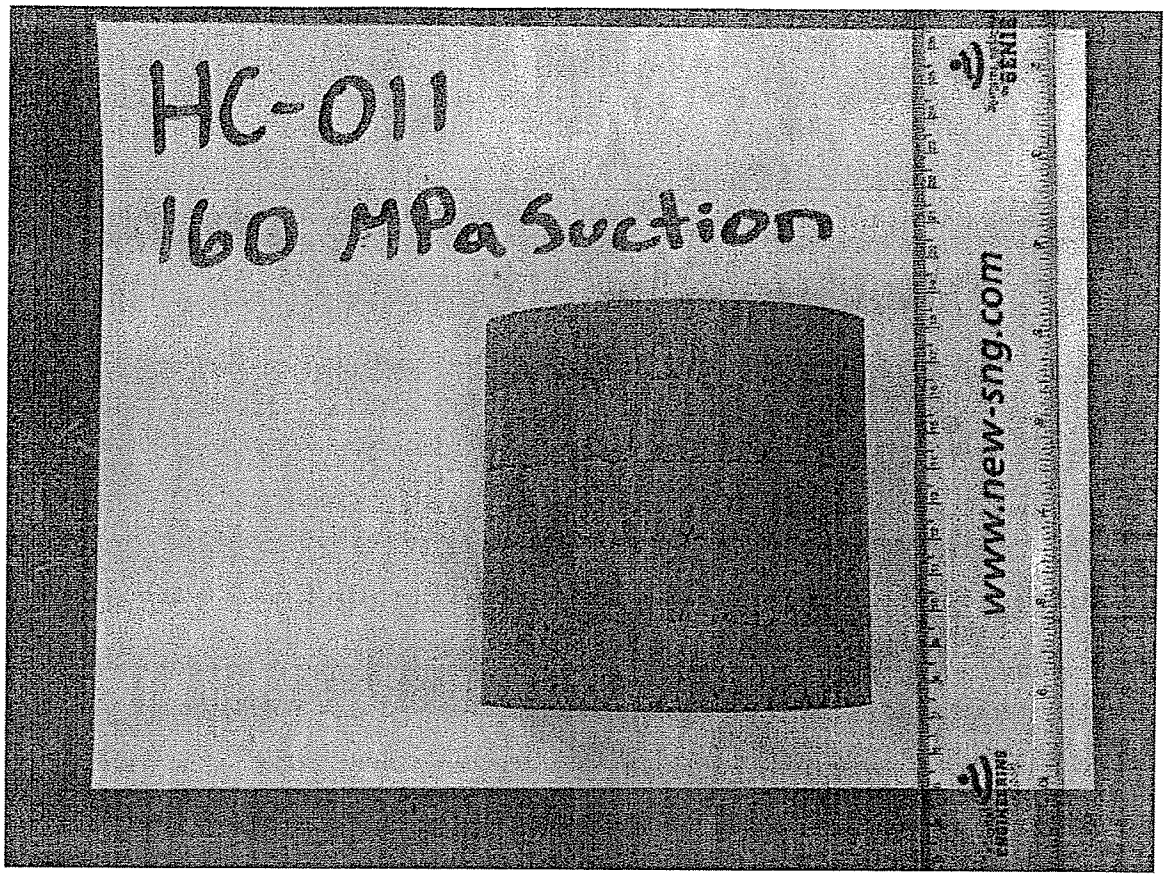

Figure 3.4 Large hydraulic characteristics specimen

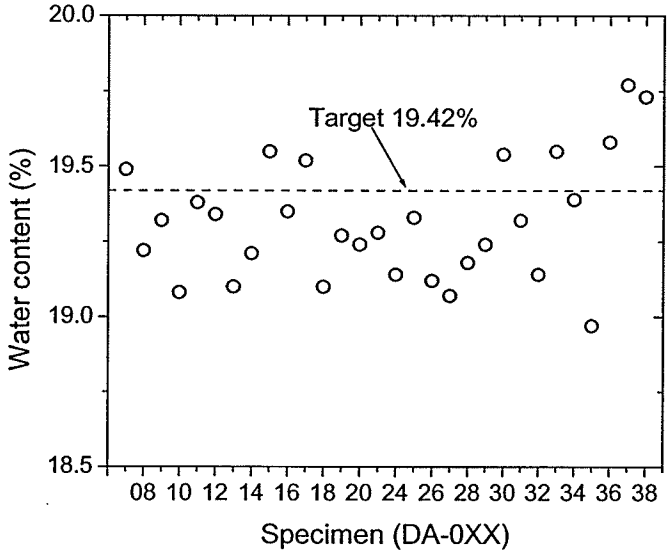

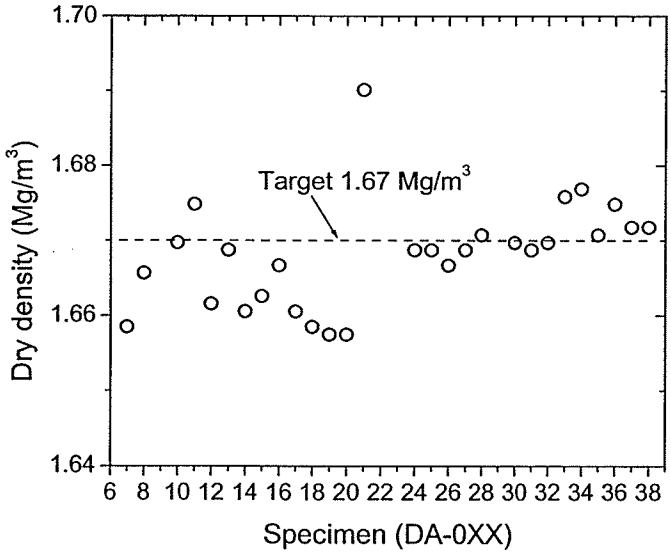

Figure 3.6 Water content and dry density of all triaxial specimens

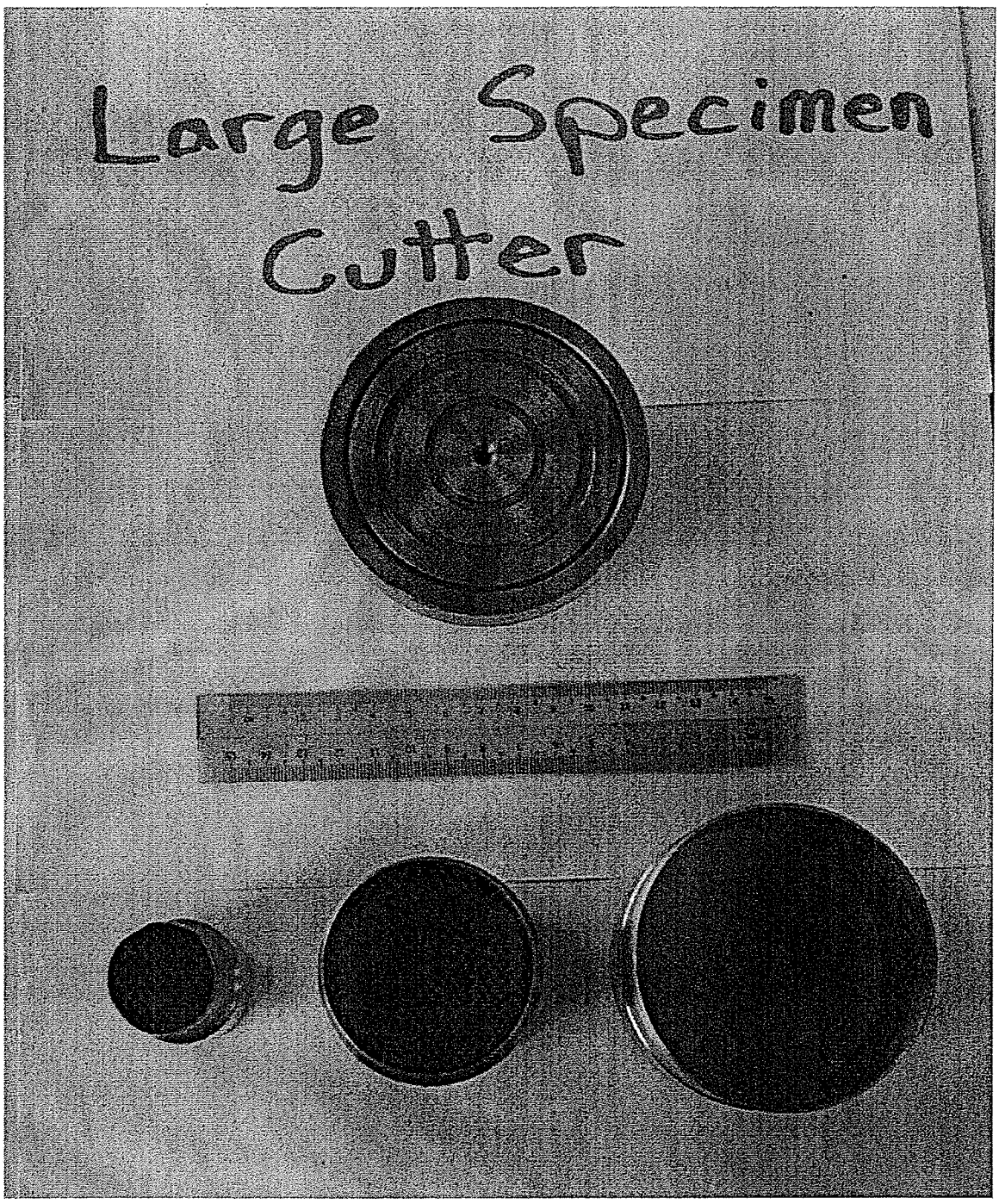

Figure 3.5 Large specimen cutting shoe apparatus

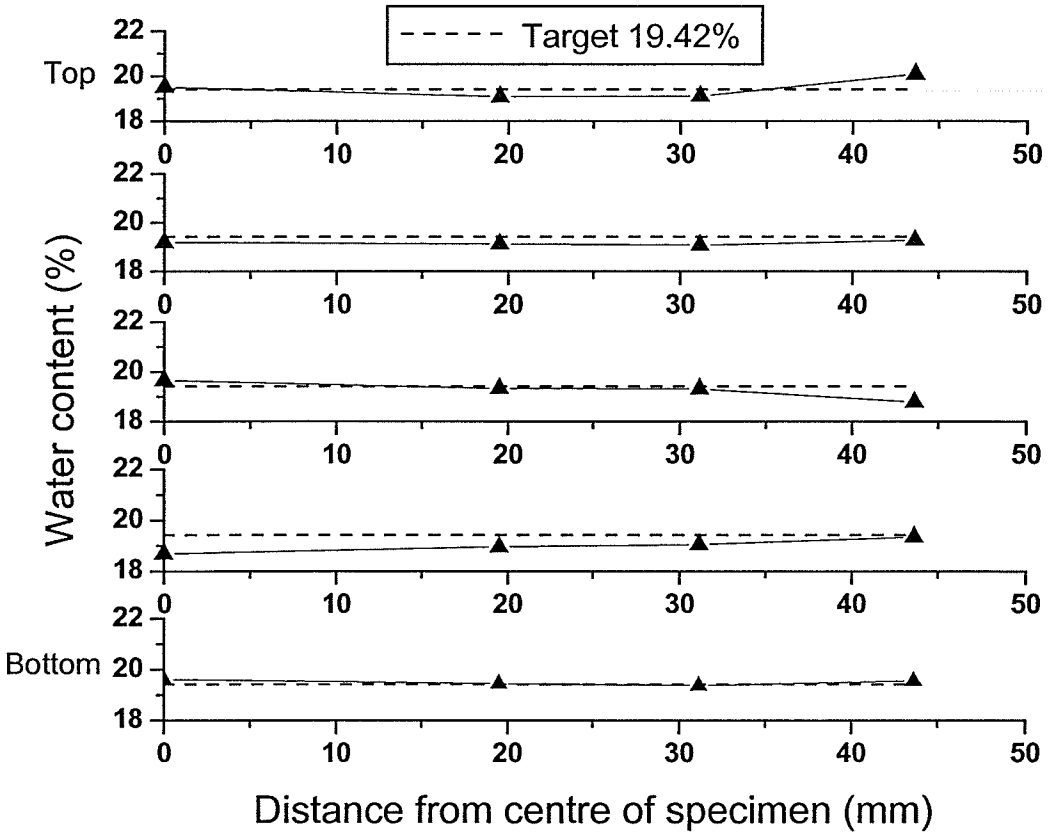

Figure 3.7 Water content distribution of the large quality control specimen

4.0 EQUIPMENT FOR TRIAXIAL TESTS

4.1 Introduction

Triaxial testing is a widely used method to measure the mechanical behaviour of soils. This chapter describes the triaxial equipment used in the testing program undertaken in this research. The equipment is described in some detail to document new developments undertaken during this program. Photographs are also provided along with a description of the apparatus.

4.2 High Pressure Triaxial Tests

This section describes the triaxial apparatus used during the testing program. The main component of the testing was completed using the existing high temperature, high pressure (HITEP) triaxial cells at the University of Manitoba. Researchers at the University of Manitoba have previously presented a detailed description of the HITEP cells and their design; see for example Lingnau *et al.* (1996). The HITEP cell is mounted in a strain controlled load frame, which is described in Blatz (2000). The load frame is an ELE25-310 Series Steplessly Variable Drive load frame, capable of running at strain rates from 2.5×10^{-5} mm/min to 4.0 mm/min. A strain rate of 0.0139 mm/min was chosen to shear all specimens, since at this rate suction equilibration is ensured throughout the triaxial specimen during shearing (Blatz *et al.* 1999) but may not ensure suction equilibration along the shear plane as well.

Two membranes separate the specimens from the cell fluid (silicon oil), which are held in place in the cell with 4 O-rings at the bottom pedestal and 3 at the top loading cap as shown in Figure 4.1. Also shown in Figure 4.1 are the two

radial linear variable displacement transformers (LVDT's), the vertically mounted LVDT to measure axial displacements, and the load cell. Calibration of all instrumentation was conducted to ensure a linear R^2 regression coefficient of 0.98 or better.

4.2.1 Data Acquisition and Control System

As mentioned earlier, monitoring of high pressure triaxial tests at the University of Manitoba initially used a Campbell Scientific CR7 Data Acquisition system. All instruments and power supplies were monitored with this system. The CR7 was connected to a PC for data storage and visualization. The software package PC208W, which was distributed for use with the CR7, created a data file, which allowed data to be stored and viewed during testing. This software also provides a detailed output of all of the instruments in graphical format.

Implementation of a new fully automated data acquisition and stress path control system was undertaken in the spring of 2001 (Figure 4.2). The system was custom built on the basis of sketches and specifications of how the software interface and automation controller should operate the triaxial apparatus. Feedback control algorithms were created for the automation processes, which utilize a programmable logic controller. This logic controller is customizable by the user to modify testing as required for testing programs. An important feature, that is extremely valuable, is that the system can be monitored and controlled securely over the Internet. This is especially useful for longer duration tests that can potentially take up to 30 days.

Calibration of all existing HITEP cell instrumentation is completed using physical measurements and the data acquisition system. The new system uses a Windows-based software package RSView to display the data graphically in real time and to store the data in a file. When running the data acquisition program (RSView) separate windows are used to display each type of test, isotropic compression, triaxial shear, and the calibration coefficients for each instrument. From each of these windows the user can modify either the tests or the calibration coefficients as required.

Control of stress paths can be carried out during either isotropic compression or triaxial shear. Prior to implementation of this system, all stress paths were controlled manually by hand. To follow target stress paths using the new system, a series of equations relating the area to control parameters (p and q), deviator stress and mean stress, were developed. As changes to the cross-sectional area of the specimen, cell pressure or load occur, new values of the control parameters are calculated to maintain the target path. The control system uses an electrical motor, Figure 4.3, to adjust the pressure regulator to achieve the target cell pressure. To avoid damage to the motor or pressure regulator during cell pressure adjustment, minimum and maximum ranges were set on the regulator using sensors. Once either of these sensors has been triggered, the control system stops increasing or decreasing the cell pressure (depending on which sensor was triggered). The motor currently uses two speeds to adjust the cell pressure. A long turn rate (motor turns regulator for 1 second) when the desired cell pressure is more than 150 kPa beyond the

actual cell pressure being measured, and a short turn rate (motor turns regulator for 1 tenth of a second) when the cell pressure is within 150 kPa of the desired cell pressure. The control system continually searches for the correct cell pressure until the actual cell pressure is within 25 kPa of the desired cell pressure. With this control system, a sensitivity of 25 kPa is not mandatory but can be changed by the user to meet any specific requirements. Along with changing the sensitivity, the turn rates can also be adjusted by the user if required.

With this new system, testing can follow any isotropic or shear stress path that may be desired. All that is required from the user is a "recipe" (listing times and pressures) for the stress path. During isotropic compression, up to 20 different steps can be used to isotropically compress or unload the specimen with each step lasting as long as the user desires. For stress paths during triaxial shearing, the user must enter the desired q/p ratio. If a constant-p stress path is desired, the user selects a pre-set constant-p stress path test.

The data-logging rate during all testing is defaulted to one reading per second. The user can change the default reading interval to any length of time between each successive reading to the data file. The data-logging rate does not affect the rate at which the cell pressure is adjusted during any phase of testing. The control system checks the cell pressure every 3 seconds to determine whether or not the actual cell pressure is within 25 kPa of the desired cell pressure. The user can also change the length of time between each update of the cell pressure.

4.3 Summary of Triaxial Testing Equipment

This chapter presented the equipment used during the triaxial testing program of this research. A description of a new fully automated data acquisition and stress path control system was also presented. This new system allows for generalized stress paths under triaxial conditions to be accurately examined in q-p space. Examination of these stress paths in q-p space provides required experimental evidence to add further confidence to numerical modeling activities. The subsequent chapters present the data obtained using this new system.

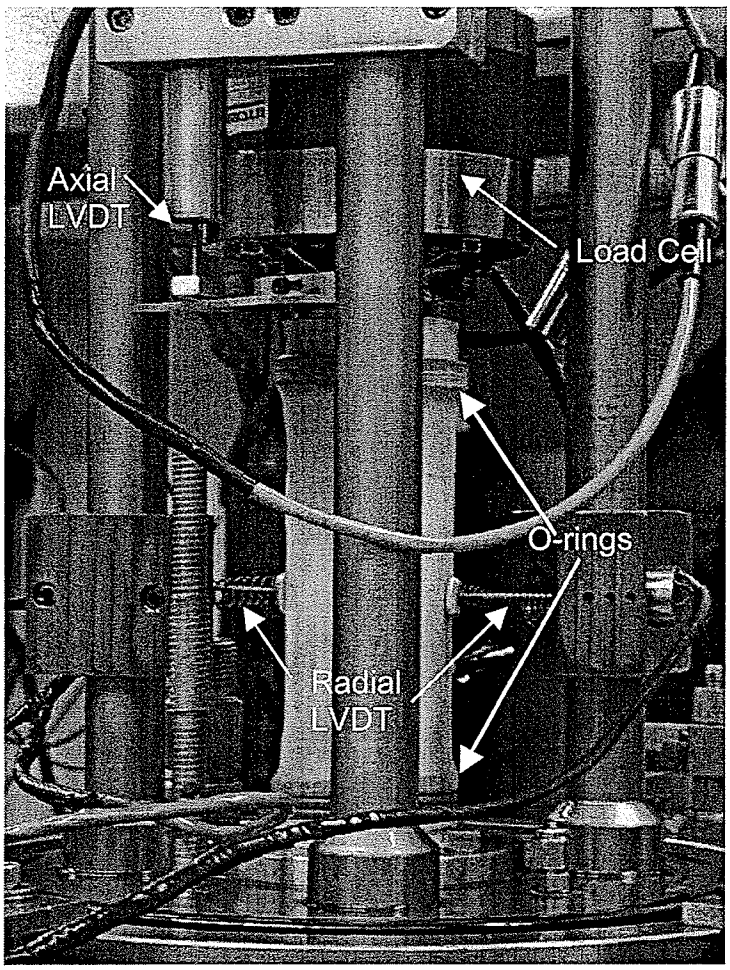

Figure 4.1 Specimen in HITEP cell

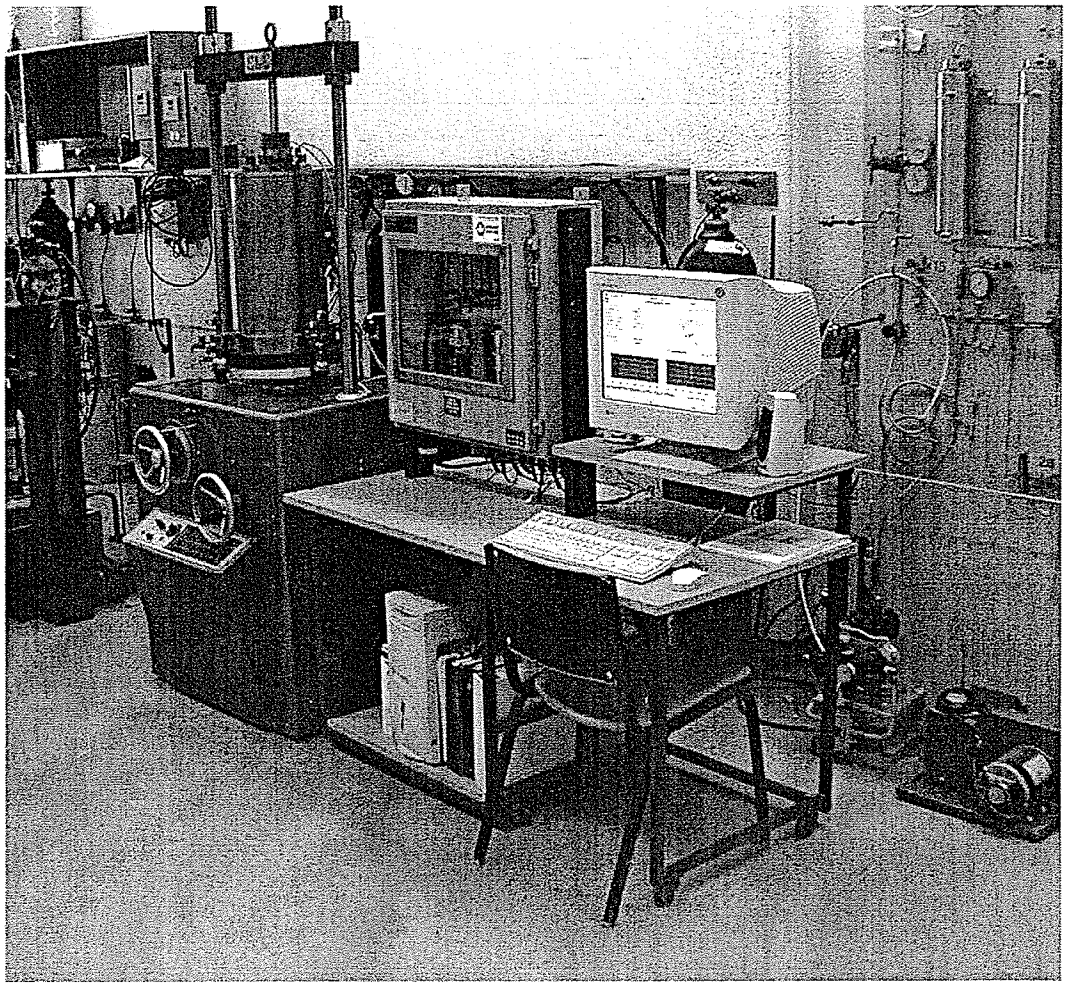

Figure 4.2 Photograph of new automated stress path triaxial testing system

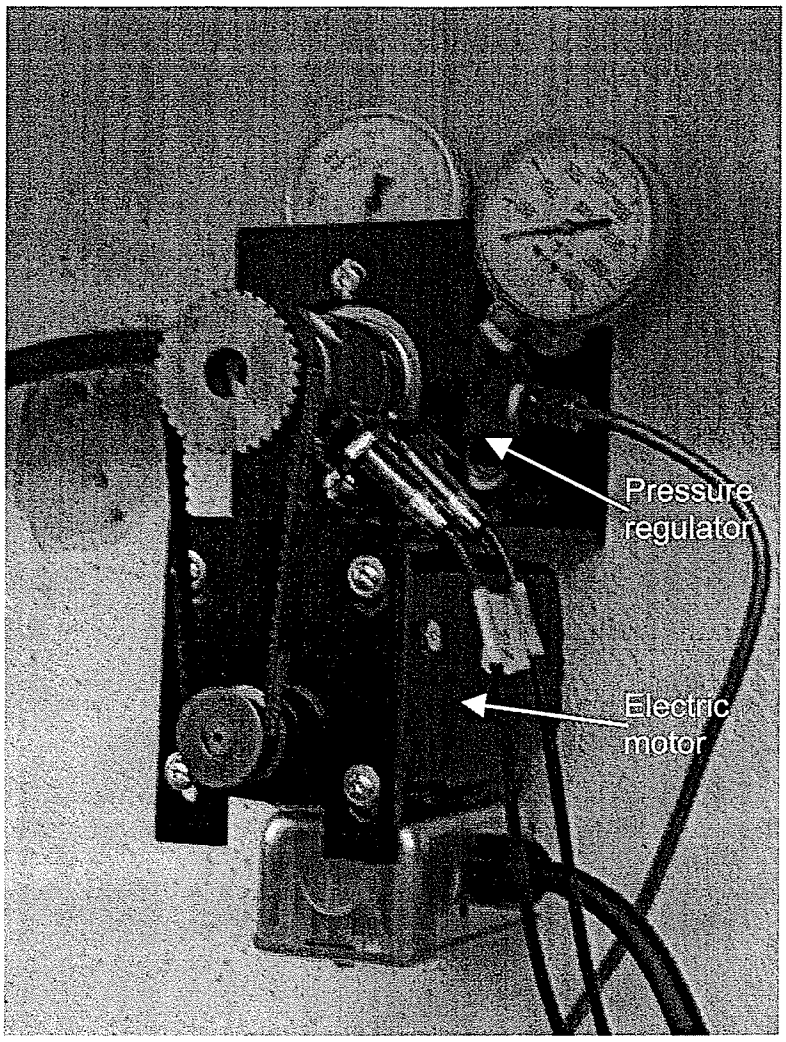

Figure 4.3 Pressure regulator and electrical motor for the new data acquisition and control system

5.0 SHRINKAGE CHARACTERISTICS OF BUFFER

5.1 Introduction

A first step in understanding the behaviour of unsaturated, compacted buffer is in understanding the behaviour of the material when subjected to changes in suction. Measurement of volume changes under conditions of no external applied stress represents a plane in p-S-V space, since p is atmospheric pressure (zero pressure). With suction and volume changes now lying on a single plane, volume change behaviour of the material can be examined using a two-dimensional plot.

This chapter presents the shrinkage characteristics of Saskatchewan and Wyoming buffers under increasing applied suctions. The results provide insight into the volume change behaviour of compacted buffers when subjected to increasing suctions. The results show that as suction increases, shrinkage also increases for both buffers, to a limiting value.

5.2 Shrinkage Tests

Five desiccators were used to produce five different values of target suction (10, 20, 40, 80, and 160 MPa) to be applied to the specimens. The concentrations of sulphuric acid used to establish the suctions were calculated using relationships outlined in Stokes and Robinson 1948. Compacted specimens were placed in the desiccators after the sulphuric acid solutions had equilibrated with the vapour pressure in the headspace (3 days). The evacuation of the desiccator headspace upon placement and removal of specimens from the desiccators is not accounted for, as these changes would be very difficult to

quantify. Specimens were removed from the desiccators after equilibration (30 days for 50 mm diameter specimens, Tang 1999) and dimensions and mass were measured manually using calipers and digital scales in the laboratory. Density, volume and water content changes were then determined from these measurements.

Specimens DA-007 to DA-021 and DA-024 to DA-038 were used in the shrinkage tests. The first set of buffer specimens (DA-007 to DA-021) was made using Wyoming bentonite while the second set of specimens (DA-024 to DA-038) used Saskatchewan bentonite. After the shrinkage tests were complete, the specimens were then used in the isotropic compression and triaxial shearing testing programs. The results of these further tests are discussed in Chapter 6.

5.2.1 Suction Environments

During equilibration in the desiccators, each specimen underwent water exchange with the sulphuric acid solution. In all cases, the initial total suctions (4 MPa) in the specimens following compaction were less than the target suctions (10 MPa and greater). This meant that during the time in the desiccator, water was drawn from specimens by the lower partial vapour pressure present in the desiccator headspace. Removing water in this way increased suctions in the specimens. Because of the constant mass environment inside the desiccator, the water drawn from the specimens resulted in an increase in the mass of water in the sulphuric acid solution. Small losses due to the opening of the lid and invasion of the headspace by atmospheric pressure were not accounted for, as it would be very difficult to quantify these losses. After the removal of specimens,

the suction level in each desiccator was recalculated, assuming that all water removed from the specimens was taken up by the sulphuric acid solution. This correction allows for the direct comparison of results between Blatz (2000) and this research. Table 5.1 summarizes the initial suctions used in the tests and how they reduced after water exchange with the specimens.

	Desiccator 1 (MPa)	Desiccator 2 (MPa)	Desiccator 3 (MPa)	Desiccator 4 (MPa)	Desiccator 5 (MPa)
Wyoming Initial	10	20	40	80	160
Wyoming Final	9.3	17.7	34.1	65.8	126.3
Saskatchewan Initial	10	20	40	80	160
Saskatchewan Final	9.6	18.5	34.5	66.1	129.7

Table 5.1 Suction in desiccators

5.3 Soil Water Characteristic Curves for Buffer

The soil water characteristic curve for each of the two buffers was developed using water content measurements of specimens placed in the target suction environments. Figure 5.1 shows the soil water characteristic curve obtained from the shrinkage tests for each buffer. Also included in the figure are results for Saskatchewan buffer from Blatz (2000) for comparison. It must be remembered that all of the specimens were compacted to RBM parameters, as were the specimens in Blatz (2000). All suctions used to plot the data have taken into account the changes in mass balance that occur between specimen and sulphuric acid solution and the resulting reduction in suction, using the final

value of suction after all specimens have been removed from the desiccator. When suction is reported in any of the figures in this document, it is total suction that is being reported. When osmotic or matric suction is being presented, this will be explicitly indicated in the figure.

Figure 5.1 illustrates that as suction increases, the water content decreases. The soil water characteristic curve for the Saskatchewan buffer coincides very well with the one presented by Blatz (2000). There are only small differences between the soil water characteristic curves for Saskatchewan and Wyoming buffer. The Wyoming buffer has higher water contents than the Saskatchewan buffer at the same suction level for water contents greater than ~7%.

5.3.1 A Simple Mathematical Model for the SWCC

Due to the difficulty in direct measurement of suction, it is common practice to obtain water contents of soils in the field but not the corresponding suction. The suction in the soil is very important since it is the suction that generates volume change in the soil and affects both the strength and the compressibility. In order to understand the volume changes that are associated with suction changes, the changes in water content must also be considered. To do this, a mathematical formulation that relates water content to suction (known as the SWCC) must be developed.

A mathematical function has been fitted to each of the soil water characteristic curves shown in Figure 5.1 for each of the buffers. A best-fit exponential decay function was fitted to the experimental results. The resulting

equation relates total suction to water content over the suction range examined in this research. The equation for the Saskatchewan buffer is:

$$S = 326.06 \exp\left(-w / 4.439\right) \qquad [5.1]$$

and the equation for the Wyoming buffer is:

$$S = 510.92 \exp\left(-w / 3.577\right) \qquad [5.2]$$

where S is the total suction in MPa and w is the gravimetric water content. These equations are valid over the suction ranges of 9.6 MPa to 129.72 MPa and 9.3 MPa to 126.25 MPa for Saskatchewan and Wyoming buffers, respectively.

These mathematical relationships allow suctions to be determined using known water contents for either Saskatchewan or Wyoming buffers, provided the suction is inside the specified ranges of suction presented in the previous paragraph. Also, these equations only apply to drying paths and not wetting paths, as they were not considered in this testing. Using the suction of the buffer, volume change behaviour can be examined for each of the buffers using the ideas and data shown in the following section.

5.4 Volume Change Behaviour

Measurement of shrinkage produced by constant suction environments was examined. After equilibration under the applied suctions, specimen dimensions were measured manually. Volume strains were inferred from multiple point measurements of diameter and length. Figure 5.2 shows the relationship between axial and radial strain components of the volume strain *versus* suction for both buffers following equilibration in the desiccators. As has been stated by previous researchers (Tang 1999 and Blatz 2000), suction is an

isotropic stress, which acts independent of direction. This figure shows that for both buffers the strain components are close to isotropic. This is of interest because during compaction, specimens were anisotropically compacted with zero lateral strain conditions. A possible explanation is that the shrinkage is dominated by microstructural volume changes in the peds instead of the macrostructural volume changes of the ped structure, which may be more anisotropic in nature (Blatz 2000). Looked at in more detail, Figure 5.2 shows that radial strains are slightly larger than the axial strains in both buffers. Also, the Wyoming buffer experienced larger strains at comparable suctions than the Saskatchewan buffer.

Volumetric shrinkage curves of both buffer materials are shown in Figure 5.3 (volumetric strain has been calculated from $\varepsilon_v = \varepsilon_a + 2\varepsilon_r$). Also included in the figure are data from Blatz (2000) for direct comparison of results from two separate researchers for Saskatchewan buffer. As shown on Figure 5.3, as the suction increases, the measured volumetric shrinkage also increases to an apparent upper limit for both buffers. The Saskatchewan buffer shows a limit of approximately 8% volume strain while the Wyoming buffer shows a limit of approximately 10% volume strain. There is a small difference between the author's data for Saskatchewan buffer and the results from Blatz (2000). This may be attributed to the sand that was used in the two separate test programs, as the difference in limiting volume strain is approximately 1%. Although the sand blends in both programs followed and satisfied the specifications outlined in Chapter 3 (Figure 3.1), slight differences in the grain

size distribution may have generated enough difference in the sand component of the buffer to produce slight differences in limiting shrinkage.

The shrinkage results in Figure 5.3 are consistent with the soil water characteristic curves in Figure 5.1 for water contents greater than ~7%. At the same suction level, slightly more water is removed from the Wyoming buffer resulting in slightly greater shrinkage as compared to the Saskatchewan buffer. This however is somewhat counter-intuitive since the activity of the Wyoming bentonite is much higher than the Saskatchewan bentonite according to the Atterberg Limits. The slight differences may not be statistically significant considering the experimental precision and close groupings of Saskatchewan and Wyoming buffer data points. In all cases, the water content of each specimen was far below the plastic limit, (w_p ~ 45%), which were almost the same for both types of bentonite. It appears that at low water contents the two bentonites behave in a similar fashion whereas at higher water contents, above the plastic limit, the bentonites may behave less similarly.

The limit of measured volumetric shrinkage (not the shrinkage limit, which is an Atterberg Limit and is expressed as a water content) is reached at approximately 30 MPa suction in both the Saskatchewan and Wyoming buffers (Figure 5.3). It is postulated that shrinkage at the 30 to 40 MPa level is inhibited through transfer of stresses from the clay phase to the sand phase of the material. Initially the buffer material behaviour is dominated by clay with sand in the matrix. As the clay component shrinks under increased suctions it is postulated that the bulk volumetric shrinkage occurs in the clay until the sand

dominates the behaviour. This is noted in Figure 5.3 as the sharp non-linearity, drawn by hand, that occurs at approximately 8 to 10 % strain. Further increases in suction no longer increase the (compressive) volumetric straining of the buffer. However, the water content will continue to decrease as water is pulled from the clay, which can still shrink in the spaces provided by the sand skeleton. This hypothesis cannot be verified with the experimental data gathered in this program. Further work is required to explore this by testing specimens of pure bentonite to compare its volumetric shrinkage limit with that of the buffer mixture. This concept is important for modeling, as two separate soil models (one for the clay behaviour and one for the sand behaviour) may be required to describe the full range of behaviour of the buffer as volumetric strains occur.

Figure 5.4 shows changes in bulk and dry density under applied suction conditions. Also included in the figure are data from Blatz (2000). The Saskatchewan and Wyoming buffer again show similar behaviour. As suction increases so does the dry density to an apparent limit of approximately 1.8 Mg/m^3, which is reached around 30 MPa. This density coincides with the suction at the limit of measured volumetric shrinkage. This behaviour is consistent with the sand grains being brought into contact. Increases in dry density would indicate that shrinkage is taking place. Once 30 MPa is reached, shrinkage and hence increases in dry density stop. The bulk density is shown to remain relatively constant (about 2.0 Mg/m^3) at suctions less than 30 MPa, it then decreases with further increases in suction. At suctions less than 30 MPa the constant bulk density represents a loss in water content that is being

counteracted by a gain in dry density. After 30 MPa, the bulk density decreases because water is still being drawn from the specimens while there is very limited volumetric shrinkage. The bulk and dry density will eventually become equal when suction is high enough to remove all of the free water.

An important component of this testing series is the examination of volume changes as a function of suction when total stress is held constant. As stated earlier, this condition represents a plane in the p-S-V volume state space. Figure 5.5 shows the specific volume data plotted against suction after equilibration in the desiccators. Included in the figure are results from Blatz (2000) for Saskatchewan buffer. This figure again shows similarities in behaviour between the two programs on Saskatchewan buffer. The Wyoming buffer tends to behave in a similar fashion. As shown by the shrinkage curves in Figure 5.3, Wyoming buffer tended to shrink slightly more than Saskatchewan buffer at comparable suction levels. As expected, the specific volume of the Wyoming buffer is also slightly lower than the Saskatchewan buffer at similar suctions. As suction increases the specific volume decreases until approximately 30 MPa suction, after which, the specific volume remains close to constant. This once again is as expected, since at approximately 30 MPa the measured shrinkage (Figure 5.3) has almost, if not completely, stopped. Therefore, changes in specific volume should also stop at this point.

5.5 Summary of Shrinkage Characteristics

Previous sections of this chapter have presented volume change behaviour of two buffers compacted to RBM parameters and then subjected to

drying conditions. The results can be used to provide a simplified representation of the volume state surface in p-S-V space at zero total mean stress (atmospheric pressure). These results help in the interpretation of the behaviour of buffer when subjected to isotropic and triaxial shear conditions, since the initial volume state of the materials can be defined by their suction, water content and associated shrinkage.

The Saskatchewan and Wyoming buffers were found to have slightly different behaviour under increased suction loading. This however may not be the case at higher water contents (lower suctions). Higher water contents result in more water being available to the montmorillonite minerals in the buffer. This could result in observed differences in behaviour between the two buffers as would be suggested by the Atterberg Limits of the two constituent bentonites (Chapter 3). Also, the occurrence of a possible transition between clay dominated behaviour and sand dominated behaviour has been postulated. It has been associated with an apparent limit to volume shrinkage that occurs at approximately 30 MPa suction. Further evidence that potentially supports this assumption will be presented in Chapters 6 and 8.

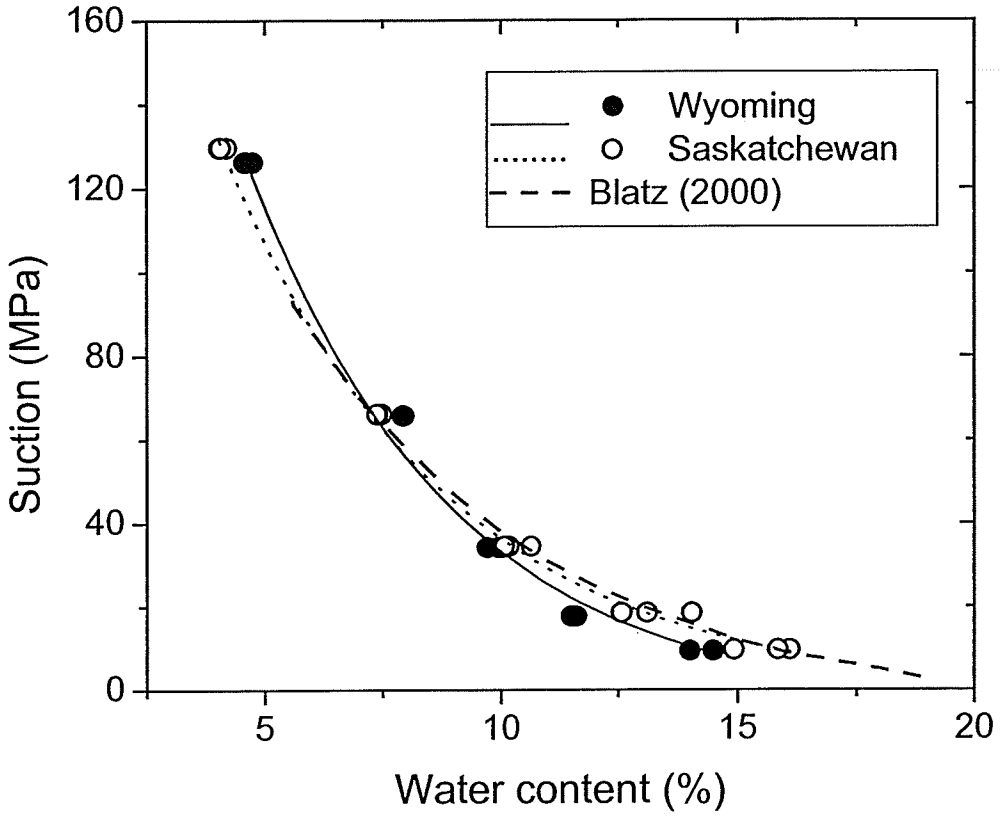

Figure 5.1 SWCC for Saskatchewan and Wyoming buffers

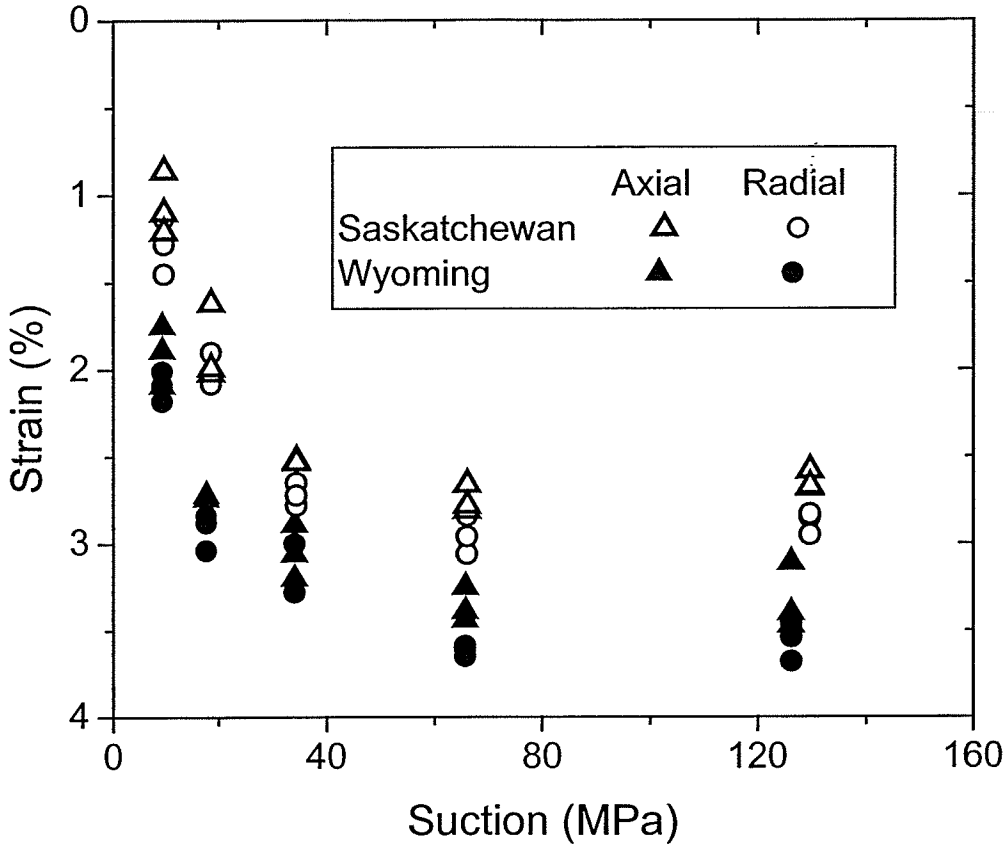

Figure 5.2 Axial and radial strain components produced after suction equilibration

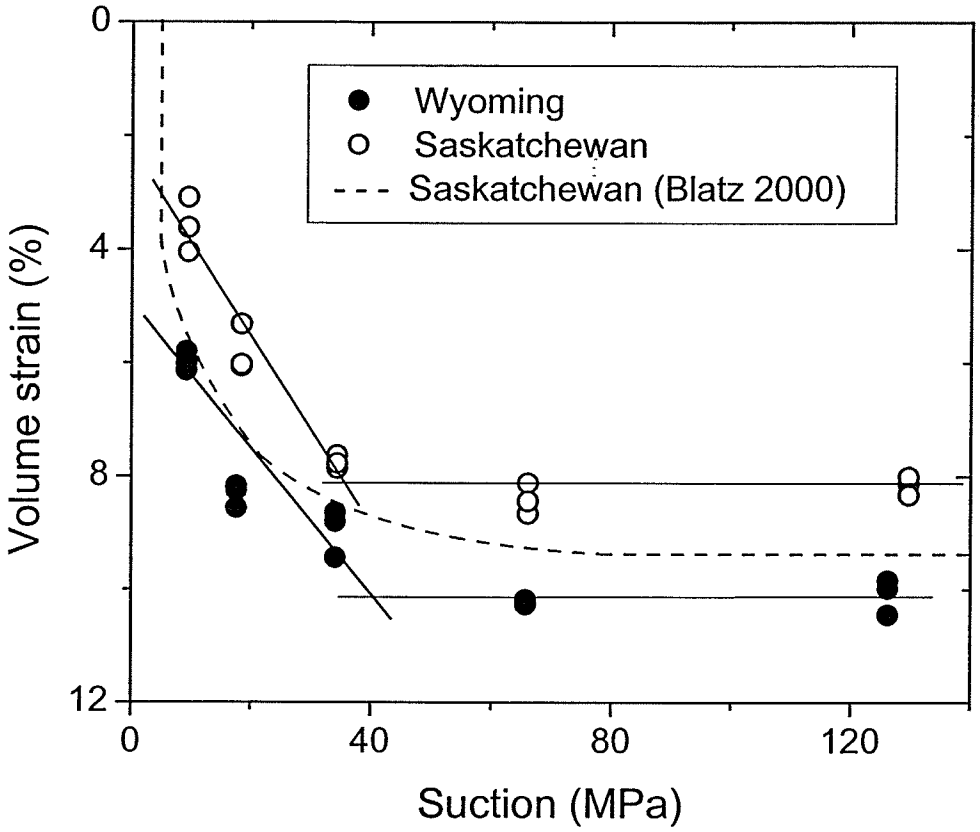

Figure 5.3 Shrinkage curves for Saskatchewan and Wyoming buffers

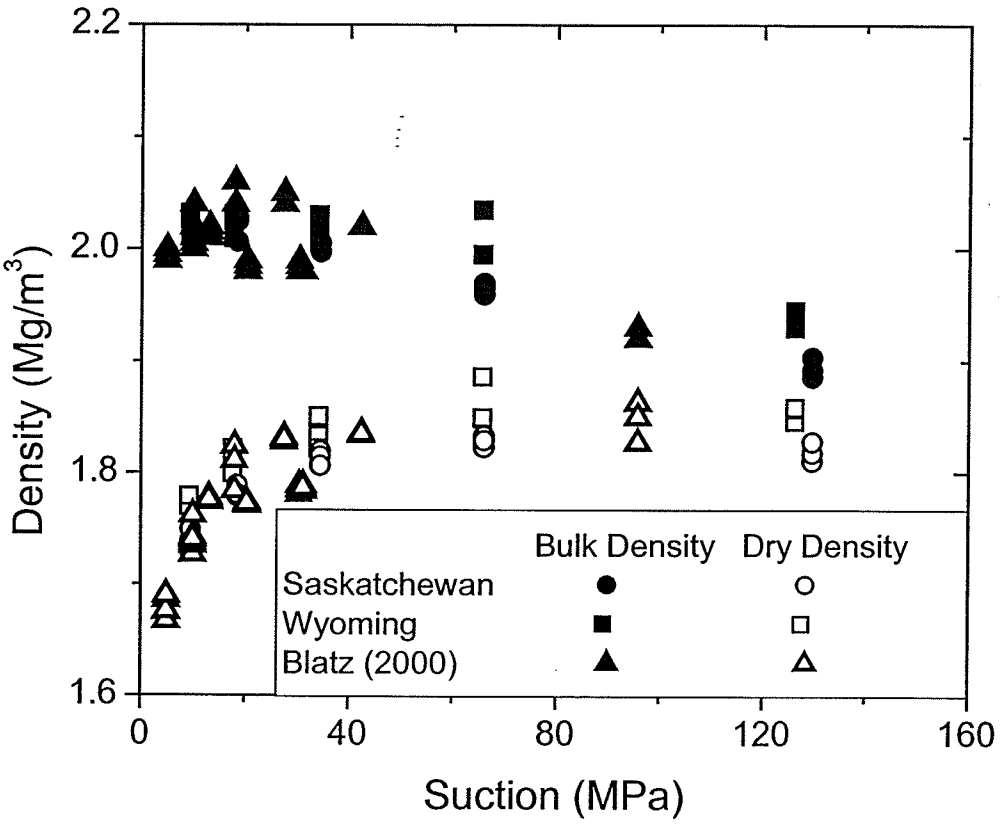

Figure 5.4 Bulk and dry density of Saskatchewan and Wyoming buffers

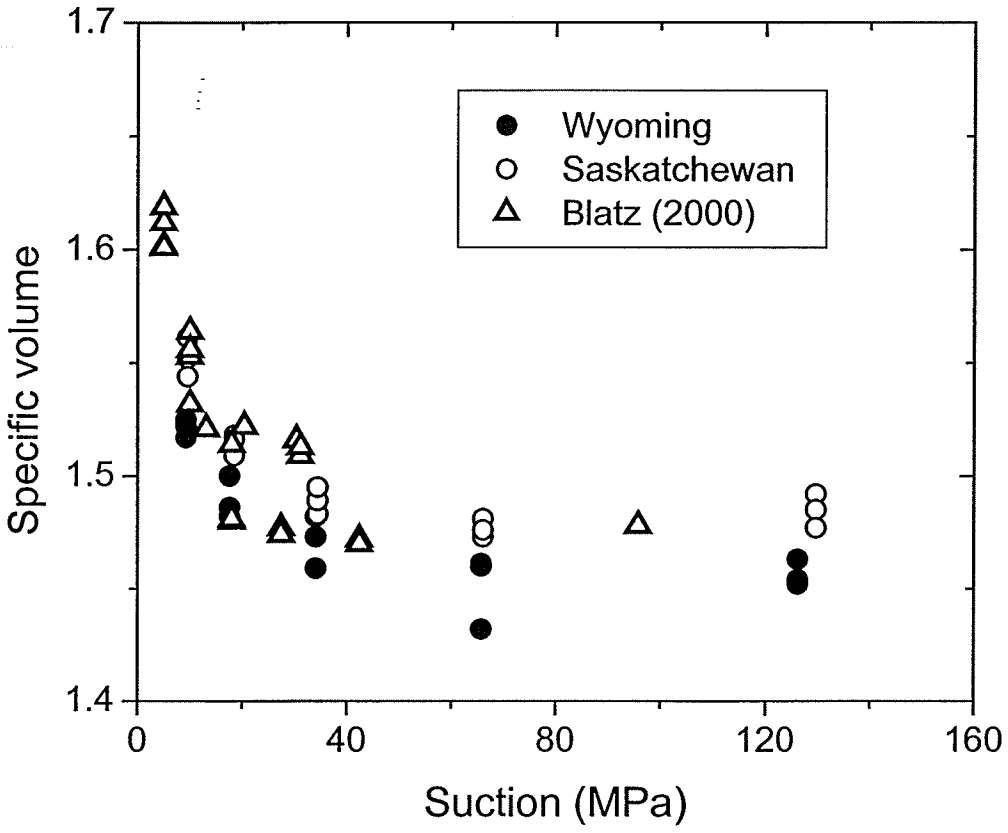

Figure 5.5 Specific volumes for Saskatchewan and Wyoming buffers

6.0 ISOTROPIC COMPRESSION AND TRIAXIAL SHEAR TEST RESULTS

6.1 Introduction

This chapter presents results of isotropic compression and triaxial shear testing on two buffers compacted to RBM parameters (Chapter 3) and subsequently dried to different suction levels. Stresses and strains are recorded continuously throughout both testing programs. These testing programs utilized new testing equipment (Chapter 4) that controls the cell pressure to achieve a desired stress path (q-p space) during both isotropic compression and triaxial shear. During all phases of testing, suction was not measured but instead was inferred from known initial suctions (after removal from desiccator) and previously measured suction *versus* pressure relationships. The generalized stress paths are limited to the triaxial stress space and a calculated value of suction. These results provide valuable insight into the behaviour of unsaturated buffers at various suction levels.

6.2 Measurement of Yielding

A major consideration in defining the behaviour of a material is the determination of the point at which yielding occurs. A material can yield under a number of different forms of loading (tests). For instance, isotropic compression, triaxial shearing or suction loading can each cause yielding to occur in soil depending on the past history and properties of a particular specimen. Strains that occur after yielding, result in permanent deformation of the material, meaning the strains can not be recovered upon unloading. As yielding is observed in response to different types of loading, plots of these yield points can

be used to generate yield envelopes and in three dimensional space, yield surfaces. With the use of these envelopes (or surfaces) and the observed behaviour of the material, numerical modeling can be used to predict behaviour when the material is subjected to different types of loading conditions.

This research project involved investigation of two forms of yielding in compacted buffers. The first form is yielding due to isotropic loading and the second form is yielding due to triaxial shear. Results of these tests provide an improved understanding of the behaviour and more specifically yielding of compacted buffers.

6.3 Isotropic Compression

The initial compaction of buffer develops an initial yield state related to the microstructure of the compacted material. This initial yield state as defined by Alonso *et al.* (1990) is represented by a curve called the Load Yield (LY) curve (Figure 2.3 (a)). This LY curve represents the boundary between elastic (recoverable) and plastic (non-recoverable) behaviour for total mean stress increments. Loading to this boundary is associated with elastic straining of the material. Once the boundary is reached, plastic straining (with an elastic strain component) and expansion of the elastic region begins or contraction of the boundary surface for strain softening materials.

Isotropic compression tests were begun after the specimens had equilibrated in the shrinkage testing component of this research. Specimens used were DA-007 to DA-021 (Wyoming buffer) and DA-024 to DA-038 (Saskatchewan buffer). After equilibration in the desiccators, each specimen

was placed into the high pressure, high temperature (HITEP) triaxial cell following manual measurements of the dimensions and mass. The isotropic loading paths were selected to evaluate compressibility, strength and yield characteristics for specimens at target suction levels of 10, 20, 40, 80, and 160 MPa.

Specimens were initially compressed using selected cell pressure increments up to a maximum value of 5 MPa (with the exception of the three specimens loaded to 6 MPa previously discussed). The cell pressure increments were applied every 24 hours to ensure suction and volume change equilibration between increments (Blatz 2000). Figure 6.1 shows a typical plot of volume strain versus time during the isotropic compression and unloading phases of DA-011 (Wyoming buffer) at 160 MPa target suction. The vertical portions of the figure show the times that the cell pressure was either increased or decreased.

No drainage was permitted from specimens during compression. The tests are therefore referred to as "constant mass" tests. Although no drainage is permitted, there is a change in suction associated with isotropic compression of the air phase. Changes in suction during the testing can be followed using a relationship with the slope of $\Delta S/\Delta p = -0.83$, where ΔS = change in suction and Δp = change in mean stress, as shown in Tang et al. (1997) and Blatz and Graham (2003). These two references also outline that upon removal of Δp, suction was recovered, that is that the decrease in suction due to compression is an "elastic" relationship. Table 6.1 lists the calculated suctions in each specimen

(1) before isotropic compression, (2) at the initial load yield (p_y), (3) after isotropic compression (p_c), and (4) after isotropic unloading (p_{ul}).

Applying the relationship, $\Delta S/\Delta p = -0.83$, to the experimental results obtained in this testing program is questionable. This is because the measurement of suctions has previously been limited to the range from 2 MPa to 8 MPa (Tang *et al.* 1997 and Blatz 2000). It must be remembered that the lowest suction applied to the specimens, even after the reduction of suctions due to the mass balance consideration in the desiccator, was 9.3 MPa as shown in Table 6.1. The previous chapter showed major changes in physical behaviour were associated with a suction of about 30 MPa. However, the author has assumed that there will be decreases in suction during compression that follow the relationship $\Delta S = -0.83\ \Delta p$. At high suctions, the adjustment relationship may be different. Checking the relationship requires instruments that can measure high suctions and their reaction to increasing and decreasing compressive loads. The validity of applying this relationship to these high suction materials beyond that which has been quantitatively assessed in previous programs is yet to be confirmed.

Figures 6.2 through 6.6 illustrate volume strain (at 24 hrs) versus logarithm of total mean stress for Saskatchewan and Wyoming buffer specimens at target suction levels of 10, 20, 40, 80, and 160 MPa. (Note that calculated suction levels have been shown in Table 6.1 for all stages of the isotropic compression tests. For purposes of comparing similar specimens, target suction levels have been used in the text (as opposed to final suctions) for clarity.) As

mentioned earlier, the loading path during isotropic compression has been assumed to follow $\Delta S/\Delta p = -0.83$ and is not along a constant suction trace in p-S space.

Figures 6.2 through 6.6 indicate that the behaviour under initial loading was stiff. This stiff initial behaviour was followed by less stiff behaviour beyond a yield stress (or load yield (LY) pressure) (p_y). Definition of the yield stress (values estimated by the Casagrande construction technique) is much more apparent at the lower suction levels as compared to the higher suction levels. As expected, the response to unloading following loading to the maximum mean stress value (5 MPa) for both buffers was stiff with a slope that was comparable (though slightly stiffer) to the slope of the initial loading portion of the curve.

Figure 6.7 summarizes results from the Wyoming specimens at each target suction. The data indicate increases in stiffness in both the pre-yield and post-yield regions of behaviour due to increased suction. Figure 6.8 shows similar relationships for the Saskatchewan buffer. Again the notable increase in stiffness of the material behaviour at higher suctions is apparent. This increased stiffness at higher suctions is attributed to the fact that after the shrinkage phase, specimens at suction levels higher than 30 MPa are likely to behave as a sand-dominated material. As such, the stiffness of the response to isotropic loading can be expected to produce results that have been observed.

Values of compression index for first-time compression, including the initial stiff portions and normally consolidated regions were measured from the experimental data. The term normally consolidated is used in the text to refer to

the plastic hardening that occurs upon further loading beyond the initial yield stress. Table 6.2 gives values for the κ_i, λ, and κ_u, along with the load yield (p_y). Figure 6.9 shows the type of models from which these isotropic parameters were obtained. The data in the table show that as the suction increases in the specimens, so does the load yield pressure. This indicates that specimens have a stiffer initial response to loading, which corresponds to a larger zone of elastic behaviour. The data also show that at the same pressure level, the Wyoming buffer exhibited consistently higher volume strains, indicating that the mixture is more compressible than Saskatchewan buffer.

Figures 6.10 and 6.11 show measured κ - and λ - values as a function of suction, respectively. Also included on Figure 6.11 are the results from tests on "Frac" sand by Ferris (2000) that show average end-of-test λ - values of 0.03. This result is consistent with the λ - values measured for the Saskatchewan buffer specimens at suctions higher than the suction at the limiting volumetric shrinkage (~30 MPa) where the sand is believed to be the dominant load-resisting component of the mixture. This result supports the earlier hypothesis that the buffer behaves differently depending on the suction present in the material, and behaves largely as a sand during isotropic compression at suctions greater than 30 MPa.

Figure 6.12 shows the relationship between load yield pressure and suction for all specimens, with a line drawn by hand to fit the data. This figure shows that load yield pressures initially increase noticeably with increases in suction. Above approximately 30 MPa, the load yield pressures increase at a

much slower rate for both buffers. This again is believed to be related to the limit of volumetric shrinkage that brings the sand grains into contact with each other so that they dominate the behaviour of the buffers. Figure 6.13 shows the average load yield pressure (at each target suction) against suction, with lines to fit the data drawn by hand. To help define the LY curve for Saskatchewan buffer, Figure 6.13 also includes data at lower suctions than tested in this program from Blatz (2000). The suctions that are used to plot the data on Figures 6.12 and 6.13 include the adjustment due to compression $\Delta S/\Delta p = -0.83$. In previous work (Blatz 2000 and Blatz and Graham 2003), the LY curve was modeled using a straight-line relationship but it was noted that the load yield appeared to be increasing at a decreasing rate with suction increase. Including the data from the testing series reported in this thesis show that the LY curve is better defined by a non-linear or a bi-linear relationship rather than a straight-line. The data also support Blatz and Graham (2003) observation that the load yield appeared to increase at a decreasing rate with high, increasing suctions.

6.4 Triaxial Shearing

Triaxial shearing was undertaken at a constant axial deformation rate of 0.0139 mm/min, which resulted in shearing specimens to 20% axial strain in approximately 24 hours. During shearing, the cell pressure was adjusted to maintain the target (q/p) stress path specified. The shearing rate was determined to ensure that suction throughout the specimens was constant during shearing (Blatz *et al.* 1999) but suction may not be constant along the shear plane. The triaxial shear tests were done on specimens after the end of the

isotropic compression testing. Specimens used were DA-007 to DA-021 (Wyoming buffer) and DA-024 to DA-038 (Saskatchewan buffer). Table 6.3 lists the calculated suctions in each specimen (1) before triaxial shearing took place (S_{is}), (2) at the shear load yield (S_y), (3) at the peak shear value (S_{peak}), and (4) at the end of test (S_{eot}). Suctions were calculated again using the initial suction and the relationship $\Delta S/\Delta p = -0.83$.

6.4.1 Strength of Saskatchewan and Wyoming Buffer

Figures 6.14 through 6.18 show the stress paths that were followed in q-p space during shearing for both Saskatchewan and Wyoming buffers at their target suctions. (Target suctions are used once again in the text. For calculated suctions during shearing refer to Table 6.3). Peak and end-of-test values of q and p can be observed on these plots. The plots in q-p space show that significant strain softening occurs after specimens have reached peak shear strength along each of the stress paths. Figure 6.19(a) shows a typical brittle mode of failure that was observed after shearing along one of these two stress paths. This mode of failure indicates a brittle failure where a well-defined failure plane is developed. When the two parts of these brittle specimens were separated, the failure planes had striations and grooves that indicated the direction of movement during shearing.

Specimens that were sheared along a 1:1 stress path produced a ductile mode of failure as shown for example in Figure 6.19(b). Here, the specimens do not develop well-defined failure planes. Instead a region of bulging or barreling is noted, along with some shear distortions.

At high suction levels, modifications had to be made to the stress path control for the 1:1 stress path because the cell pressures required to maintain the selected shearing path could not be reached with the available equipment. If, during shearing along a 1:1 stress path, the cell pressure reached 5 MPa, the (1:1) stress path was terminated and shearing continued along a triaxial path of q/p = 3/1 (that is holding the cell pressure constant) during the rest of the shearing phase. Examples of the resulting stress paths are shown in Figures 6.14 through 6.18.

Table 6.4 summarizes the parameters (q_{yield}, p_{yield}, q_{peak}, p_{peak}, q_{eot}, and p_{eot}) for the triaxial shearing stage of the testing. The table allows direct comparisons between the two different buffers. As expected, the data show that the yield, peak and end-of-test stress values depend on the stress path followed during shearing. The 3:-1 stress path produced the lowest stress values and the 1:1 stress paths produced the highest stress values at each suction level. This behaviour is seen in both buffers.

Figures 6.20 through 6.24 show typical stress-strain curves for Saskatchewan and Wyoming specimens sheared at different target suction levels. The stress paths corresponding to each stress-strain curve are indicated in the legend of the figures. The stress-strain behaviour for both materials generally shows an initial stiff behaviour followed by a distinct peak shear stress followed by varying degrees of strain softening to the end-of-test shear strength. As mentioned earlier, the stress-strain plots indicate that less brittle (more ductile) behaviour was observed for specimens sheared along the

1:1 stress paths. This less brittle behaviour has been attributed earlier to the fact that these specimens were sheared along a stress path that results in a more ductile failure.

Another key point to note is that some specimens do not appear to reach a critical state condition (i.e. steady state) by the end of the test even after approximately 20% shear strain. That is, stress-strain curves continue to slope downwards at the end of the test (Figures 6.20 through 6.24). This can perhaps be attributed to the measurement of axial and radial deformations at only a limited number of points during shearing on these specimens. Development of a well defined failure plane during triaxial shearing, results in specimens acting as two separate "wedges" (Figure 6.19(b)). Measuring the displacement of these two separate "wedges" is difficult because the orientation the failure plane can not be controlled and the measurement points are at fixed locations. If the measurement points do not occur on the proper location on the specimen upon development of the failure plane, part of the displacement could be missed. This could result in the critical state condition not being observed in the measurements, while in fact, the specimens may be reaching critical state.

6.4.2 Stiffness of Saskatchewan and Wyoming Buffer

Stiffness is another important property for describing the engineering behaviour of buffer. The stiffness is defined as the constitutive parameter that describes the relationship between strain and applied stress. In the case of this testing program, two stiffness moduli were examined. Both are secant modulus values measured from the beginning of shearing. The first is a secant modulus

measured to 1% strain ($E_{1\%}$) and the second measures the stiffness to the strain corresponding to 50% of the peak deviator stress ($E_{50\%}$).

Figure 6.25 shows a plot of $E_{1\%}$ against initial suction for all the specimens that were tested. Also included are the $E_{1\%}$ values from Blatz (2000) from quick undrained and controlled suction tests. The moduli calculated from the controlled suction tests represent values that are obtained under drained conditions because of the suction control during testing. At lower suctions, the $E_{1\%}$ values correspond very well between all tests and buffers. However at a suction of approximately 30 MPa a distinct scatter is noticed in the $E_{1\%}$ values obtained from this testing program. This is associated with the stress path along which specimens were sheared.

Figure 6.26 shows the same data but this time groups the data from this testing program by the stress paths followed, with lines fit to the data drawn by hand. This shows that the data for each stress path tend to lie along a curve with the 3:-1 stress path having the lowest $E_{1\%}$ value and the constant-p and 1:1 stress paths having higher values. These figures (6.25 and 6.26) also show the slightly less stiff behaviour of the Wyoming buffer specimens (lower modulus value) as compared to the Saskatchewan buffer specimens at comparable suction values. As usual with this level of instrumentation, there is a fair amount of scatter in the stiffness data.

A better description of the stiffness must also consider how well the modulus fits the initial portion of the stress-strain curve prior to yield. In some cases, such as along 3:-1 stress path, a value of 50% peak deviator stress in

reached before 1% strain. This leads to $E_{50\%}$ fitting the initial stiffness of the material better than $E_{1\%}$. In most cases along the 1:1 stress path, both the $E_{1\%}$ and $E_{50\%}$ values produce similar values. This is because along this stress path, 1% strain and 50% of the peak deviator stress are reached at almost the same stage during the test.

The modulus values (either $E_{1\%}$ or $E_{50\%}$) that are reached first during shearing along each stress path for Saskatchewan and Wyoming buffers are plotted on figures 6.24 through 6.28, respectively, with lines drawn to fit the data by hand. The 3:-1 stress path produces modulus values that are the lowest in figure 6.26 and the 1:1 stress paths provide the highest modulus values. This occurs because along all of the stress paths the mean stress, hence the cell pressure are being adjusted during shearing to maintain the target stress paths. Thus the cell pressure (σ_3) is affecting the stiffness of the buffers. Since, the stiffness relates the stress to the strain, and the modulus in this case uses an axial stress (σ_1) and relates it to an axial strain (ε_1), a component of the radial stress (σ_3) and the radial strain (ε_3) through the Poisson's ratio (ν), is affecting the stiffness. Along the 1:1 stress path when the mean stress (cell pressure) is being increased, these increases result in a compression of the specimens sheared along this stress path. This compression results in an increased strength, expansion of the elastic region, and a "ductile" failure of these specimens. This also happens along the other two stress paths, except that the mean stress (cell pressure) is decreased to maintain paths, which results in a brittle failure of these specimens.

When buffer specimens are dried in the desiccators, they become denser as the applied suction compresses or shrinks the material to an apparent limit of dry density (discussed in Chapter 5). The effect of density on the strength of the buffers has not been examined in detail, but Blatz (2000) raised the question of what is an appropriate way to separate the effects of density and suction on behaviour. To do this, a ratio of yield, peak and end-of-test deviator stresses during shearing to dry unit weight after equilibration in the desiccator were calculated. These values are plotted *versus* suction on Figures 6.29 through 6.31, with lines fit to the data, which are drawn by hand. The data for each stress path that was followed during triaxial shearing are plotted. Suction values are adjusted using $\Delta S/\Delta p = -0.83$. These figures show that with suction the ratio (q/γ_{dry}) increases. After a suction of approximately 30 MPa the ratio values increase at a decreasing rate. This suggests that density has a smaller effect on strength than suction at high suctions ($S > 30$ MPa). Also, the ratio values along the constant-p and 3:-1 stress paths remain fairly constant between yield, peak and end-of-test values, while the ratio values from the 1:1 stress path increase from yield to peak and then decrease to the end-of-test values.

6.4.3 Yielding in Shear

The interpretation of yielding during shear used a number of plots to establish the yield points along the three different stress paths in the program. Plots in p-V space were used to interpret yielding along the 1:1 and 3:-1 stress paths. For constant-p stress paths, plots in q-V space were used.

Figures 6.32 through 6.41 show plots of specific volume versus logarithm (total mean stress) for both types of buffer along the 1:1 stress paths. These figures illustrate the specific volume (and volume strains) for all stages of the isotropic compression and unloading followed by shearing of each specimen.

The specific volume response under the shear-loading phase of the testing is of particular interest. Both buffers show similar behaviour along the 1:1 shearing stress paths. During initial shear loading, specimens generally follow a line similar in slope to the unload relationship from isotropic compression. Once the stress path takes the specimens to a point where the maximum cell pressure during isotropic compression is reached, the relationship shows a yield due to shear loading at approximately this point as well. After this yield, the specimens continue along a line similar in slope to the normally consolidated (plastic hardening) line under isotropic compression. This continues until the stress path reaches the peak in q-p space, which corresponds to the lowest specific volume in log p-V space. It is this point that becomes the new (modified) p_c for specimens along this stress path. With continued shear loading, specimens dilate, which is shown by the almost vertical line on the figures to the end-of-test conditions.

Figures 6.42 through 6.51 show plots of specific volume versus logarithm (total mean stress) for both types of buffer along 3:-1 stress paths. These figures once again illustrate the specific volume (and volume strains) for all stages of the isotropic compression and unloading followed by shearing of each specimen. Once again during initial shear loading, both buffers follow a line similar in slope

to the unload relationship during isotropic unloading. In this case, specimens initially decrease in mean stress to a point when yield is reached. Following this, there is a marked increase in the volume (near vertical line) of the specimens, which represents dilation.

The plots used to interpret yield along constant-p stress paths are shown in Figures 6.52 through 6.61. Here, plots in q-V space are used instead of the logarithm p-V space because p remains constant and yielding can not be identified. These plots show the initial stiff response to shear loading, which continues until approximately a peak value is reached, associated with very little volume change (from 0.5% to 2% volume strain). After peak is reached, specimens soften to the end-of-test value. With shearing initially taking place in the elastic region of the state boundary surface (OCR = 2), the yield values along constant-p stress paths should be equal to the peak values along this path and this can be seen in Table 6.4.

6.5 Summary of Isotropic Compression and Triaxial Shear Results

This chapter presented the results of the isotropic compression and triaxial shear testing components of this research program. Saskatchewan and Wyoming buffers were found to behave similarly during both testing phases. The Wyoming buffer was found to compress more under isotropic loading than Saskatchewan buffer. Both buffers showed significant strain softening after a peak shear stress was reached under triaxial shear conditions. It is believed additional evidence of a transition from clay to sand dominated behaviour has been shown with the data presented in this chapter. However, testing should be

completed on specimens of pure bentonite to ensure better distinction between the clay and sand behaviour of the two buffers. Also shown is that the behaviour of the two buffers can be represented by an elastic-plastic constitutive model. This is significant because upon initial placement of the waste containers in the deep geologic repository, the buffer will behave elastically followed by plastic behaviour once the yield stress has been surpassed. The similarity in behaviour between the two buffers suggests that either buffer would be suitable for use in the deep geologic repository as proposed by AECL.

Wyoming Buffer					Saskatchewan Buffer				
Sample	S_i (MPa)	$S_{@Py}$ (MPa)	$S_{@Pc}$ (MPa)	$S_{@Pul}$ (MPa)	Sample	S_i (MPa)	$S_{@Py}$ (MPa)	$S_{@Pc}$ (MPa)	$S_{@Pul}$ (MPa)
DA-007	9.3	7.9	5.1	7.2	DA-024	9.6	8.1	5.5	7.5
DA-008	9.3	7.8	5.1	7.2	DA-025	9.6	7.9	5.5	7.6
DA-009	9.3	7.8	5.0	7.2	DA-026	9.6	7.8	5.5	7.5
DA-016	17.7	15.6	13.5	15.6	DA-033	18.5	16.1	14.3	16.4
DA-017	17.7	15.8	13.8	15.7	DA-034	18.5	16.2	14.4	16.4
DA-018	17.7	15.7	13.5	15.6	DA-035	18.5	16.3	14.4	16.4
DA-013	34.1	31.4	30.0	32.0	DA-030	34.5	32.5	30.3	32.4
DA-014	34.1	31.5	30.0	32.0	DA-031	34.5	31.9	30.3	32.4
DA-015	34.1	31.5	29.9	32.0	DA-032	34.5	32.1	30.3	32.4
DA-019	65.8	63.4	61.6	63.7	DA-036	66.1	63.7	62.0	64.0
DA-020	65.8	63.3	61.6	63.7	DA-037	66.1	63.8	62.0	64.0
DA-021	65.8	63.4	61.6	63.7	DA-038	66.1	63.6	62.0	64.0
DA-010	126.3	122.7	121.3	123.8	DA-027	129.7	127.5	125.6	127.6
DA-011	126.3	123.0	121.3	123.8	DA-028	129.7	127.0	125.6	127.6
DA-012	126.3	123.0	121.3	123.8	DA-029	129.7	127.2	125.6	127.6

Table 6.1 Suctions before, during and after isotropic compression

Sample	S_{target} (MPa)	$w.c._i$ (%)	p_y (MPa)	κ_i	λ	κ_u
Wyoming buffer						
DA-007	10	14.49	1.3	0.009	0.068	0.001
DA-008	10	14.50	1.5	0.007	0.082	0.001
DA-009	10	14.00	1.5	0.009	0.080	0.001
DA-016	20	11.63	2.5	0.007	0.074	0.003
DA-017	20	11.51	2.3	0.008	0.059	0.004
DA-018	20	11.57	2.4	0.009	0.080	0.003
DA-013	40	9.95	3.1	0.004	0.063	0.001
DA-014	40	10.04	3.0	0.013	0.076	0.007
DA-015	40	9.72	3.0	0.011	0.058	0.003
DA-019	80	7.92	3.1	0.012	0.054	0.010
DA-020	80	7.93	3.2	0.014	0.040	0.006
DA-021	80	7.95	3.1	0.012	0.031	0.006
DA-010	160	4.57	4.0	0.007	0.071	0.007
DA-011	160	4.75	3.6	0.013	0.055	0.004
DA-012	160	4.61	3.6	0.009	0.042	0.003
Saskatchewan buffer						
DA-024	10	16.10	1.8	0.006	0.081	0.001
DA-025	10	15.85	2.0	0.011	0.089	0.006
DA-026	10	14.93	2.2	0.006	0.071	0.003
DA-033	20	14.04	2.9	0.012	0.090	0.006
DA-034	20	13.11	2.8	0.020	0.073	0.006
DA-035	20	12.58	2.7	0.014	0.053	0.006
DA-030	40	10.18	2.6	0.002	0.028	0.006
DA-031	40	10.08	3.1	0.004	0.022	0.004
DA-032	40	10.66	2.8	0.012	0.042	0.007
DA-036	80	7.49	2.9	0.008	0.027	0.004
DA-037	80	7.40	2.8	0.013	0.031	0.007
DA-038	80	7.38	3.0	0.015	0.034	0.007
DA-027	160	4.20	2.7	0.012	0.036	0.006
DA-028	160	4.05	3.3	0.006	0.036	0.004
DA-029	160	4.07	3.0	0.010	0.028	0.001

Table 6.2 Isotropic compression data

Wyoming Buffer					Saskatchewan Buffer				
Sample	S_{is} (MPa)	S_y (MPa)	S_{peak} (MPa)	S_{eot} (MPa)	Sample	S_{is} (MPa)	S_y (MPa)	S_{peak} (MPa)	S_{eot} (MPa)
DA-007	7.2	7.2	7.3	7.2	DA-024	7.5	7.5	7.5	7.6
DA-008	7.2	5.8	5.4	5.8	DA-025	7.6	8.0	8.1	8.2
DA-009	7.2	7.6	7.8	7.6	DA-026	7.5	9.6	5.2	5.5
DA-016	15.6	15.6	15.6	15.6	DA-033	16.4	16.5	16.5	16.5
DA-017	15.7	16.6	16.6	16.3	DA-034	16.4	17.0	17.4	17.1
DA-018	15.6	13.8	13.5	13.5	DA-035	16.4	14.2	12.9	13.0
DA-013	32.0	32.1	32.1	32.2	DA-030	32.4	32.4	32.4	32.4
DA-014	32.0	29.9	27.1	27.3	DA-031	32.4	30.3	27.5	27.9
DA-015	32.0	33.1	32.9	32.8	DA-032	32.4	33.3	33.4	33.1
DA-019	63.7	63.7	63.7	63.7	DA-036	64.0	64.0	64.0	64.0
DA-020	63.7	61.6	59.0	59.4	DA-037	64.0	61.9	58.4	59.1
DA-021	63.7	64.6	64.6	64.4	DA-038	64.0	64.9	64.9	64.7
DA-010	123.8	123.7	123.7	124.0	DA-027	127.6	127.7	127.6	127.6
DA-011	123.8	124.8	124.8	124.6	DA-028	127.6	126.1	124.7	125.6
DA-012	123.8	121.3	117.9	118.4	DA-029	127.6	128.6	128.5	128.3

Table 6.3 Suction during shearing

Sample	S_{target} (MPa)	Stress Path	q_{yield} (MPa)	p_{yield} (MPa)	q_{peak} (MPa)	p_{peak} (MPa)	q_{eot} (MPa)	p_{eot} (MPa)
Wyoming buffer								
DA-007	10	const-p	1.7	2.5	1.9	2.4	1.4	2.5
DA-008	10	q/p = 1	1.6	4.2	2.1	4.7	1.6	4.2
DA-009	10	q/p=-3/1	1.8	2.0	2.1	1.9	1.6	2.0
DA-016	20	const-p	3.6	2.5	3.6	2.5	3.0	2.5
DA-017	20	q/p=-3/1	2.9	1.3	3.0	1.3	2.0	1.6
DA-018	20	q/p = 1	3.0	4.7	4.2	5.0	4.1	5.0
DA-013	40	const-p	4.6	2.5	4.7	2.5	2.7	2.3
DA-014	40	q/p = 1	2.1	5.1	7.3	8.4	6.6	8.2
DA-015	40	q/p=-3/1	3.5	1.3	3.6	1.5	1.8	1.6
DA-019	80	const-p	4.7	2.5	5.0	2.5	3.3	2.5
DA-020	80	q/p = 1	2.8	5.1	10.0	8.1	8.6	7.7
DA-021	80	q/p=-3/1	3.3	1.4	3.5	1.4	2.5	1.6
DA-010	160	const-p	5.2	3.0	5.8	3.1	3.4	2.8
DA-011	160	q/p=-3/1	3.7	1.7	4.1	1.8	2.5	2.0
DA-012	160	q/p = 1	3.1	6.0	12.3	10.1	10.2	9.4
Saskatchewan buffer								
DA-024	10	const-p	2.0	2.5	2.0	2.5	1.4	2.4
DA-025	10	q/p=-3/1	1.6	2.0	2.2	1.8	1.5	1.7
DA-026	10	q/p = 1	-	-	2.8	5.3	2.2	5.0
DA-033	20	const-p	2.9	2.5	3.3	2.5	2.8	2.5
DA-034	20	q/p=-3/1	1.9	1.9	3.5	1.4	2.4	1.7
DA-035	20	q/p = 1	2.6	5.1	5.7	6.8	5.6	6.7
DA-030	40	const-p	5.1	2.5	5.6	2.5	3.6	2.5
DA-031	40	q/p = 1	2.5	5.0	10.1	8.4	8.9	8.0
DA-032	40	q/p=-3/1	3.4	1.4	3.7	1.2	2.4	1.7
DA-036	80	const-p	5.0	2.5	5.7	2.5	3.8	2.5
DA-037	80	q/p = 1	2.6	5.1	12.9	9.2	10.5	8.4
DA-038	80	q/p=-3/1	3.3	1.4	3.6	1.4	2.5	1.7
DA-027	160	const-p	4.9	2.5	5.6	2.5	3.8	2.5
DA-028	160	q/p= 3/1	5.6	4.4	10.6	6.0	7.4	5.0
DA-029	160	q/p=-3/1	3.5	1.4	3.7	1.4	2.7	1.7

Table 6.4 Triaxial shear data

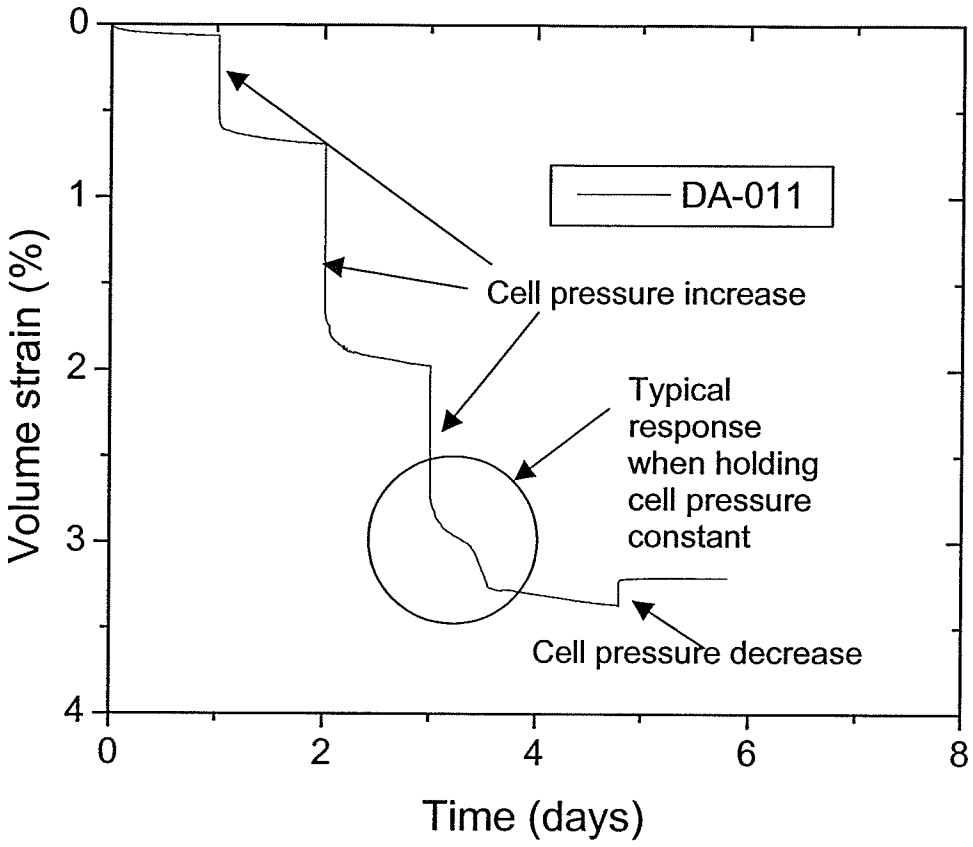

Figure 6.1 Volume strain versus time during isotropic compression

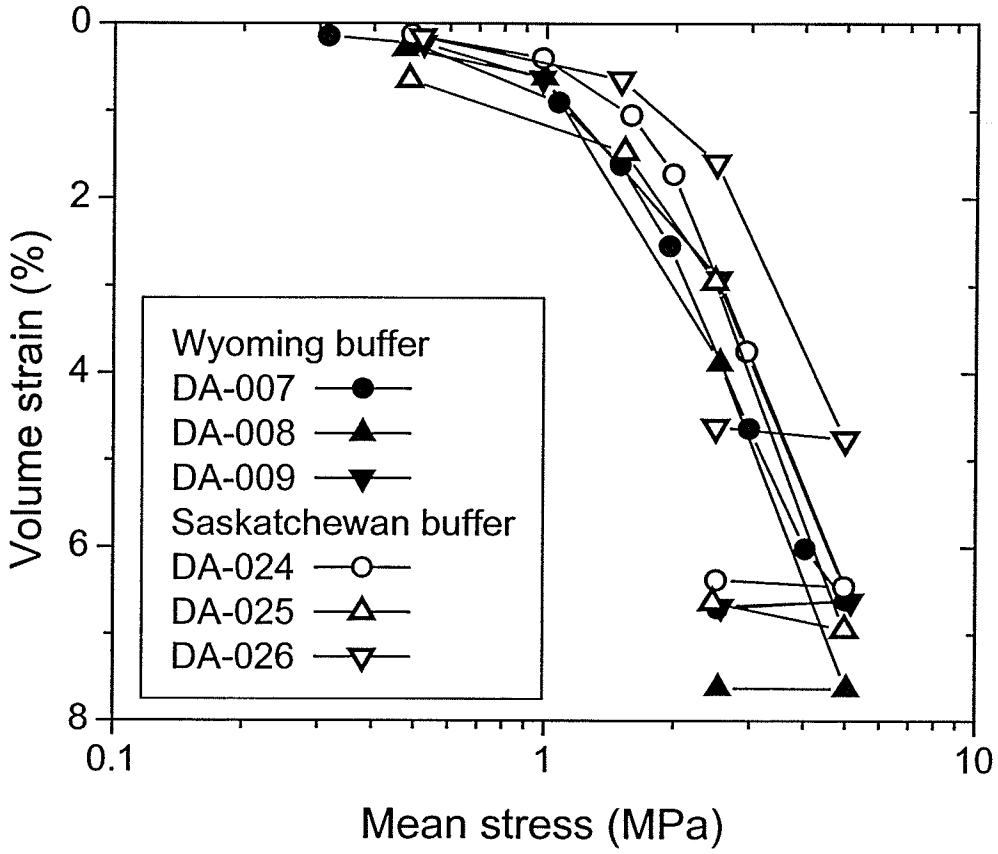

Figure 6.2 Isotropic compression curves for 10 MPa target suction specimens

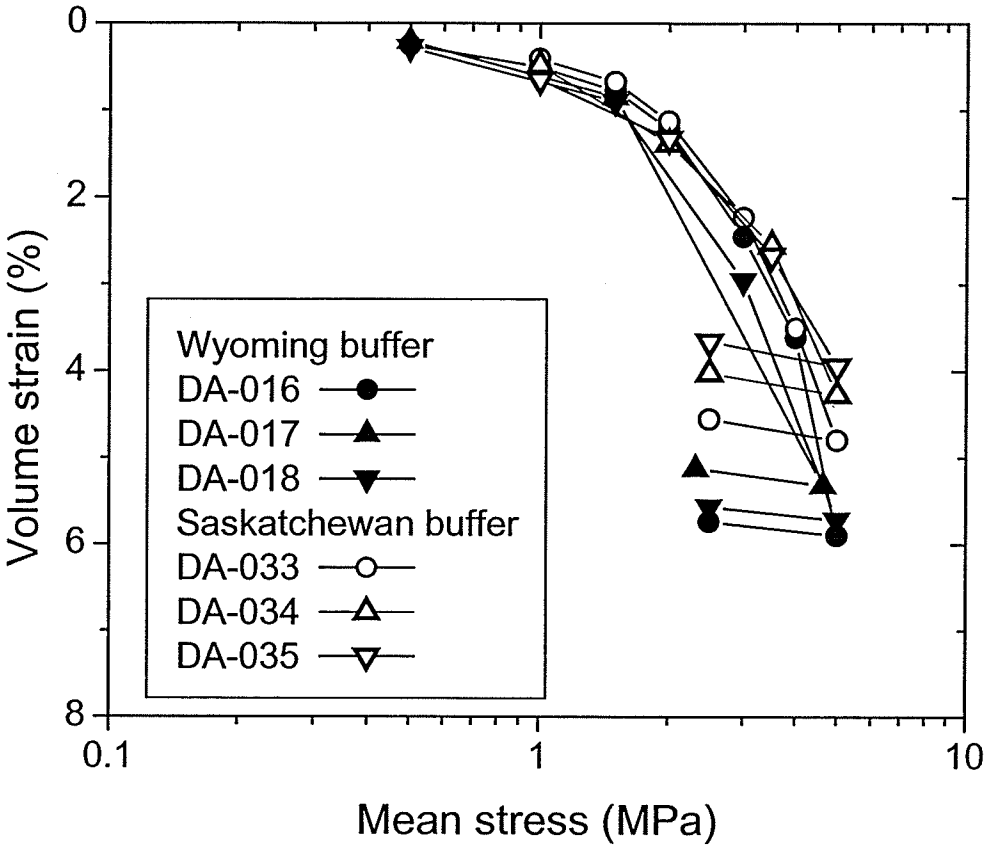

Figure 6.3 Isotropic compression curves for 20 MPa target suction specimens

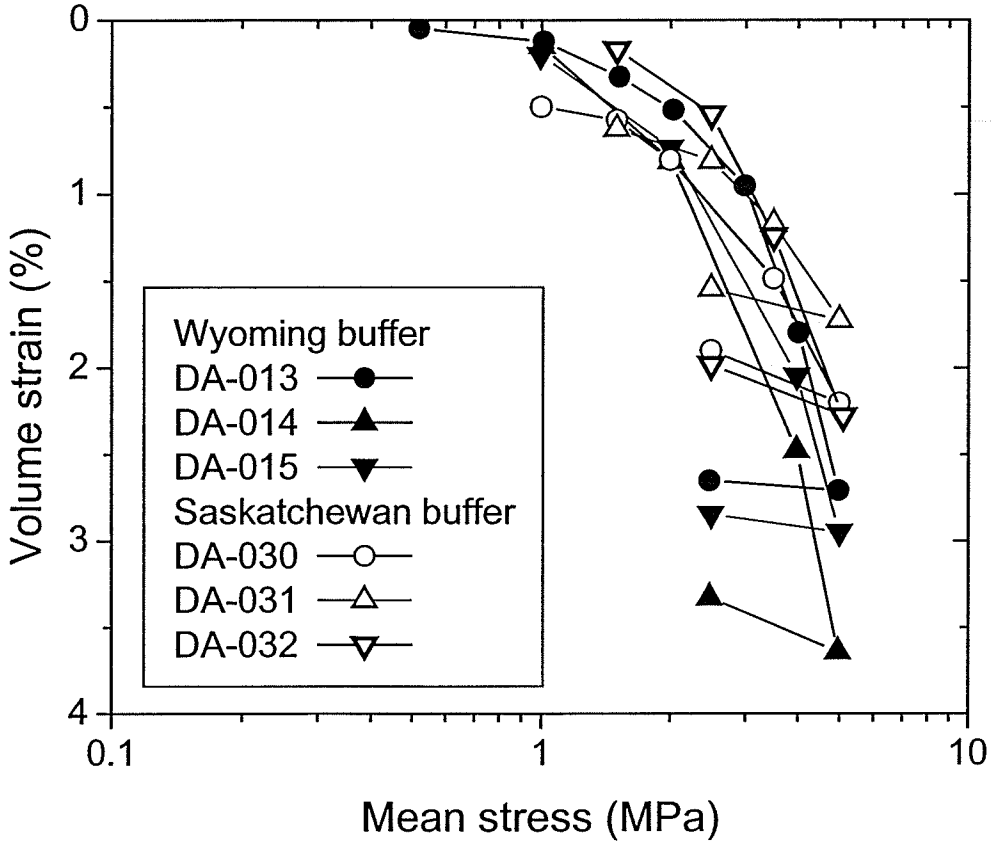

Figure 6.4 Isotropic compression curves for 40 MPa target suction specimens

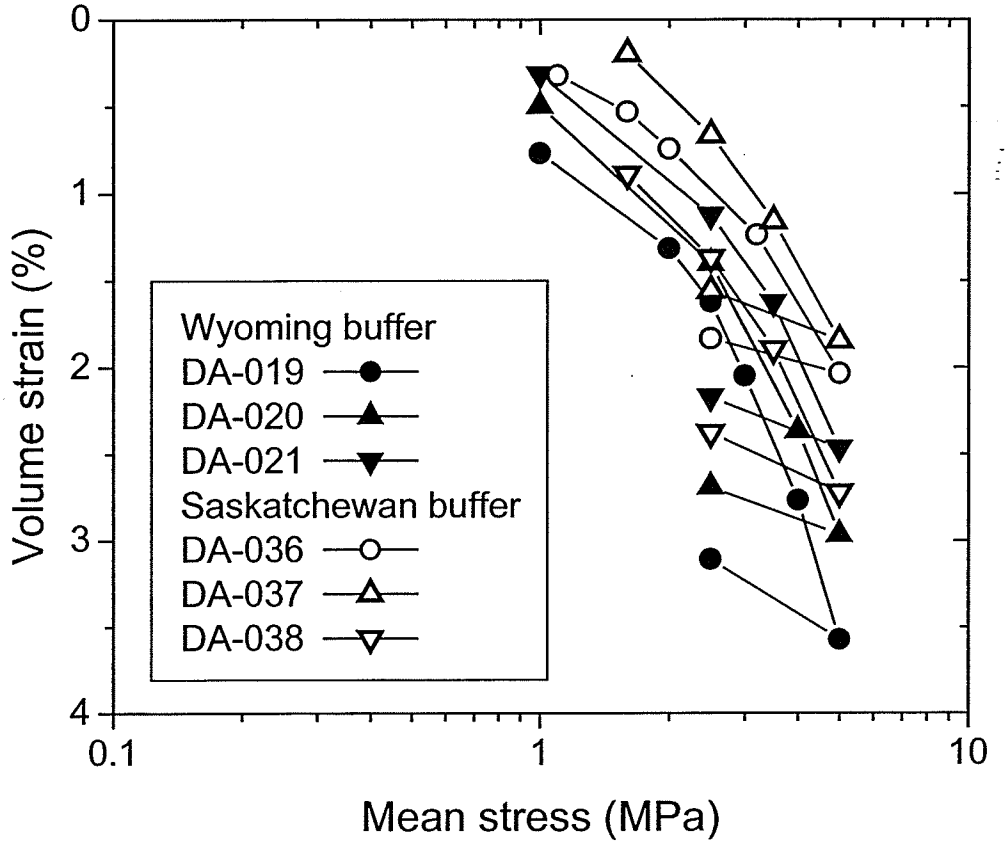

Figure 6.5 Isotropic compression curves for 80 MPa target suction specimens

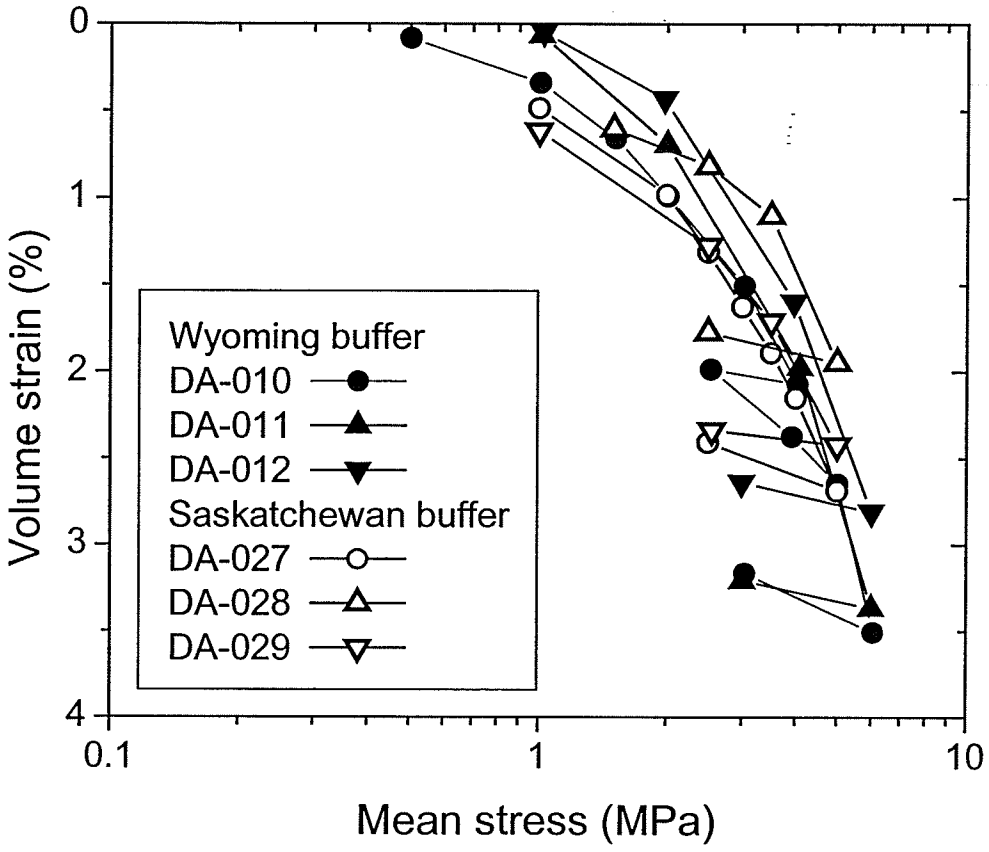

Figure 6.6 Isotropic compression curves for 160 MPa target suction specimens

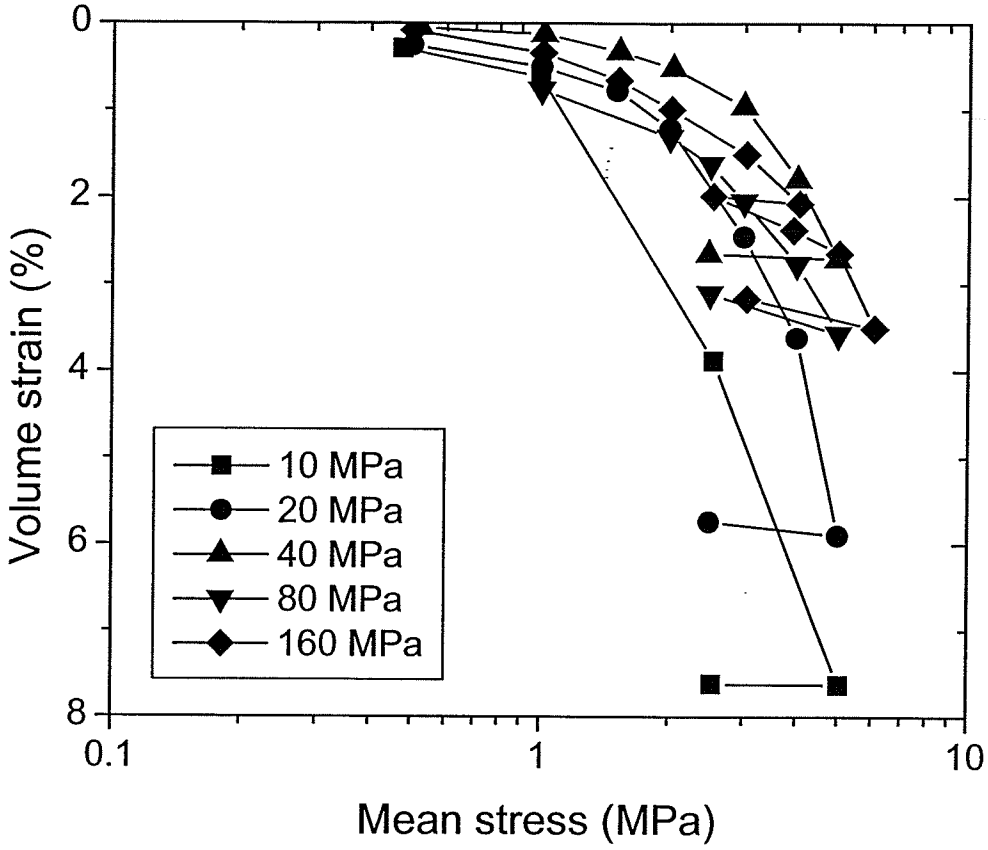

Figure 6.7 Isotropic compression curves for Wyoming buffer at all target suctions

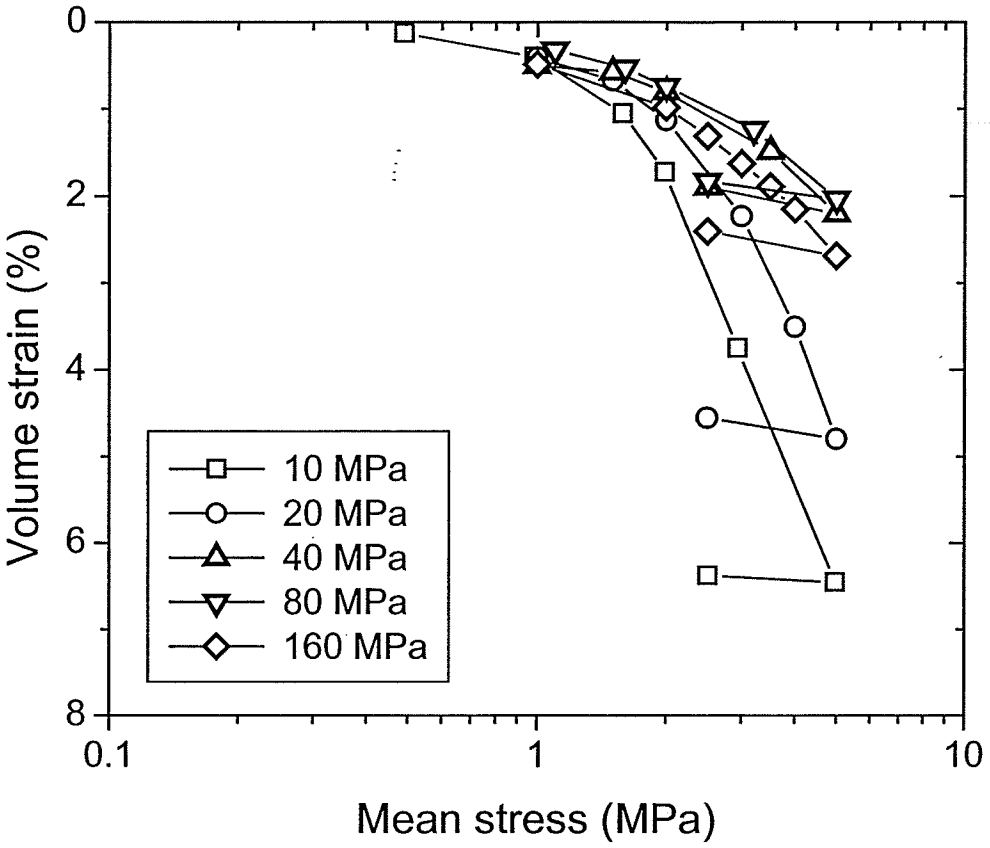

Figure 6.8 Isotropic compression curves for Saskatchewan buffer at all target suctions

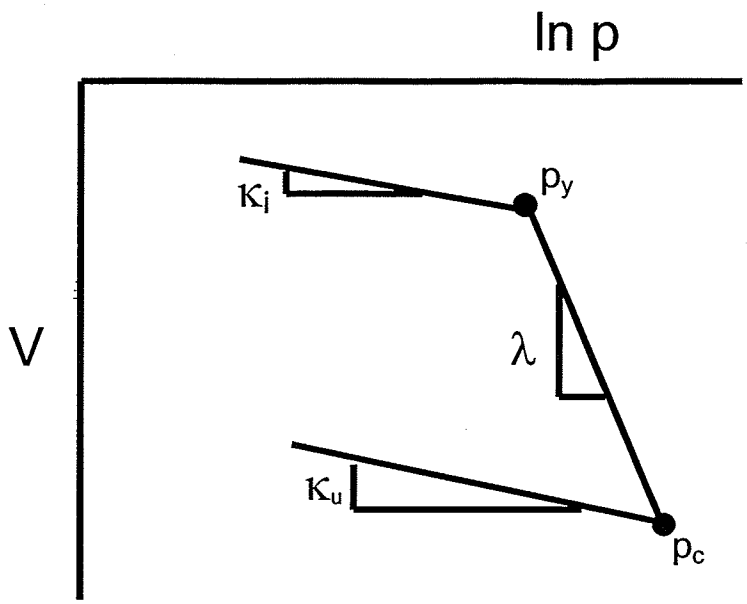

(a)

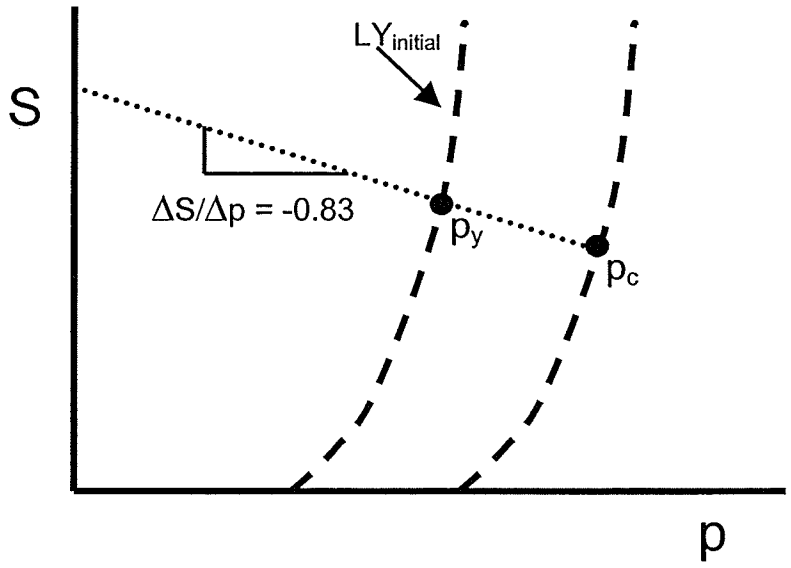

(b)

Figure 6.9 Isotropic compression parameters

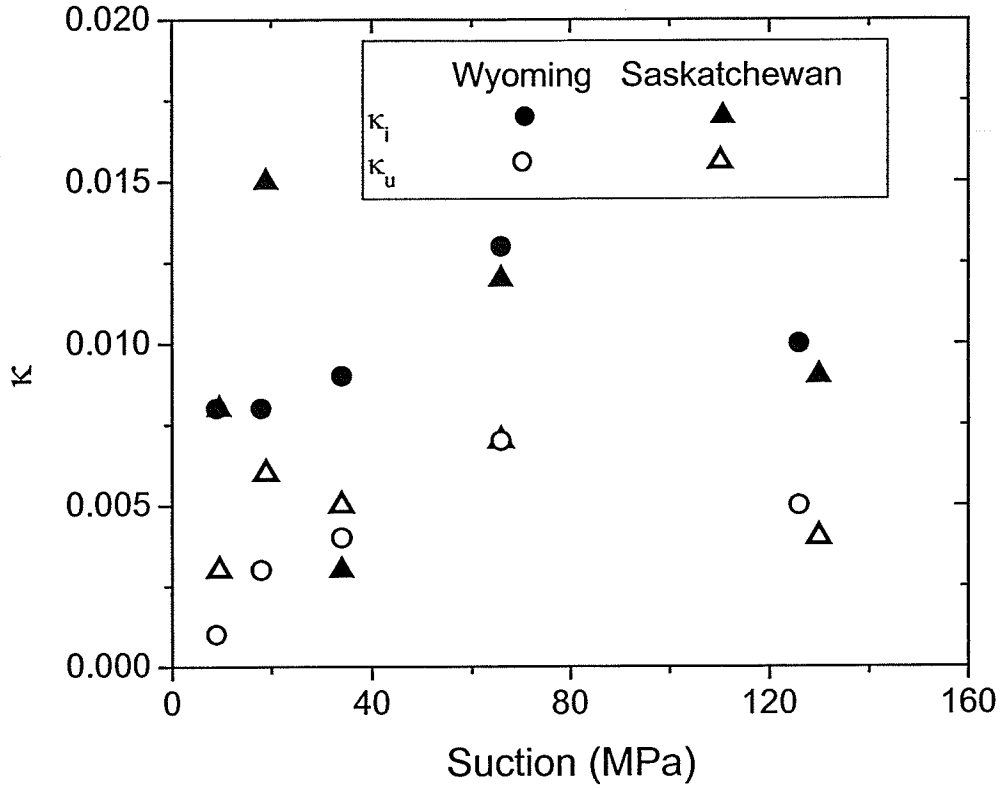

Figure 6.10 Average κ_i and κ_u indices for Saskatchewan and Wyoming buffers at varying target suction levels

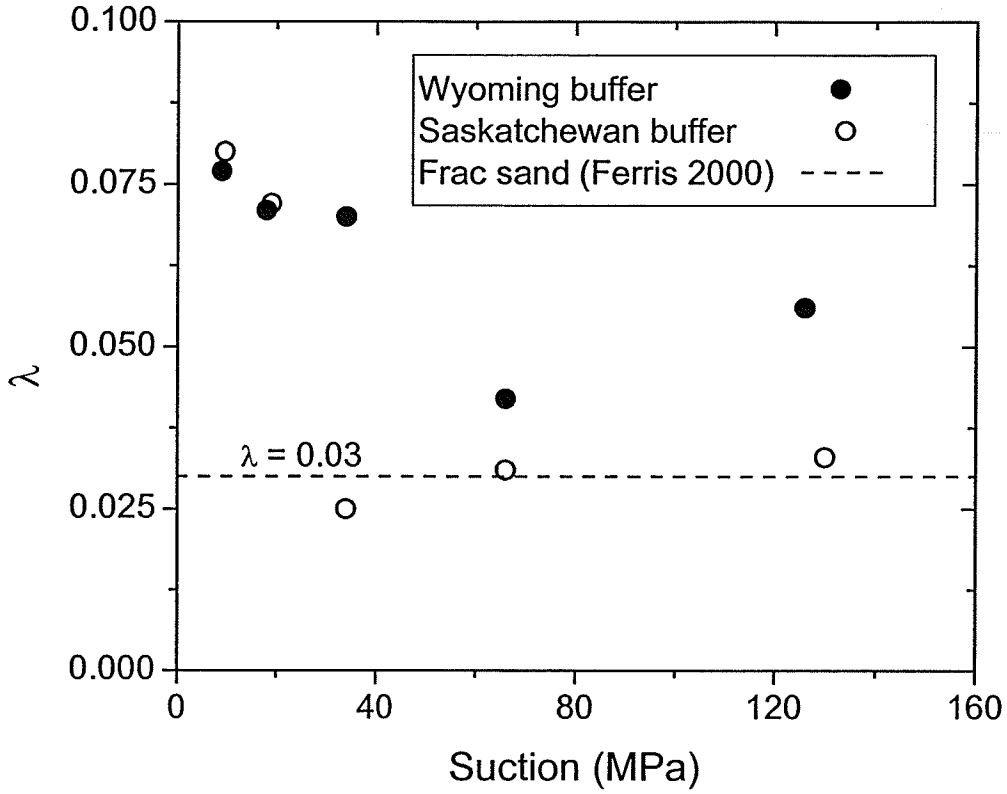

Figure 6.11 Average λ indices for Saskatchewan and Wyoming buffers at varying target suction levels

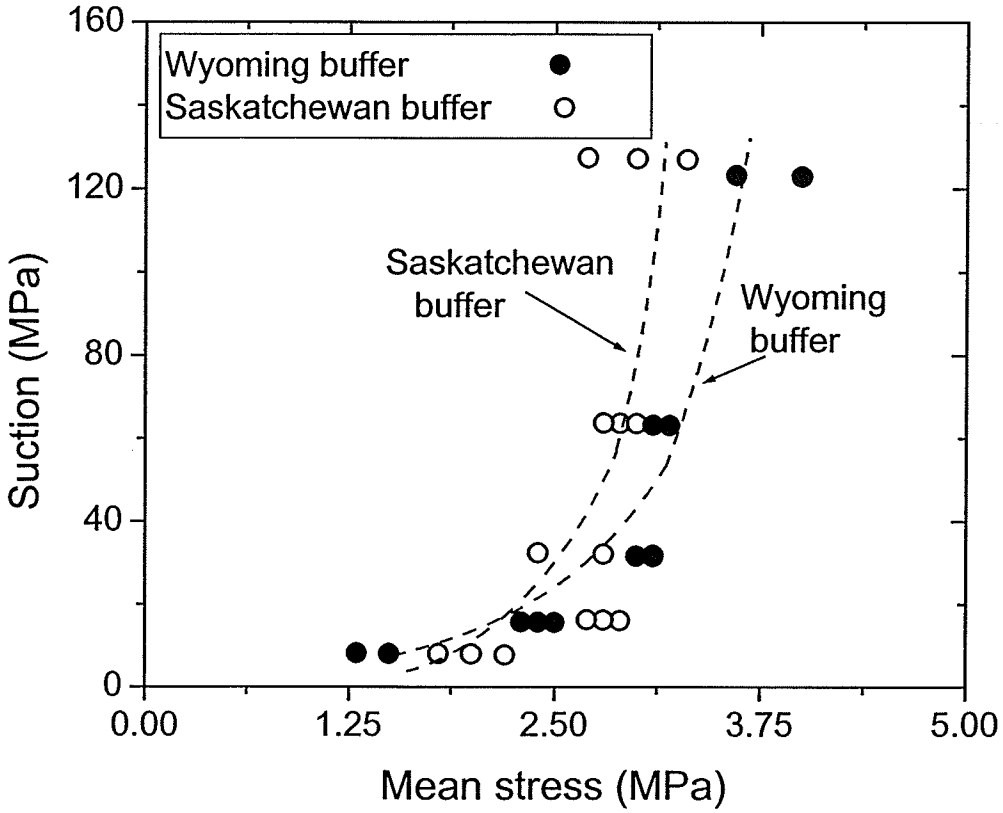

Figure 6.12 Load yield for all Saskatchewan and Wyoming buffers at varying suctions

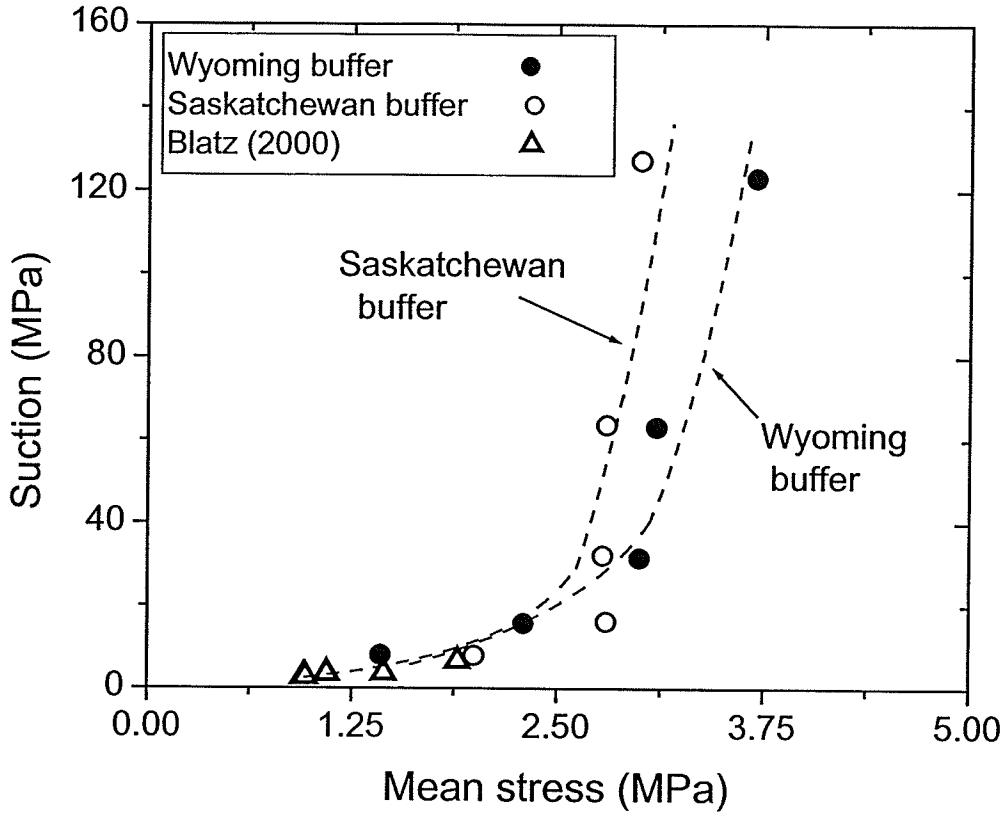

Figure 6.13 Average load yield for Saskatchewan and Wyoming buffers at varying suctions

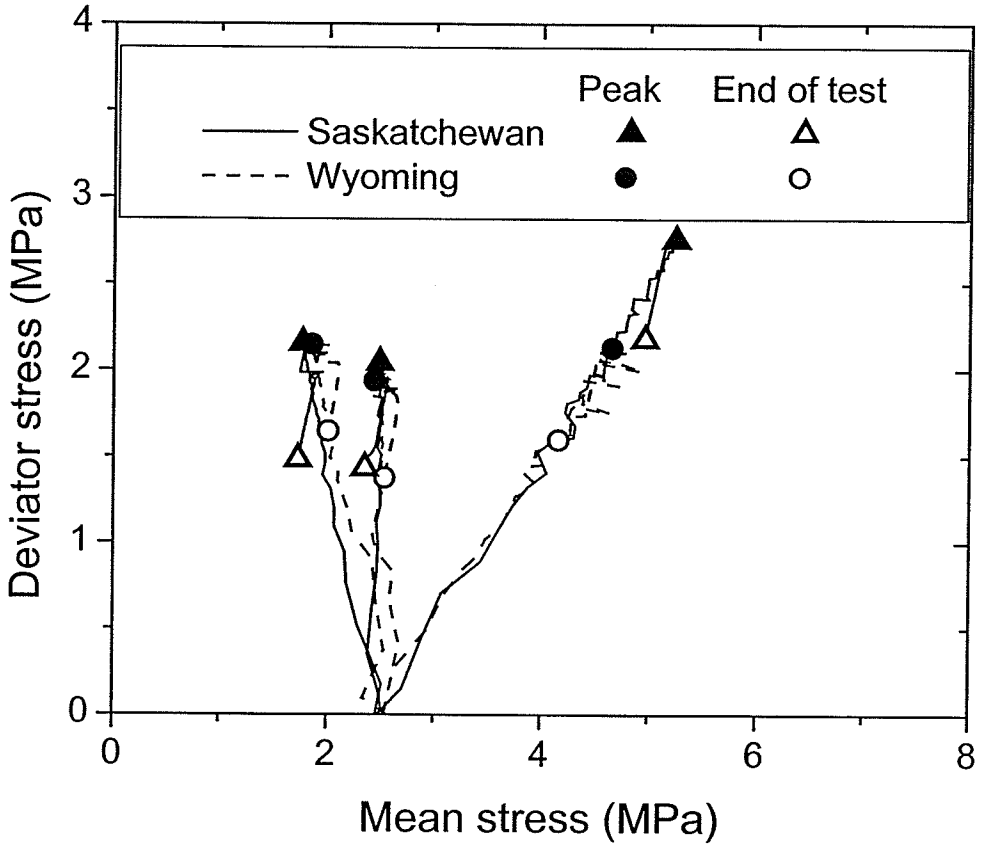

Figure 6.14 Stress paths for Saskatchewan and Wyoming buffers at 10 MPa target suction

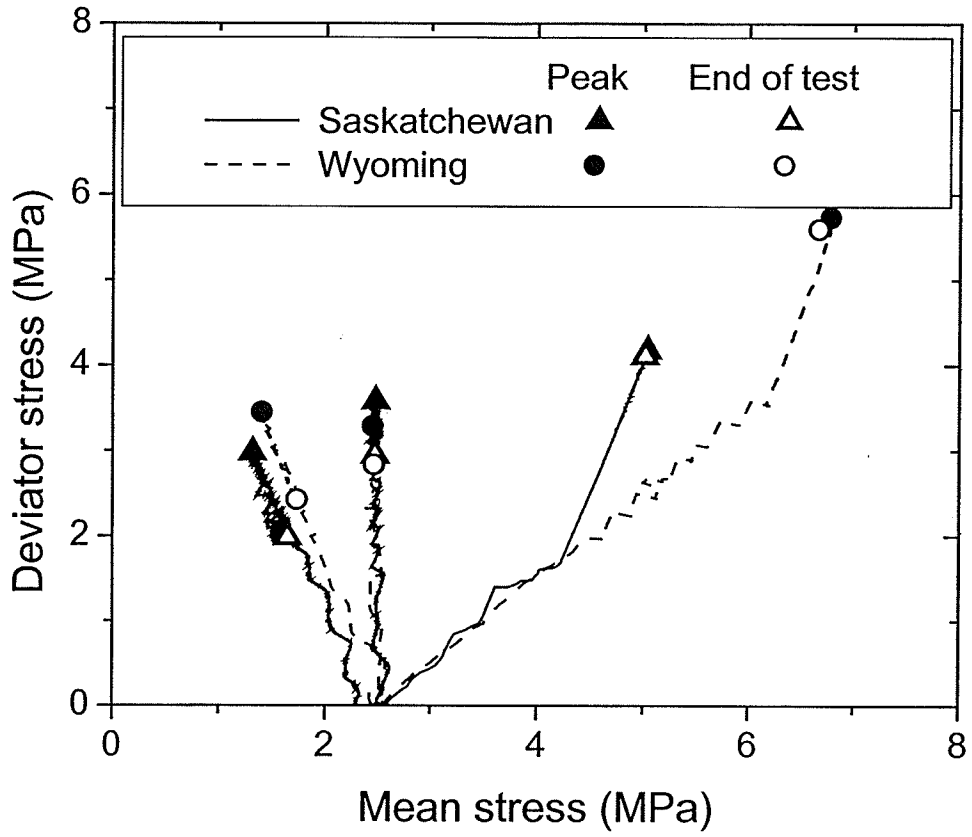

Figure 6.15 Stress paths for Saskatchewan and Wyoming buffers at 20 MPa target suction

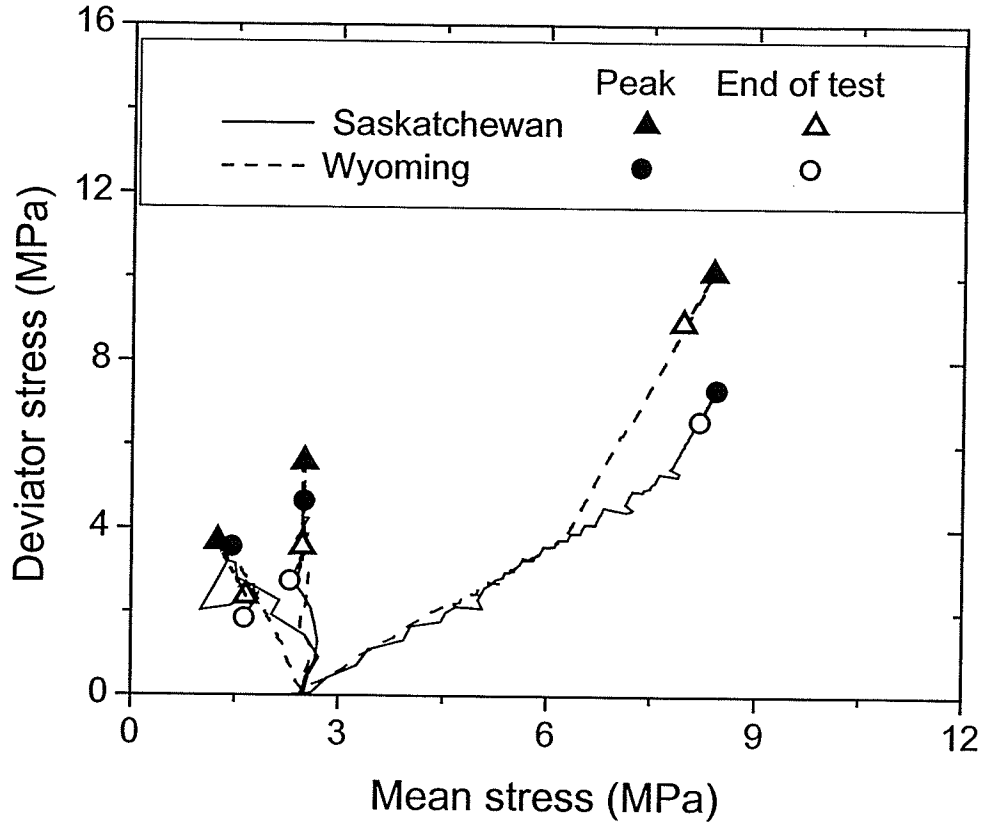

Figure 6.16 Stress paths for Saskatchewan and Wyoming buffers at 40 MPa target suction

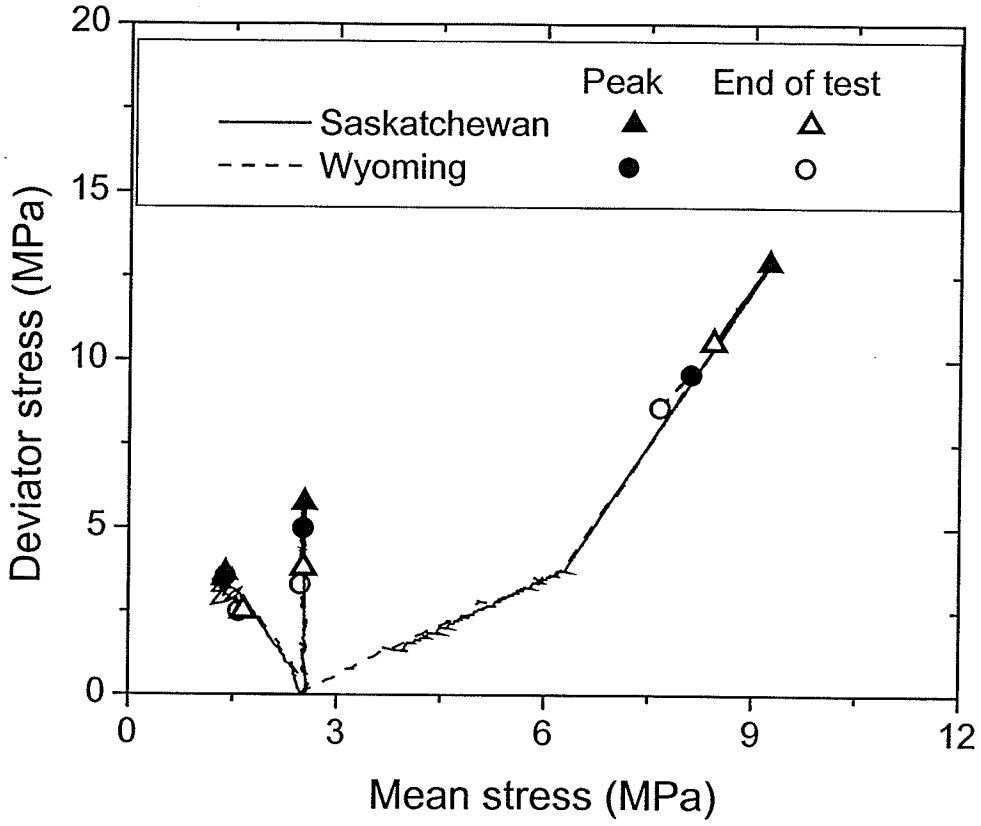

Figure 6.17 Stress paths for Saskatchewan and Wyoming buffers at 80 MPa target suction

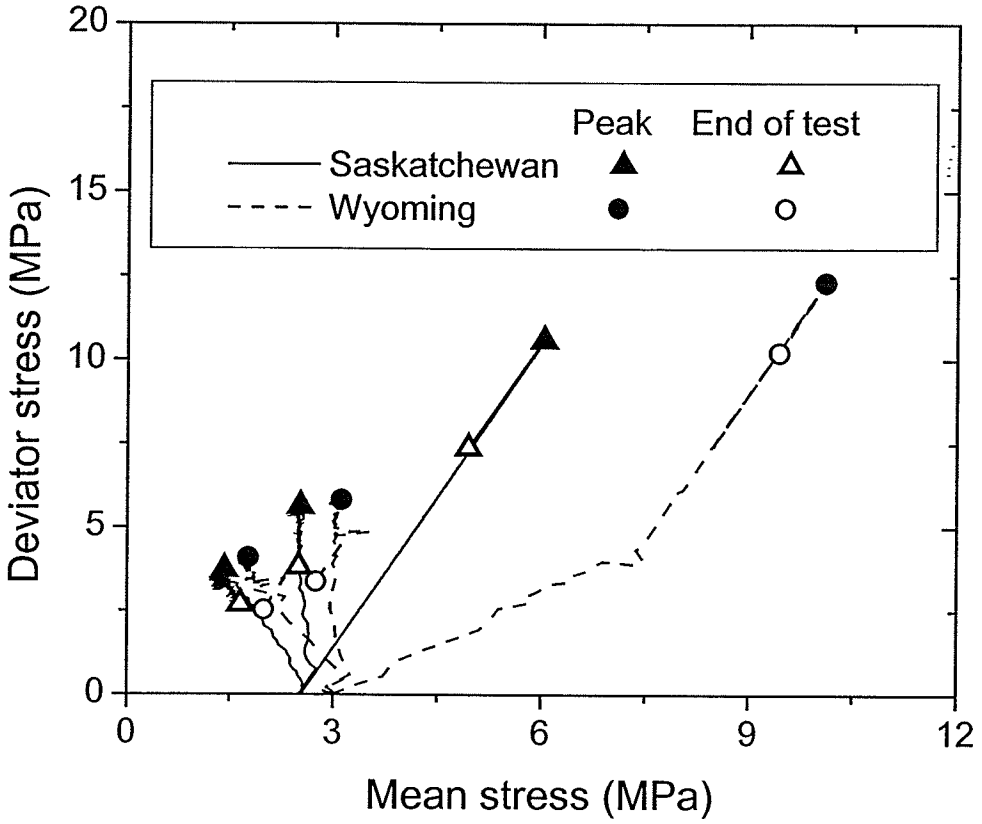

Figure 6.18 Stress paths for Saskatchewan and Wyoming buffers at 160 MPa target suction

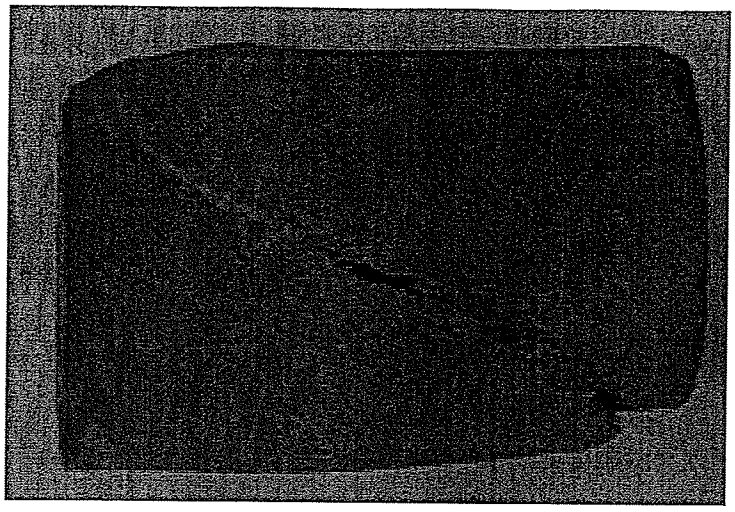

a) Brittle failure mode

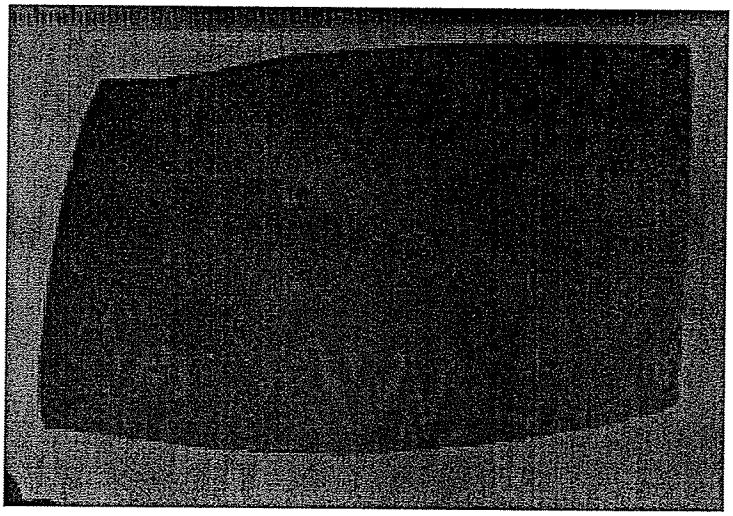

b) Ductile failure mode

Figure 6.19 Typical failure modes of sheared specimens

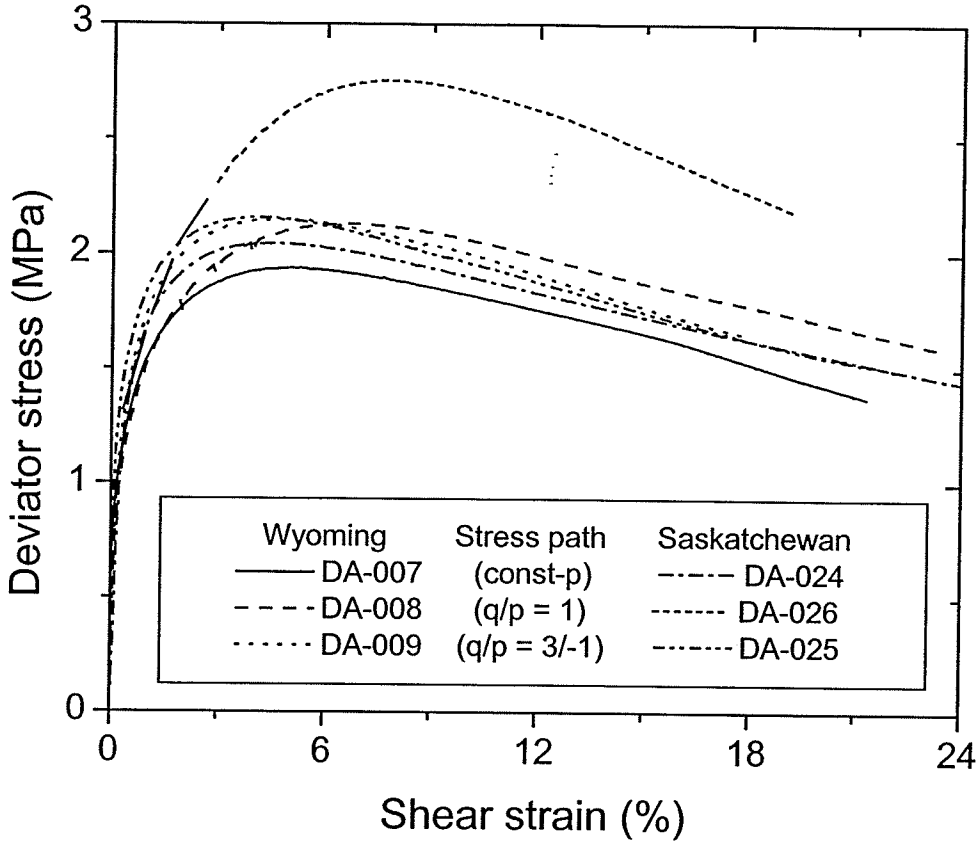

Figure 6.20 Stress-strain curves for Saskatchewan and Wyoming buffers at 10 MPa target suction

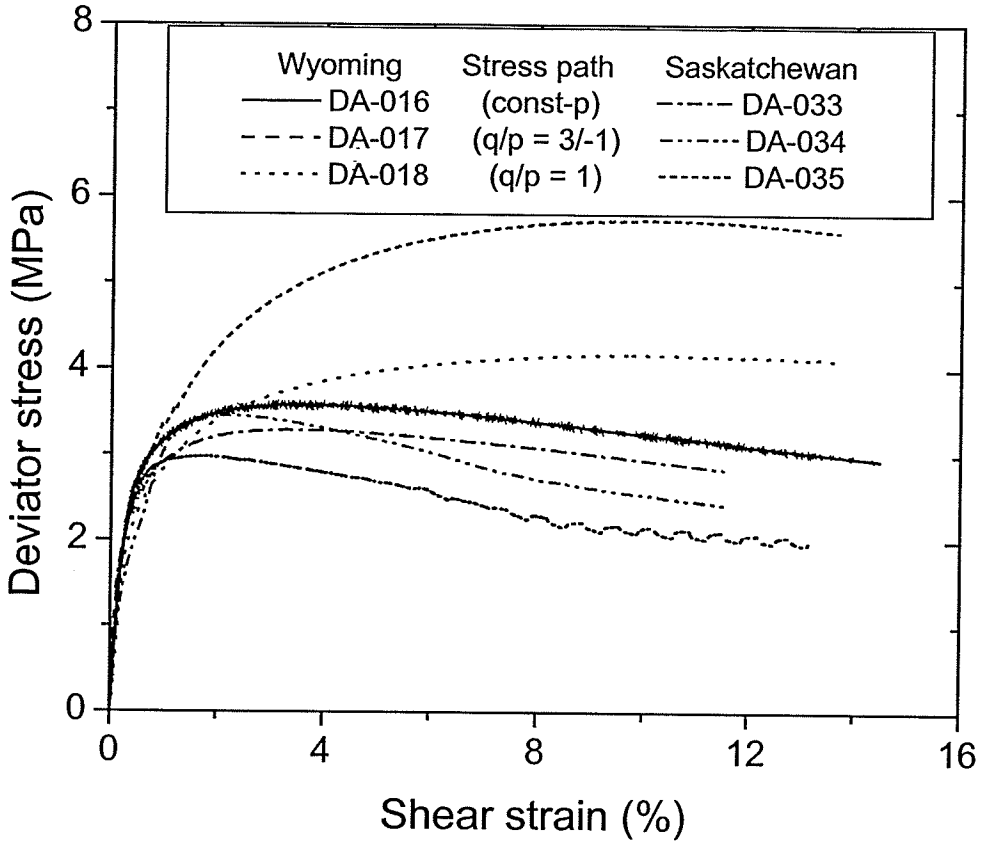

Figure 6.21 Stress-strain curves for Saskatchewan and Wyoming buffers at 20 MPa target suction

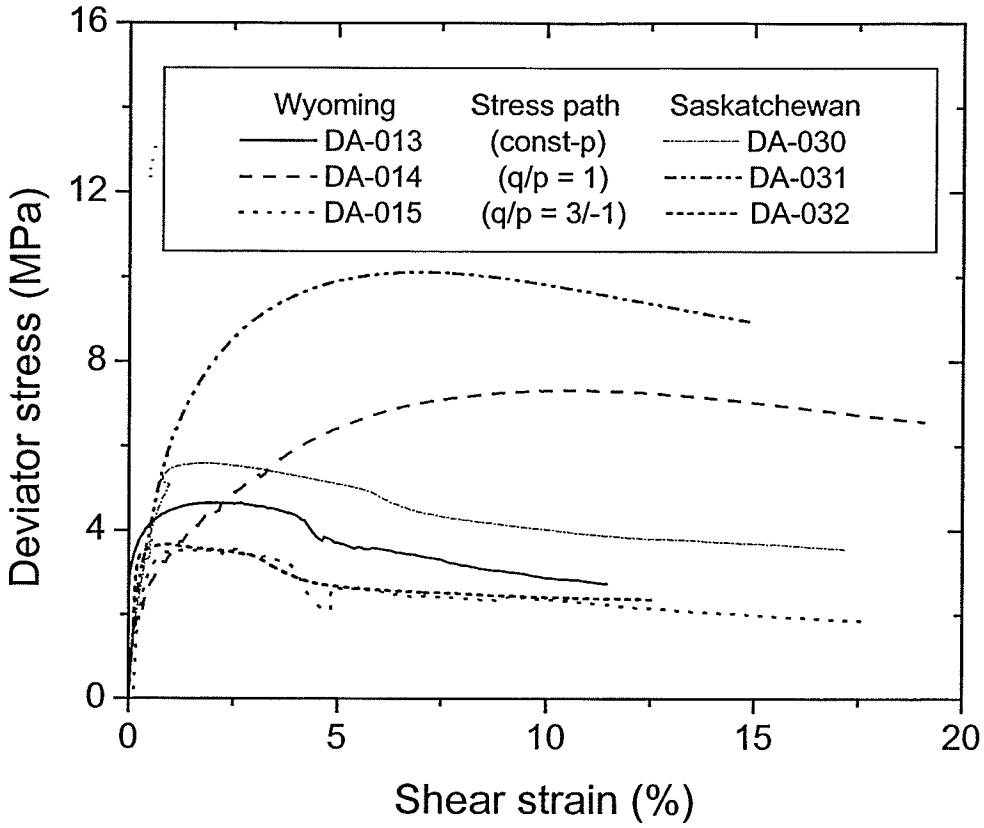

Figure 6.22 Stress-strain curves for Saskatchewan and Wyoming buffers at 40 MPa target suction

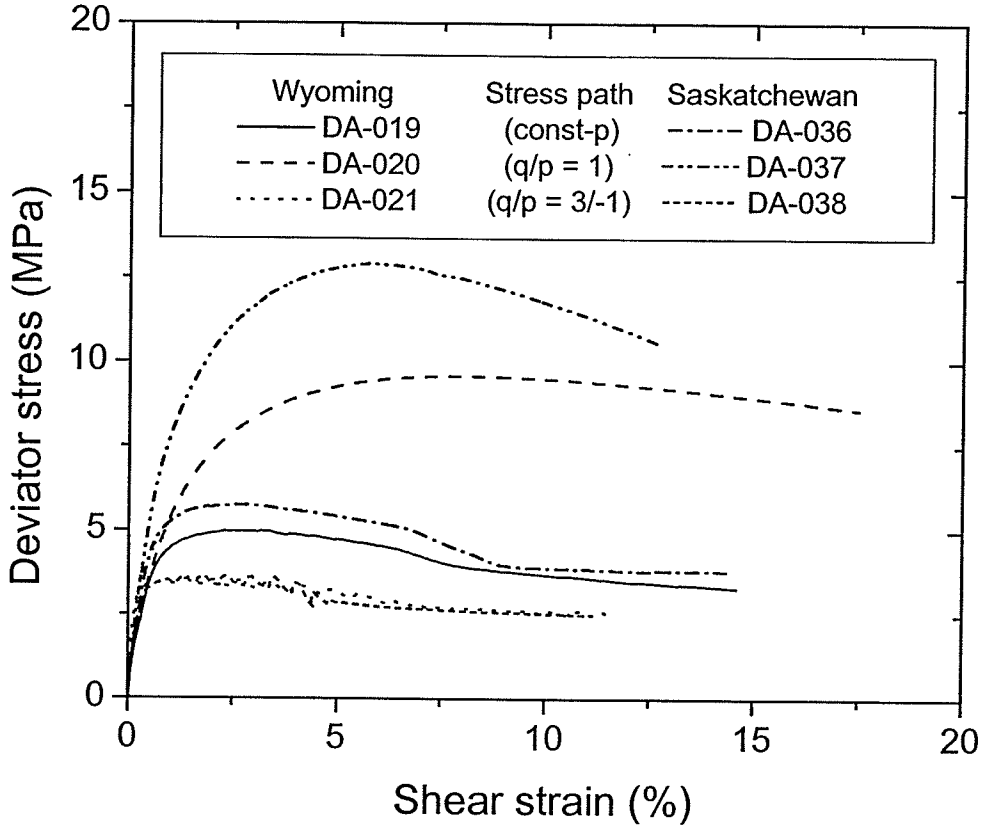

Figure 6.23 Stress-strain curves for Saskatchewan and Wyoming buffers at 80 MPa target suction

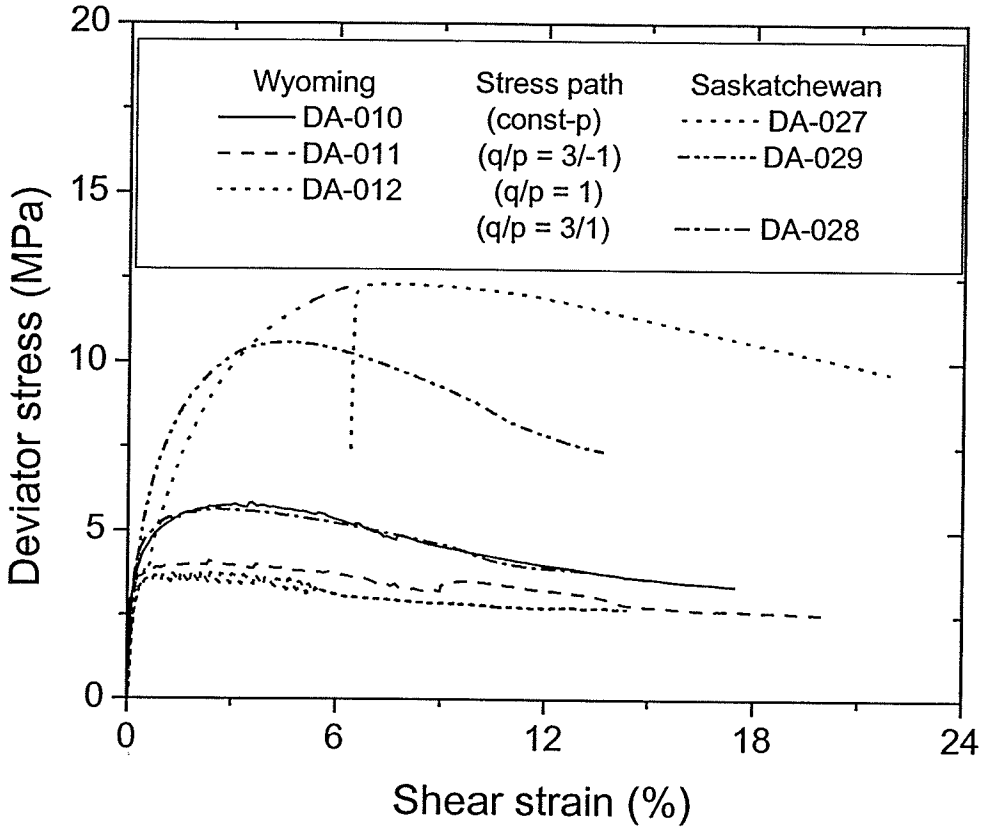

Figure 6.24 Stress-strain curves for Saskatchewan and Wyoming buffers at 160 MPa target suction

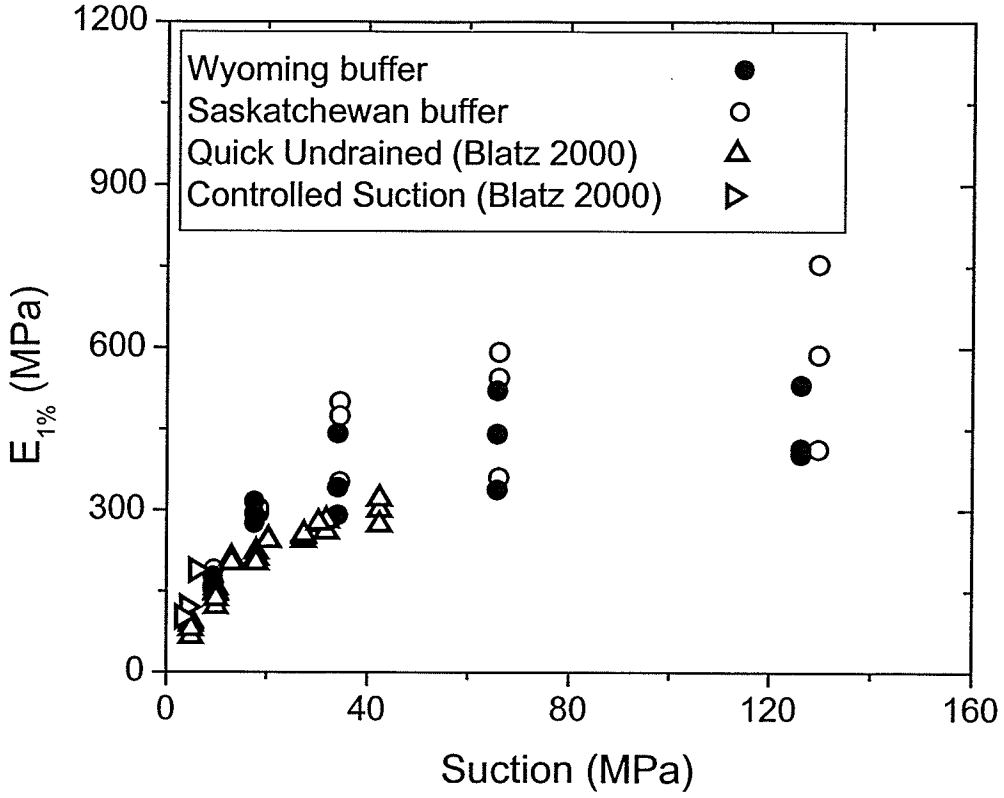

Figure 6.25 $E_{1\%}$ for all Saskatchewan and Wyoming buffer specimens at varying suction levels

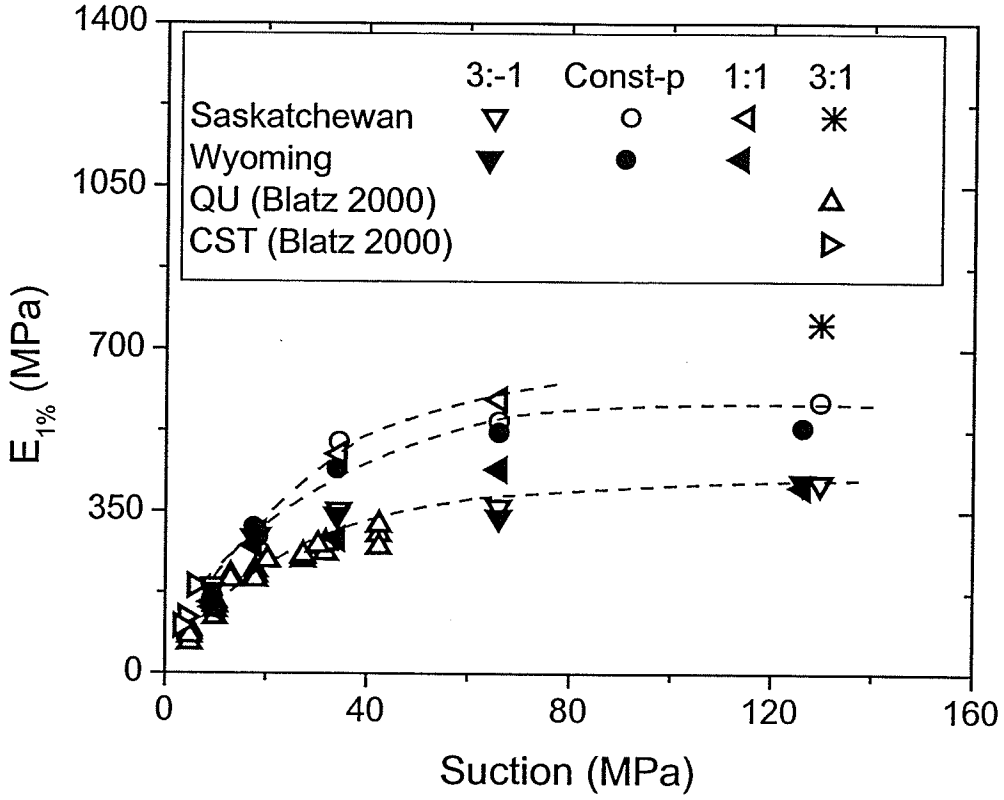

Figure 6.26 $E_{1\%}$ for Saskatchewan and Wyoming buffers at varying suctions grouped by stress path during shearing

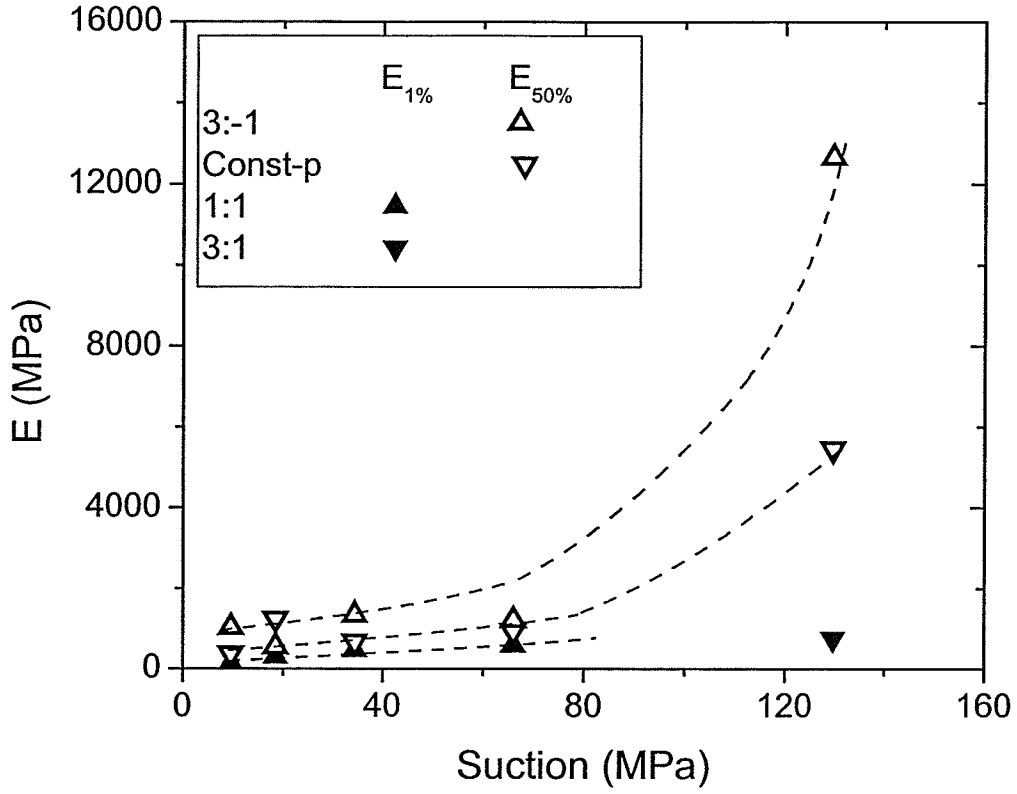

Figure 6.27 $E_{1\%}$ and $E_{50\%}$ values for Saskatchewan buffer at varying suction levels

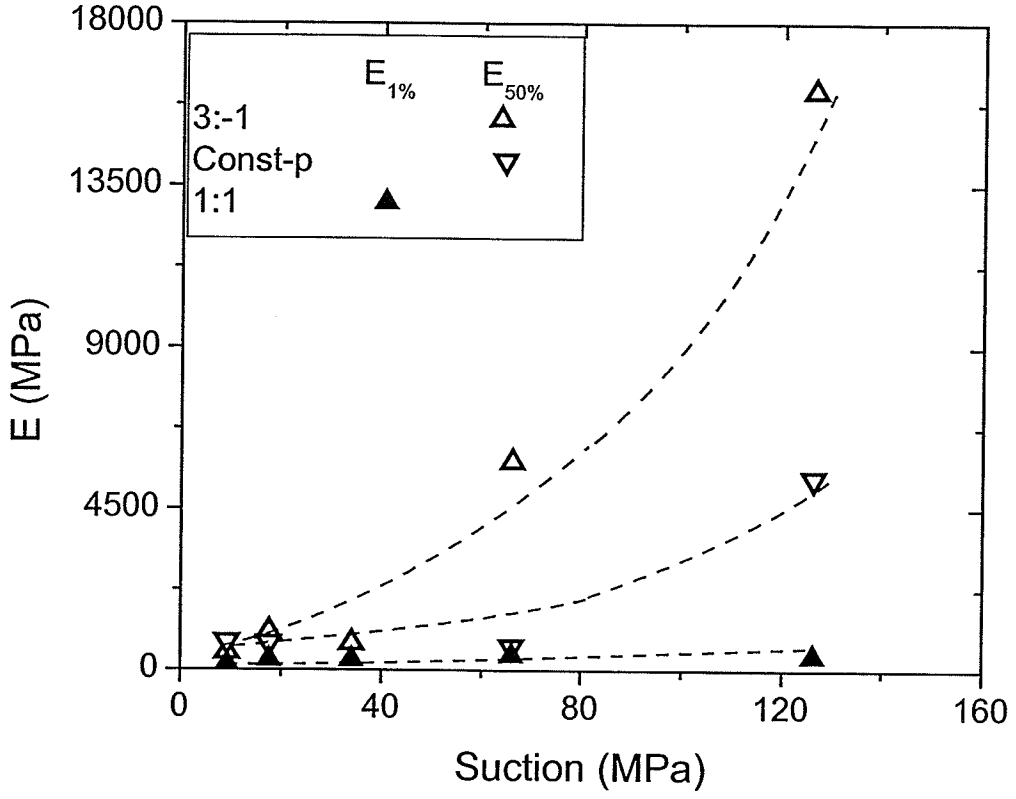

Figure 6.28 $E_{1\%}$ and $E_{50\%}$ values for Wyoming buffer at varying suction levels

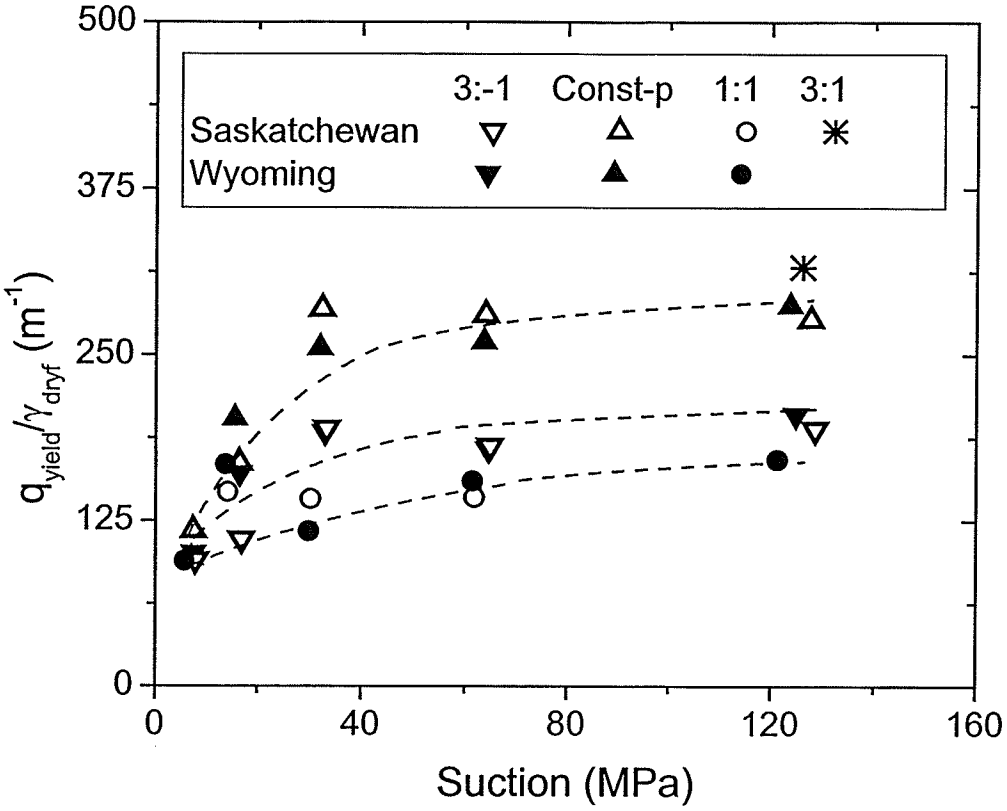

Figure 6.29 Yield ratio values for Saskatchewan and Wyoming buffers at varying suction levels

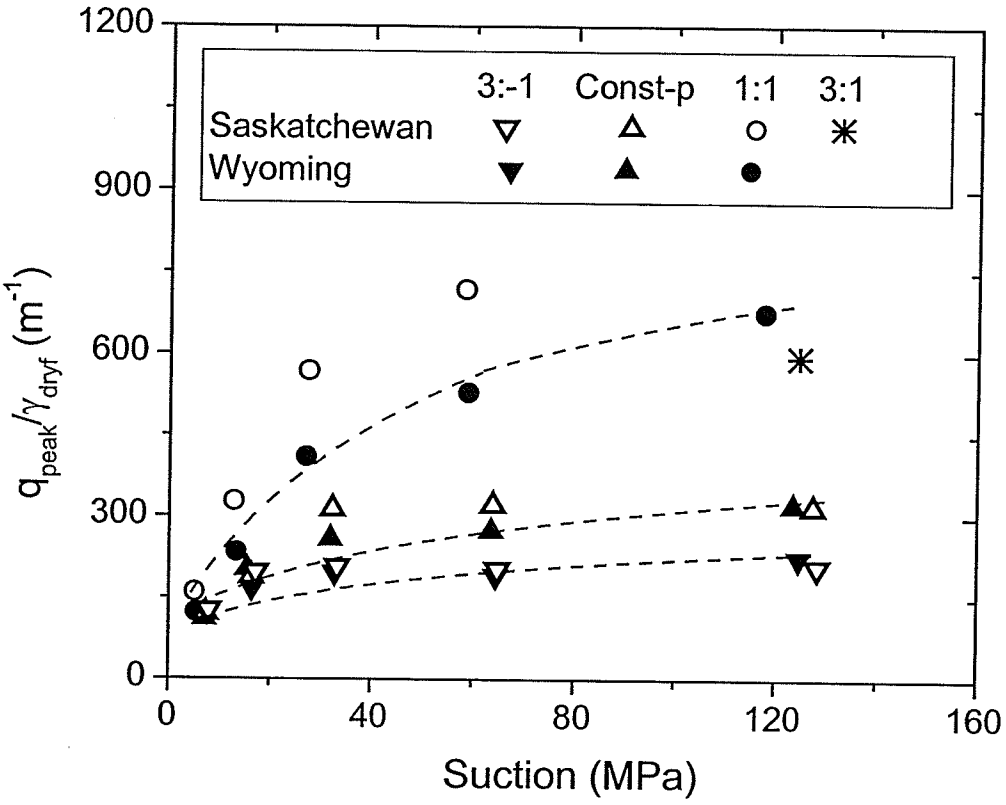

Figure 6.30 Peak ratio values for Saskatchewan and Wyoming buffers at varying suction levels

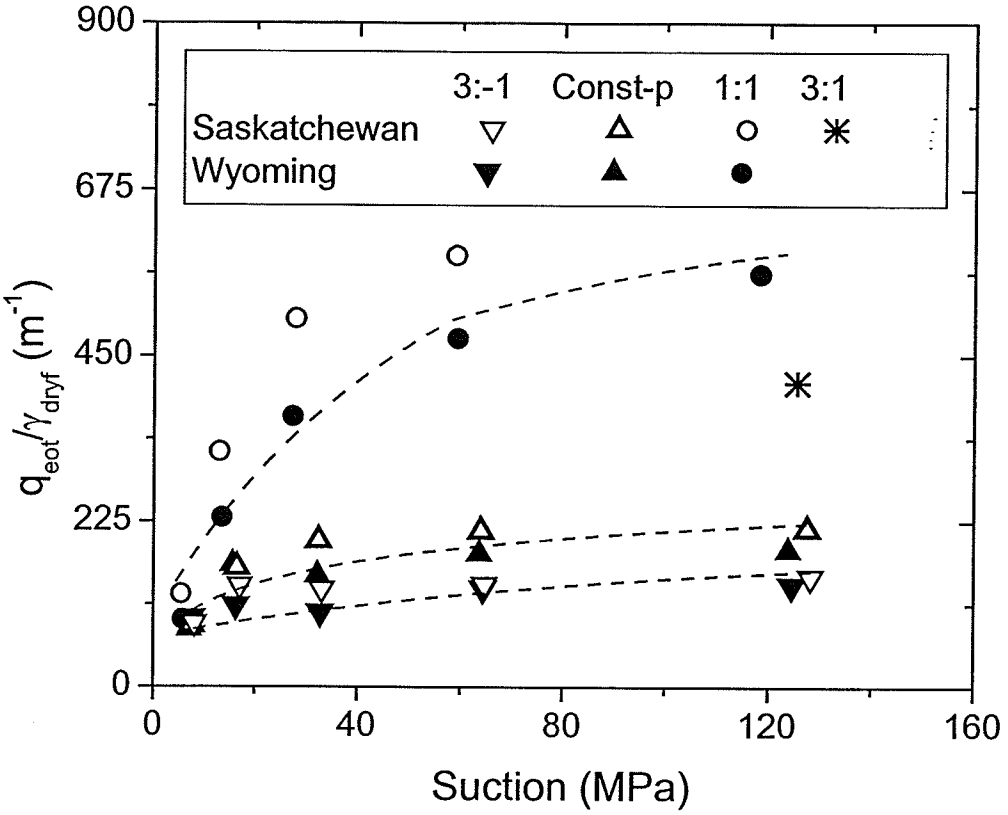

Figure 6.31 End-of-test ratio values for Saskatchewan and Wyoming buffers at varying suction levels

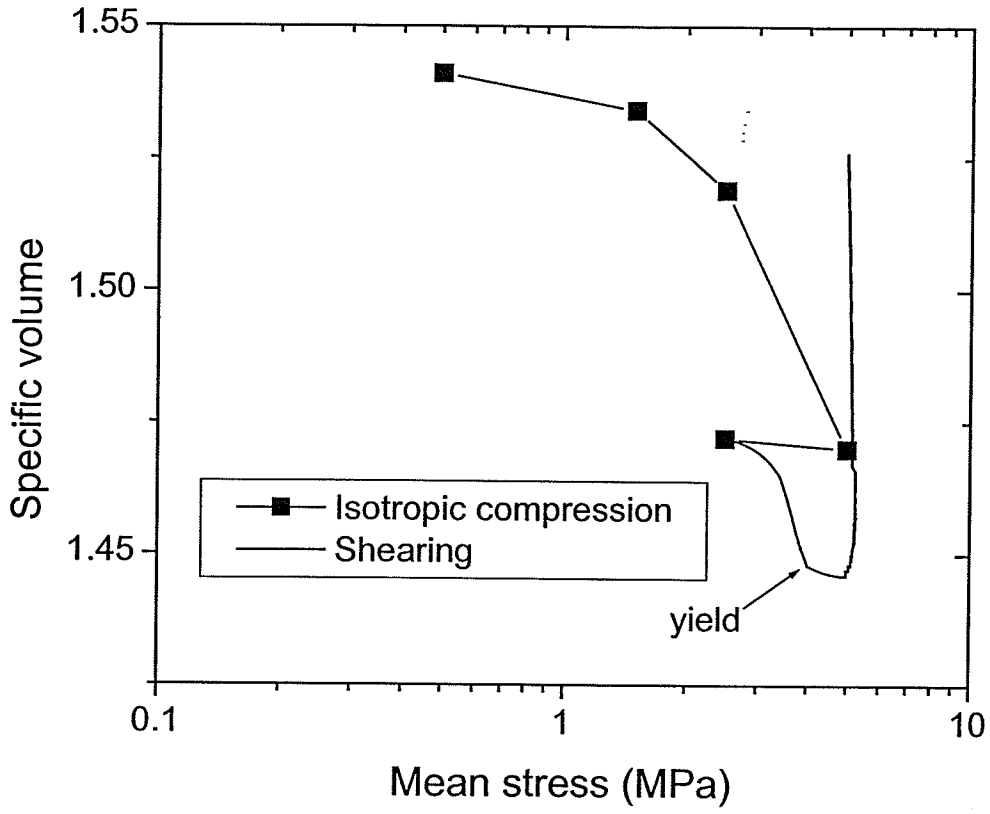

Figure 6.32 Specific volume during all phases of triaxial testing of DA-026 at 10 MPa target suction

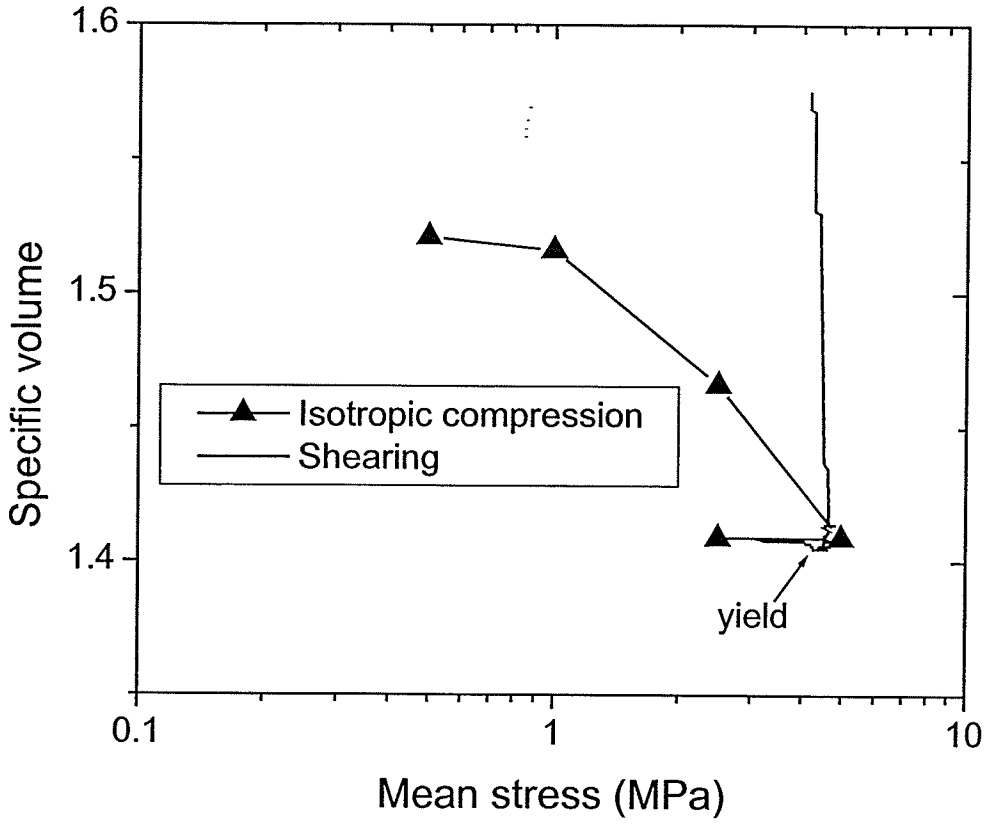

Figure 6.33 Specific volume during all phases of triaxial testing of DA-008 at 10 MPa target suction

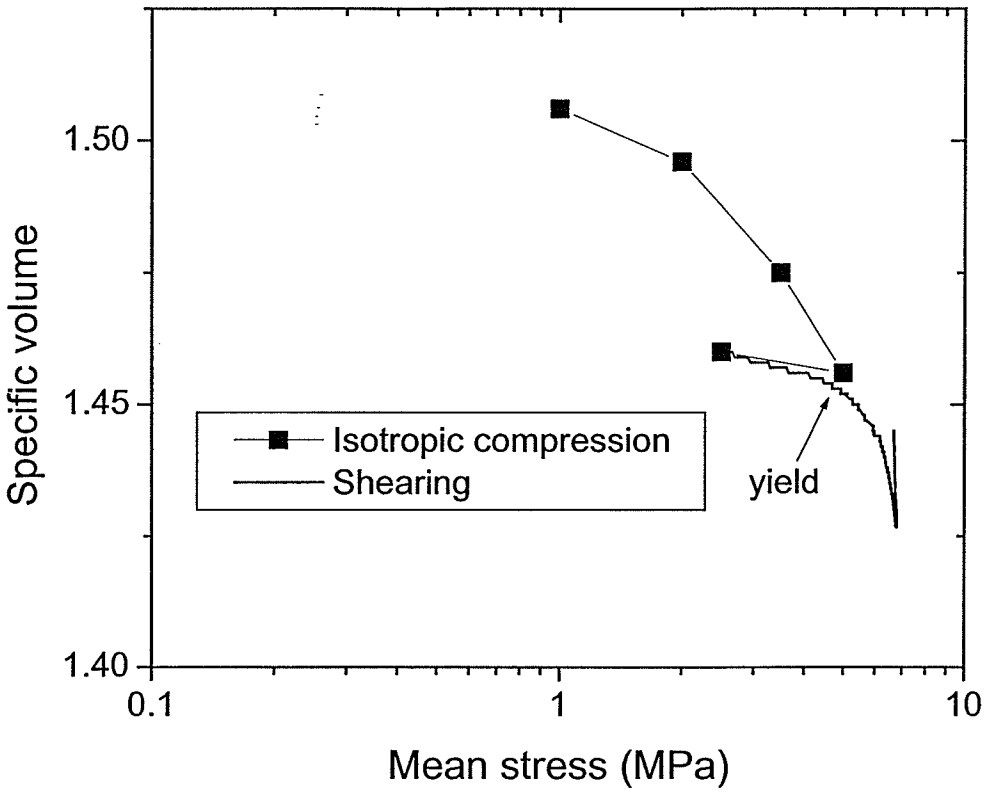

Figure 6.34 Specific volume during all phases of triaxial testing of DA-035 at 20 MPa target suction

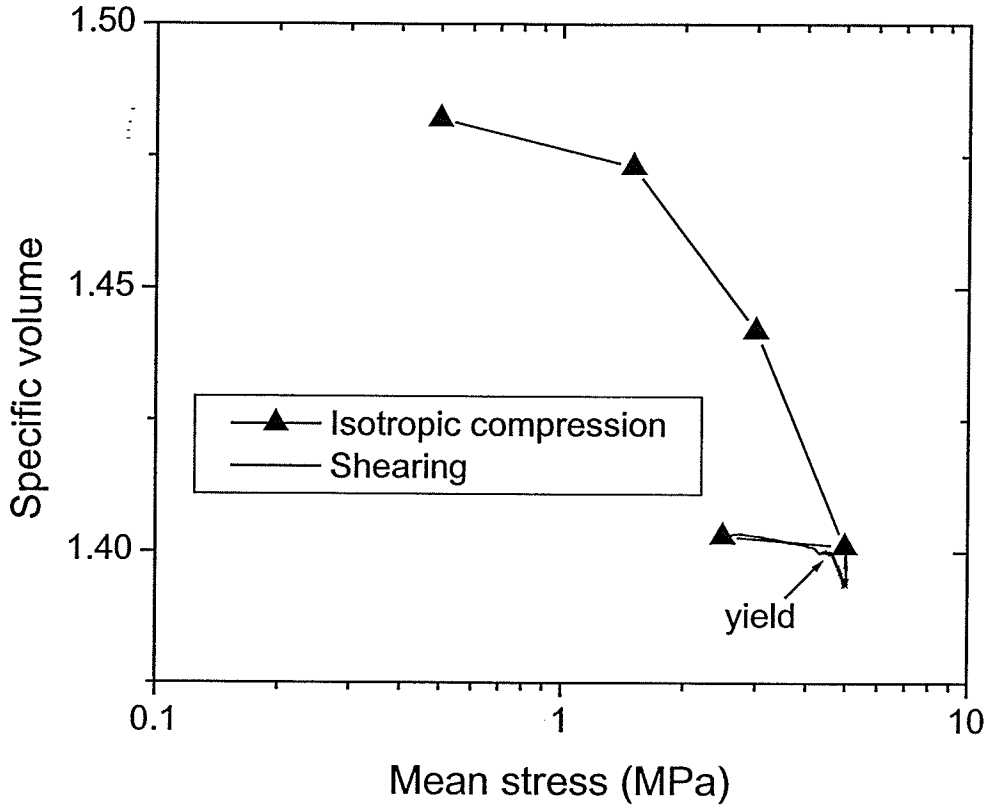

Figure 6.35 Specific volume during all phases of triaxial testing of DA-018 at 20 MPa target suction

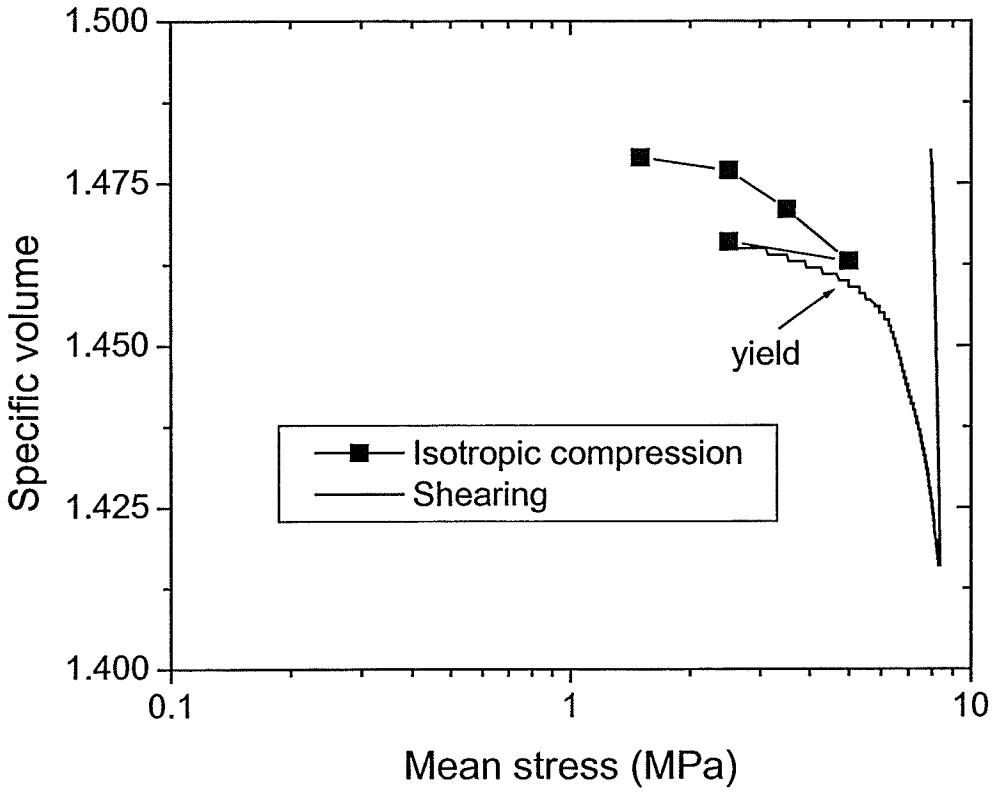

Figure 6.36 Specific volume during all phases of triaxial testing of DA-031 at 40 MPa target suction

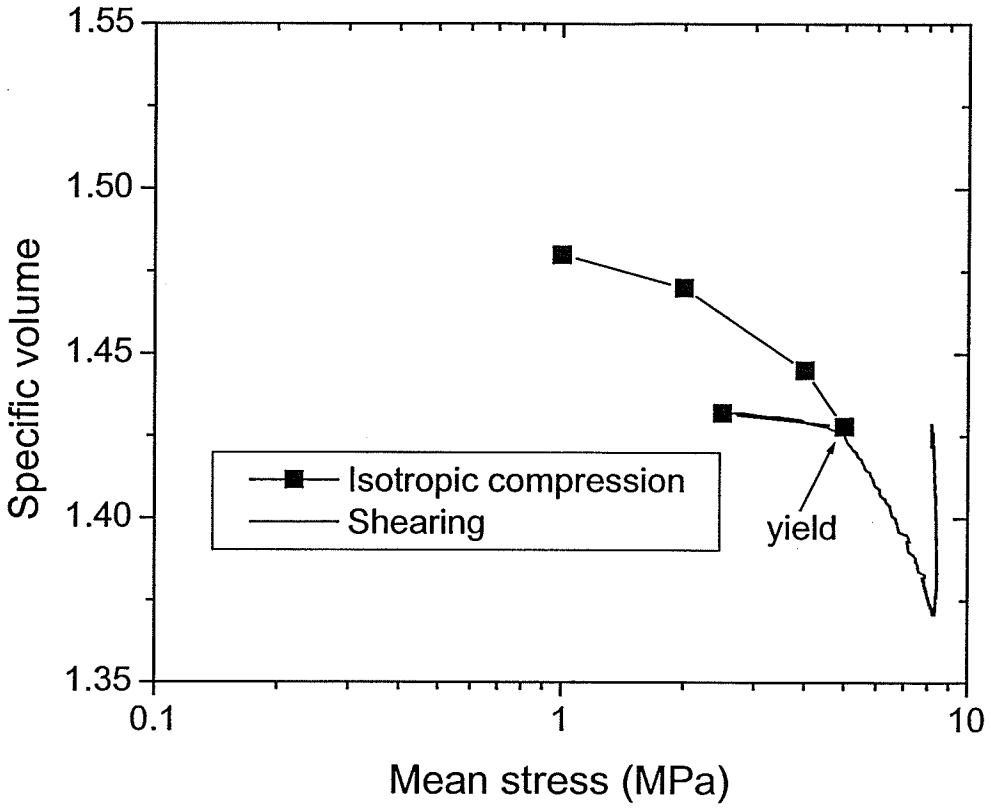

Figure 6.37 Specific volume during all phases of triaxial testing of DA-014 at 40 MPa target suction

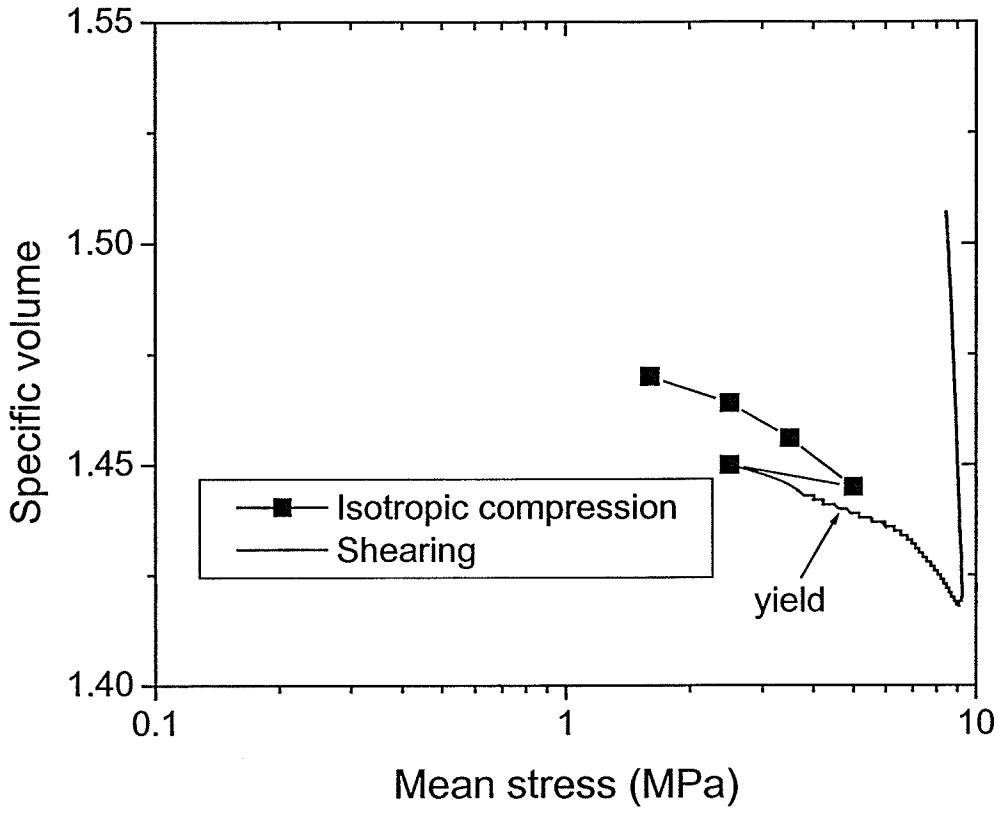

Figure 6.38 Specific volume during all phases of triaxial testing of DA-037 at 80 MPa target suction

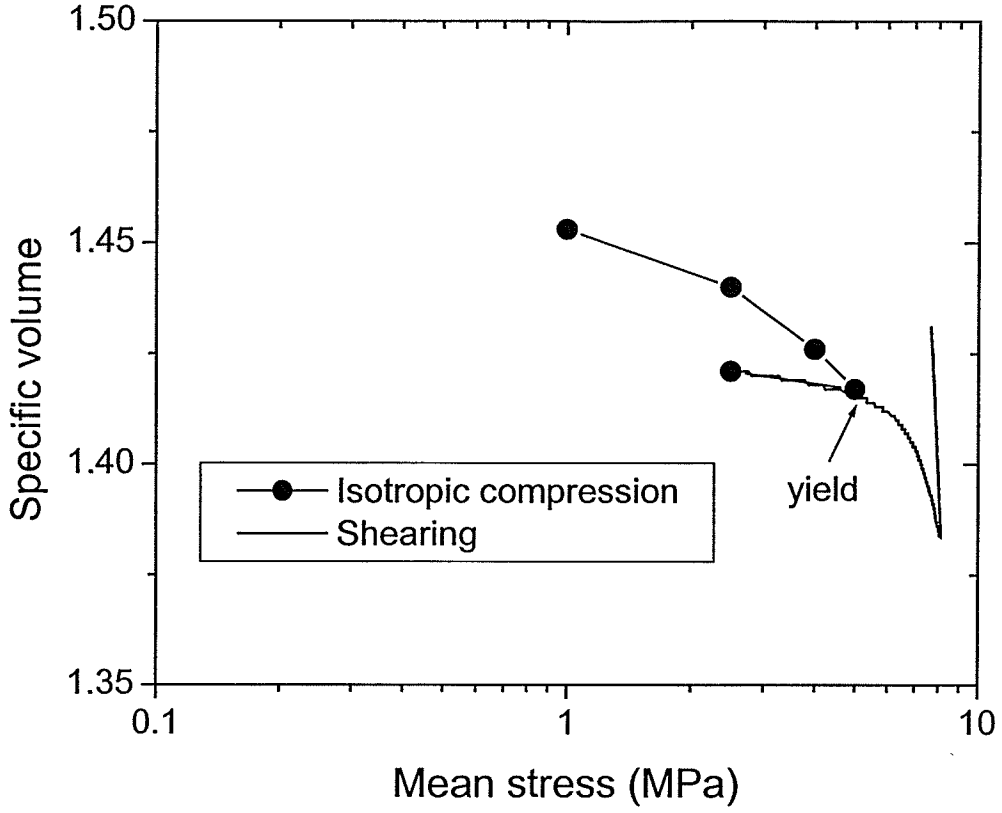

Figure 6.39 Specific volume during all phases of triaxial testing of DA-020 at 80 MPa target suction

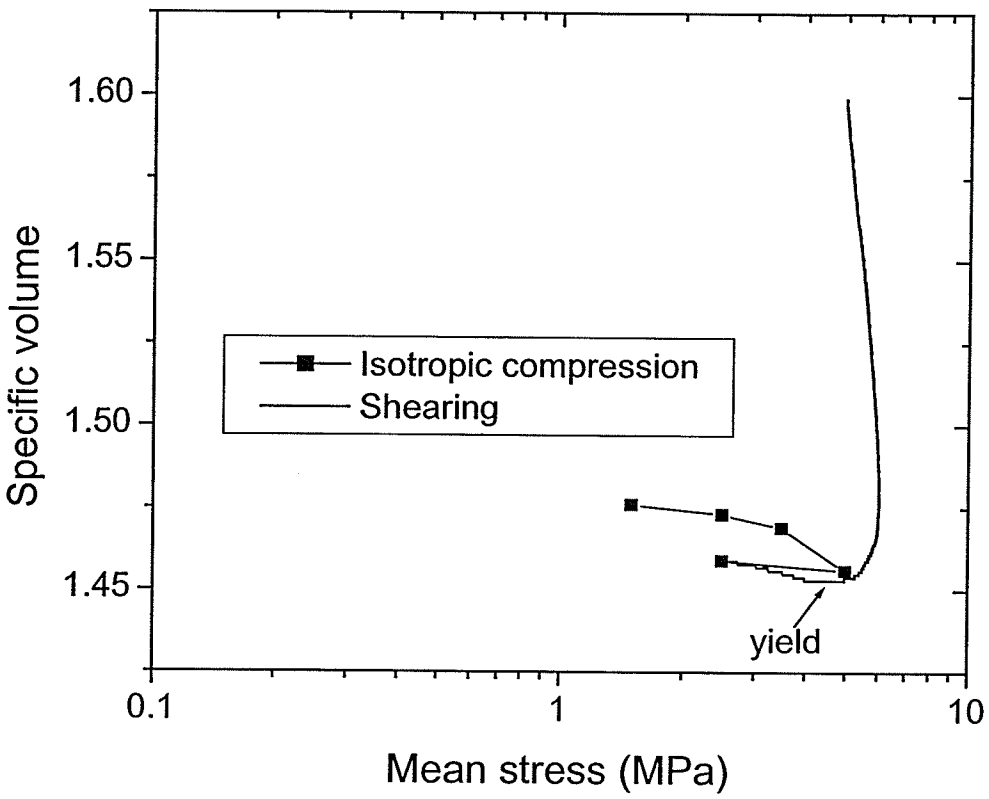

Figure 6.40 Specific volume during all phases of triaxial testing of DA-028 at 160 MPa target suction (3:1 stress path)

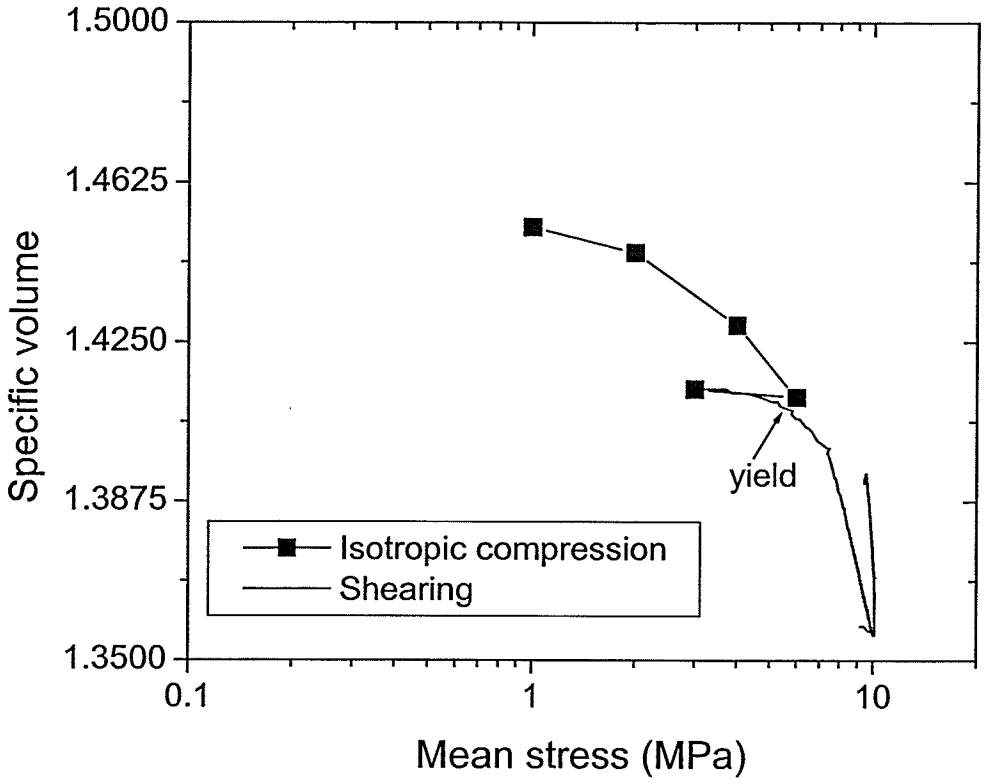

Figure 6.41 Specific volume during all phases of triaxial testing of DA-012 at 160 MPa target suction

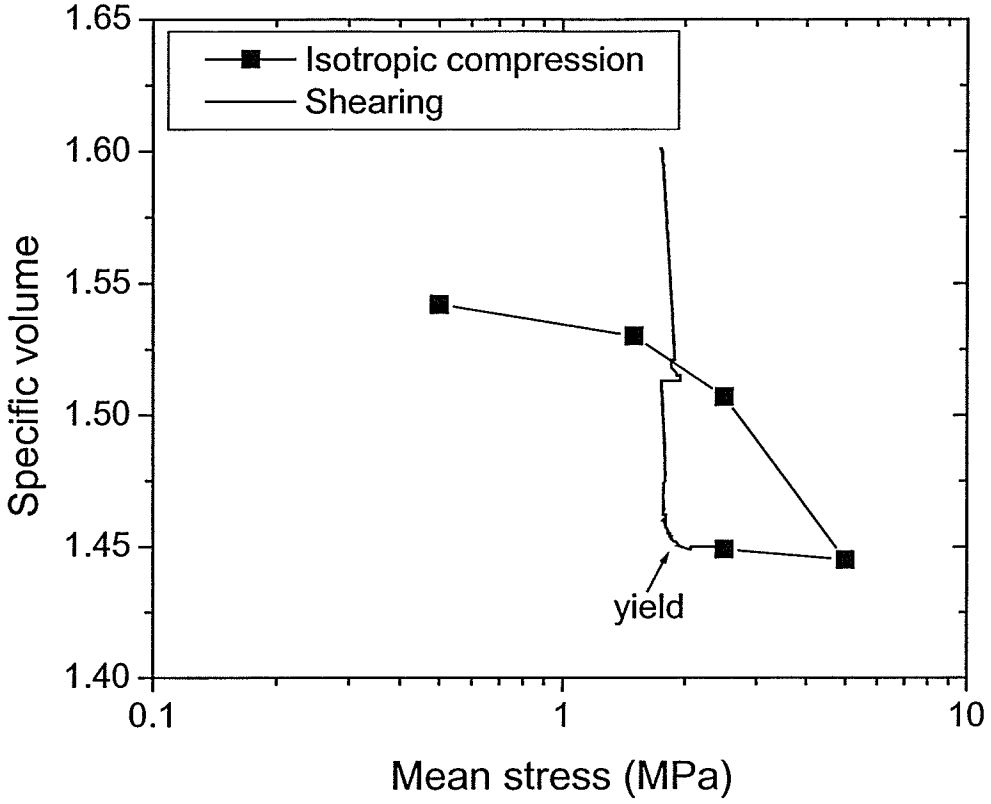

Figure 6.42 Specific volume during all phases of triaxial testing of DA-025 at 10 MPa target suction

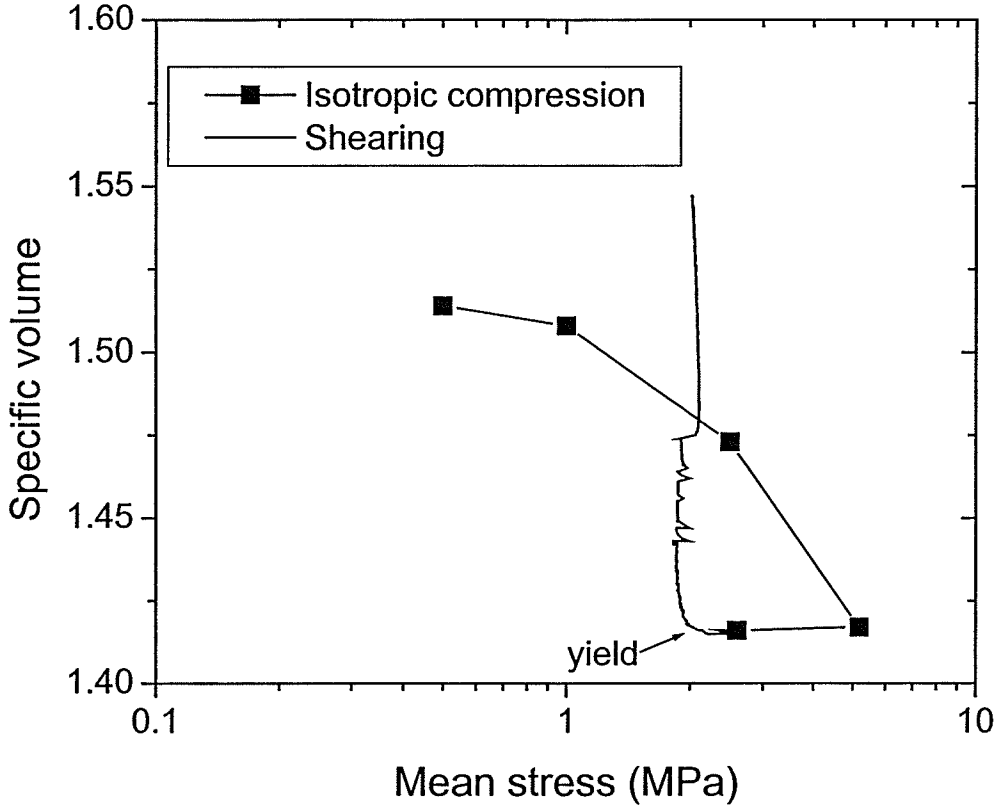

Figure 6.43 Specific volume during all phases of triaxial testing of DA-009 at 10 MPa target suction

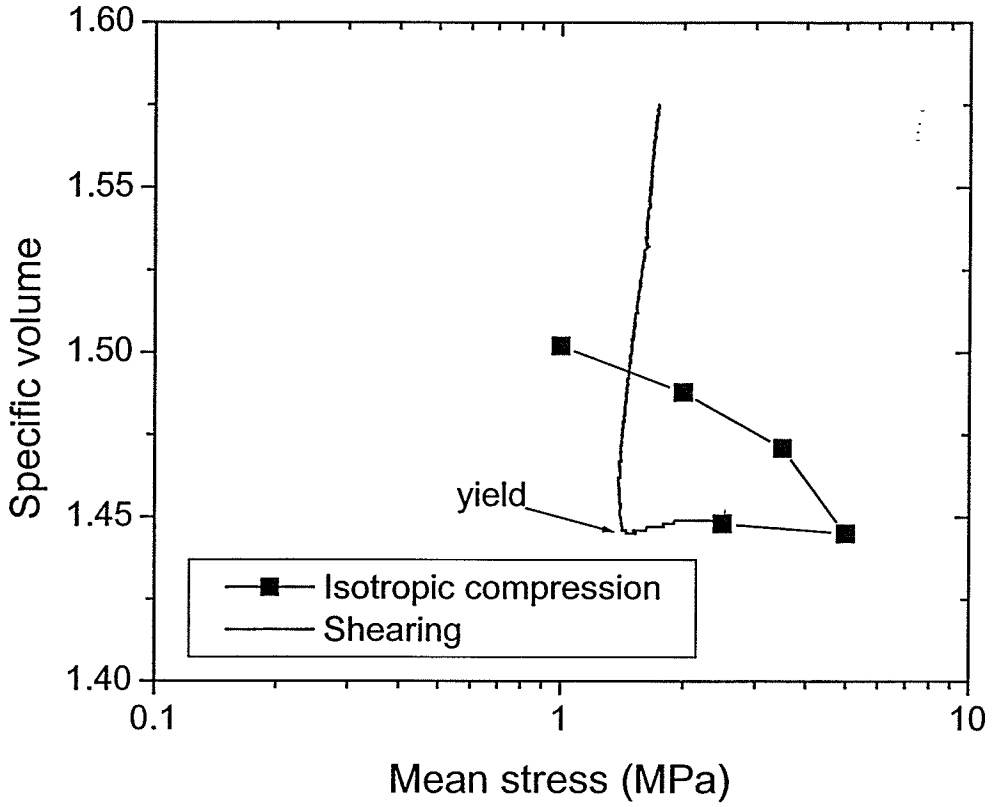

Figure 6.44 Specific volume during all phases of triaxial testing of DA-034 at 20 MPa target suction

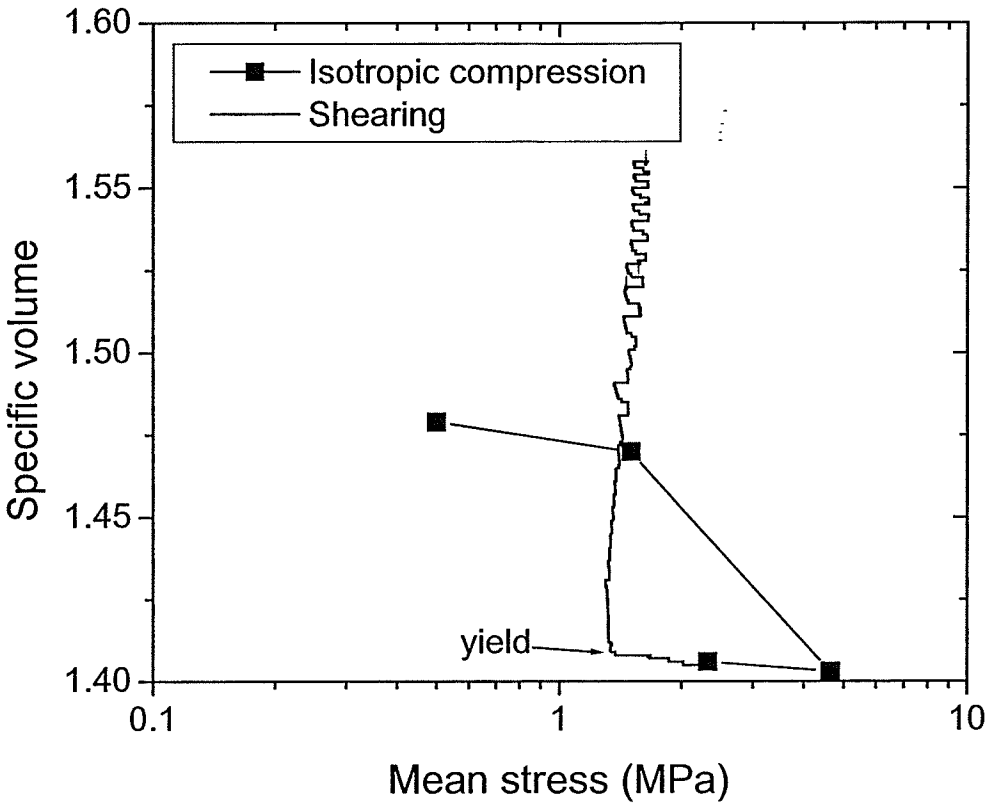

Figure 6.45 Specific volume during all phases of triaxial testing of DA-017 at 20 MPa target suction

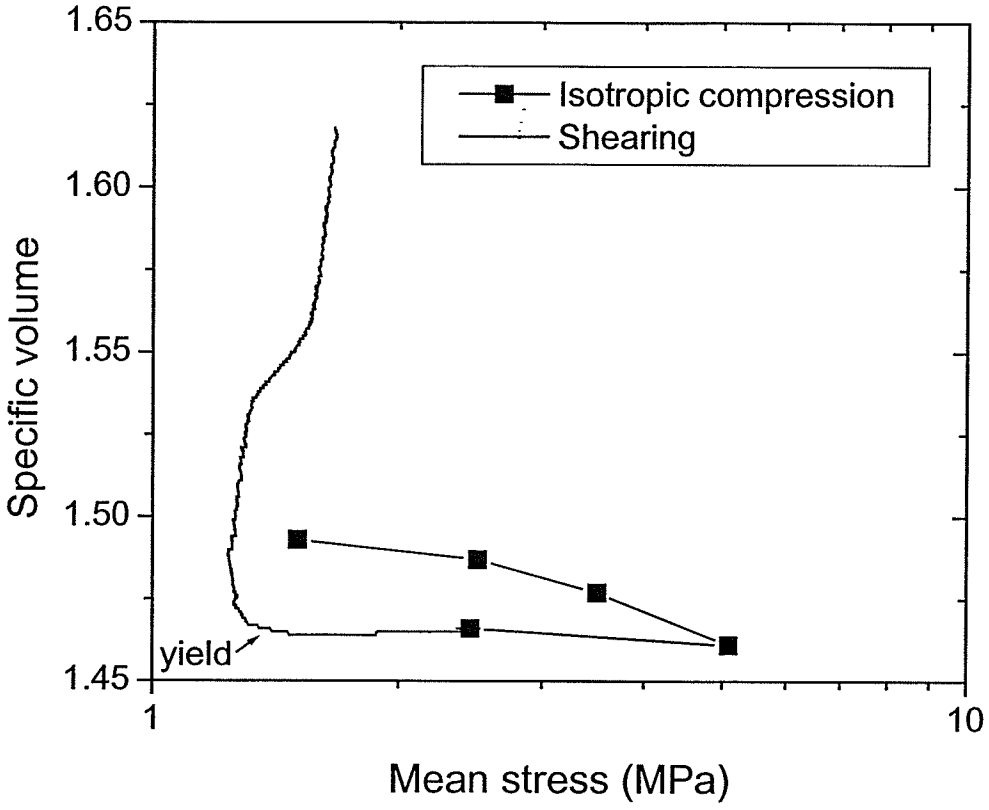

Figure 6.46 Specific volume during all phases of triaxial testing of DA-032 at 40 MPa target suction

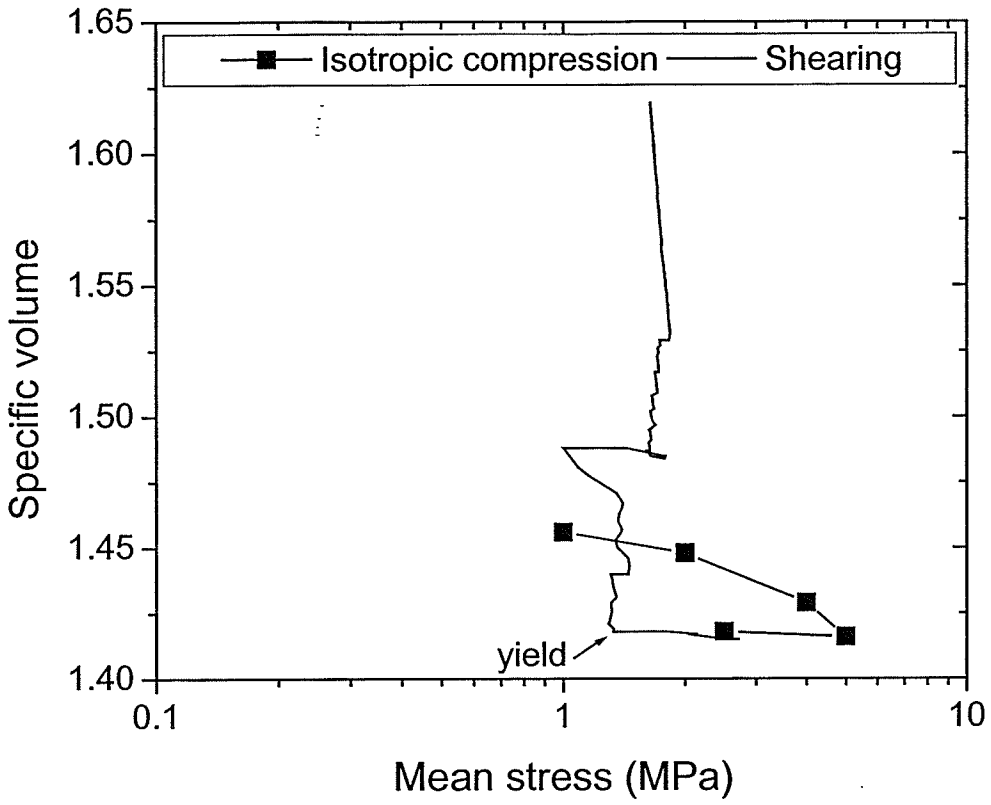

Figure 6.47 Specific volume during all phases of triaxial testing of DA-015 at 40 MPa target suction

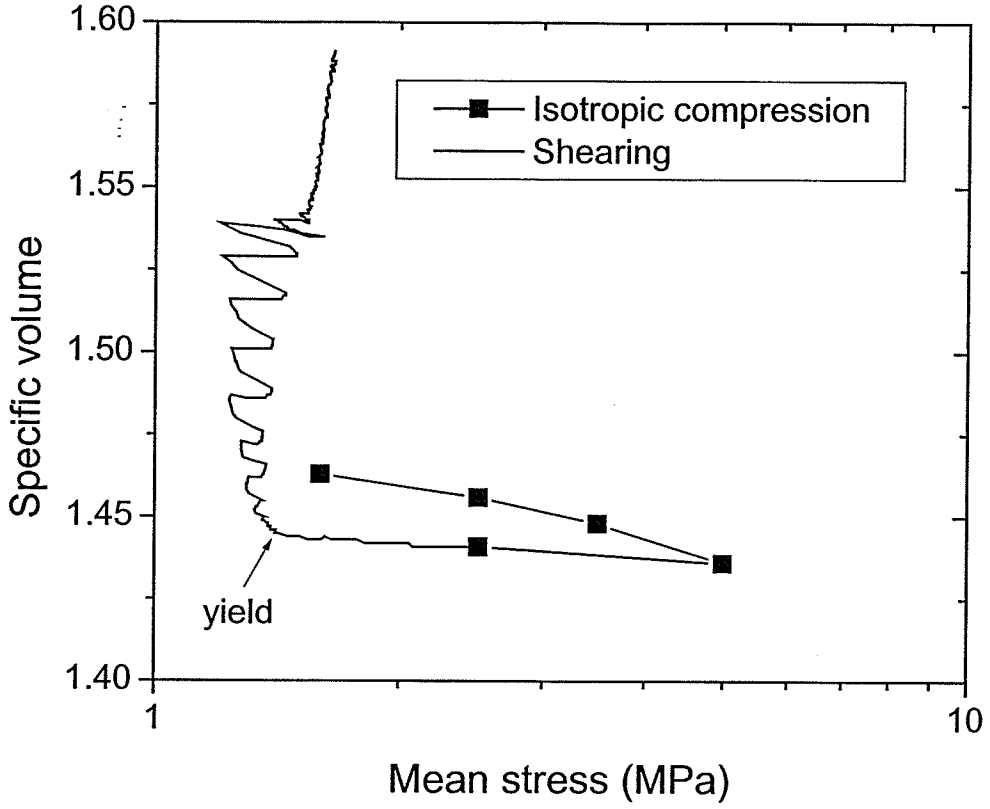

Figure 6.48 Specific volume during all phases of triaxial testing of DA-038 at 80 MPa target suction

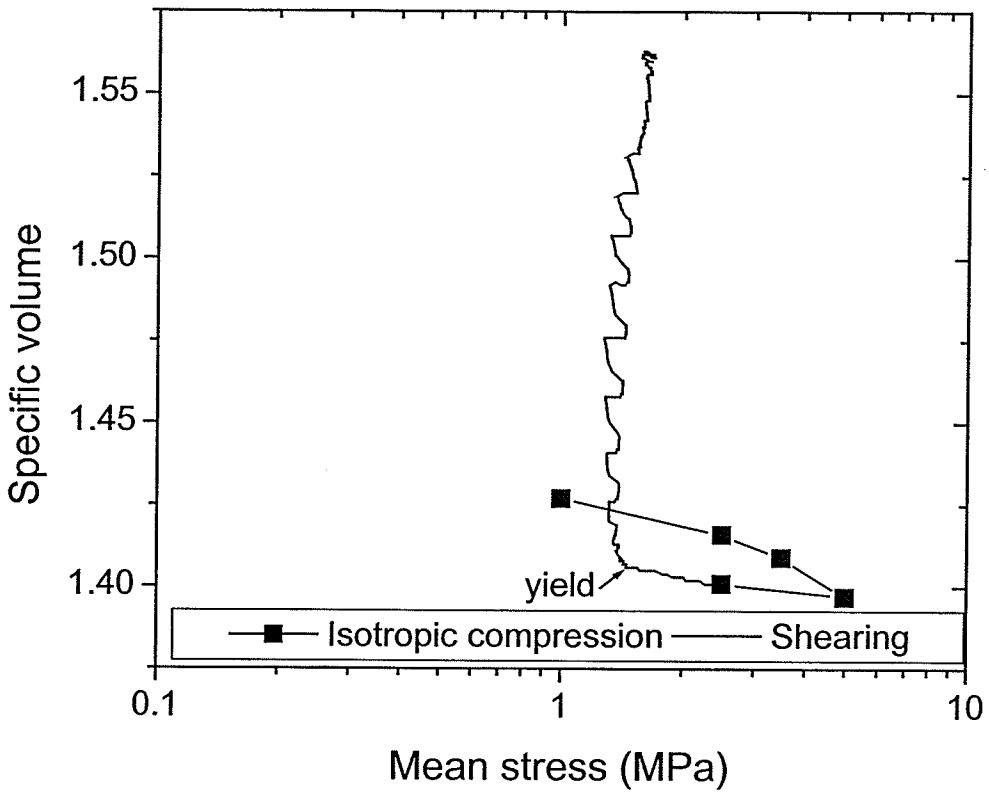

Figure 6.49 Specific volume during all phases of triaxial testing of DA-021 at 80 MPa target suction

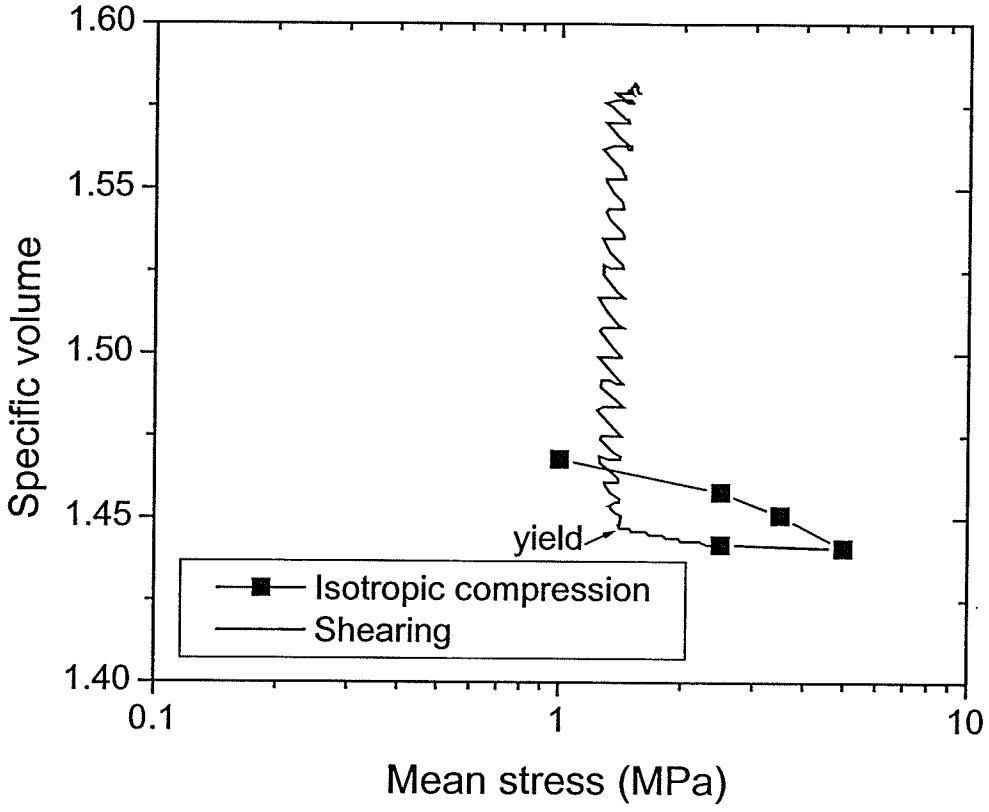

Figure 6.50 Specific volume during all phases of triaxial testing of DA-029 at 160 MPa target suction

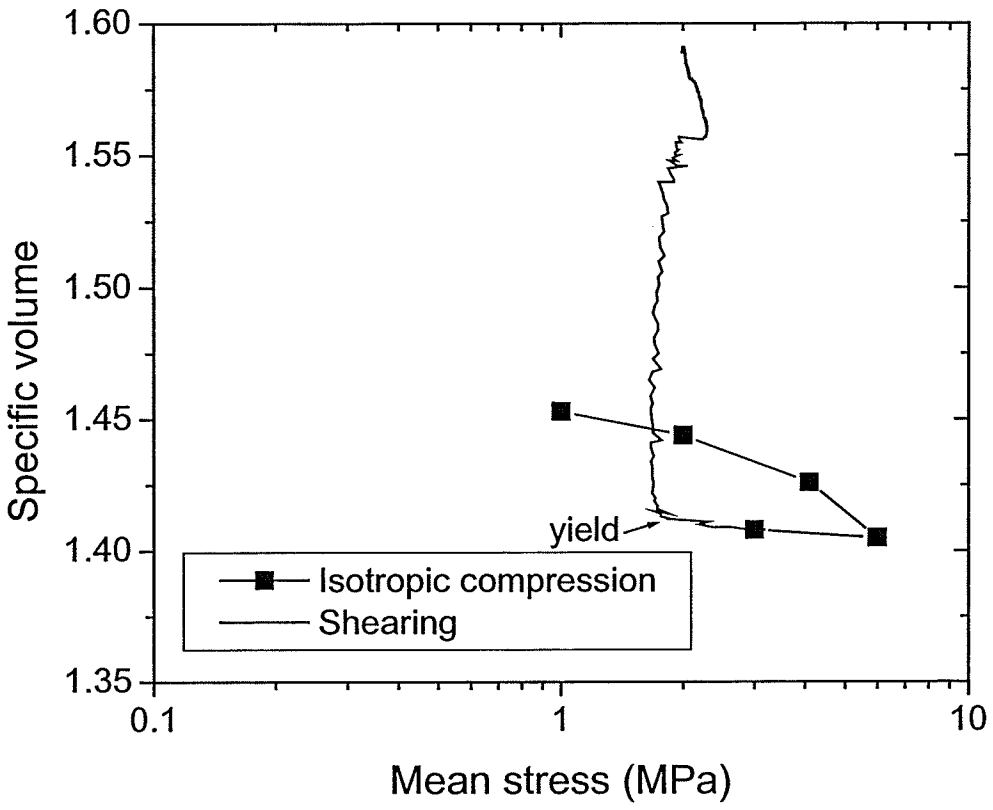

Figure 6.51 Specific volume during all phases of triaxial testing of DA-011 at 160 MPa target suction

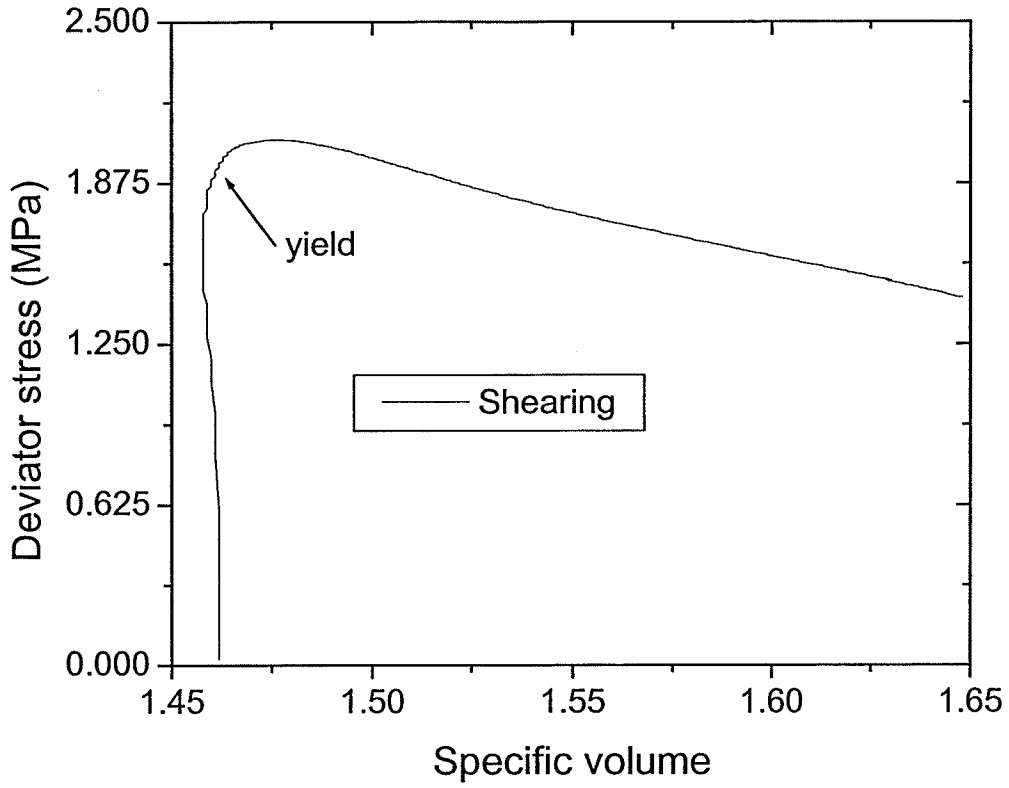

Figure 6.52 Deviator stress versus specific volume during triaxial shearing of DA-024 at 10 MPa target suction

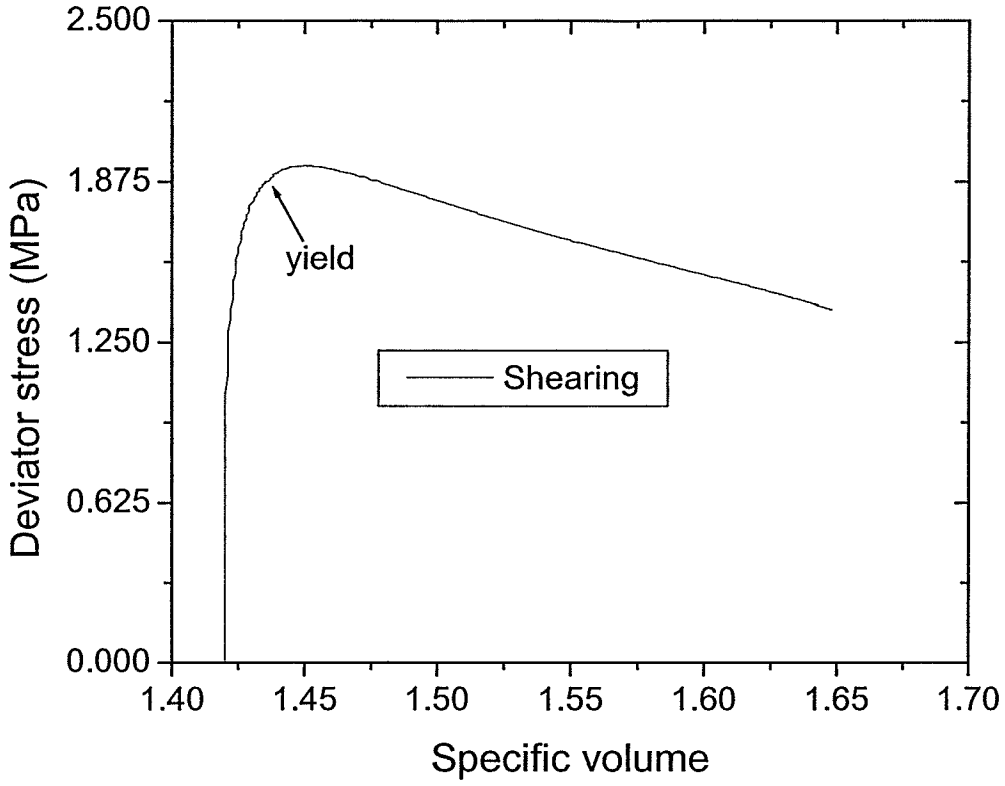

Figure 6.53 Deviator stress versus specific volume during triaxial shearing of DA-007 at 10 MPa target suction

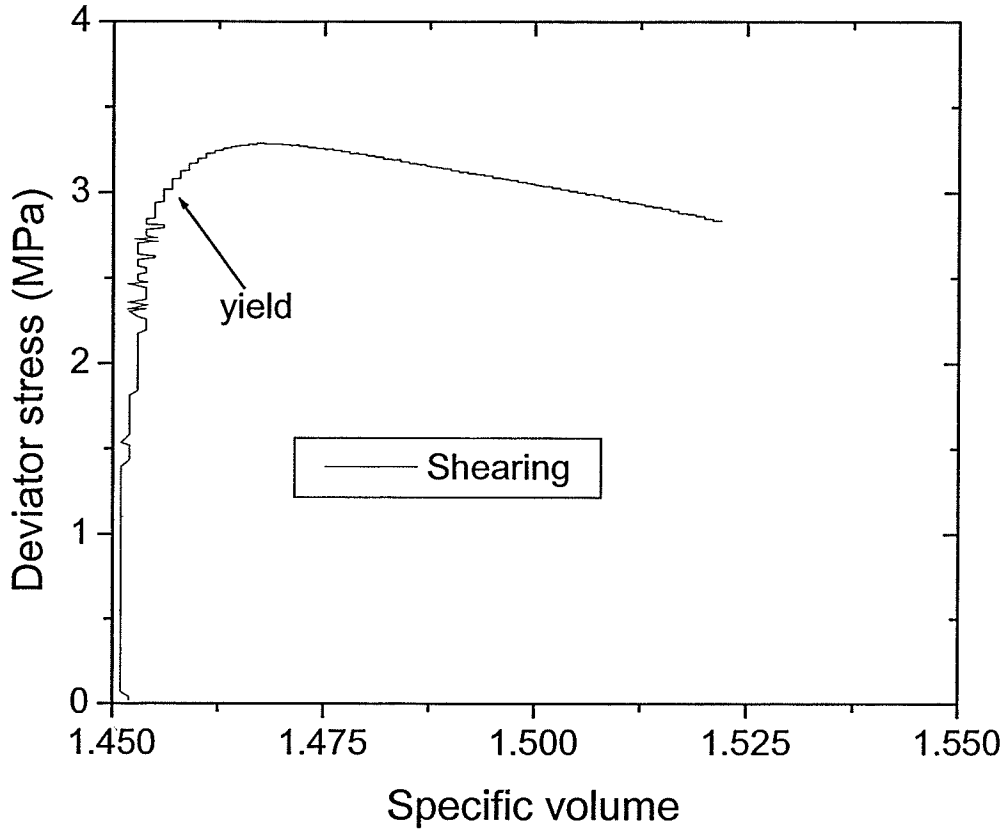

Figure 6.54 Deviator stress versus specific volume during triaxial shearing of DA-033 at 20 MPa target suction

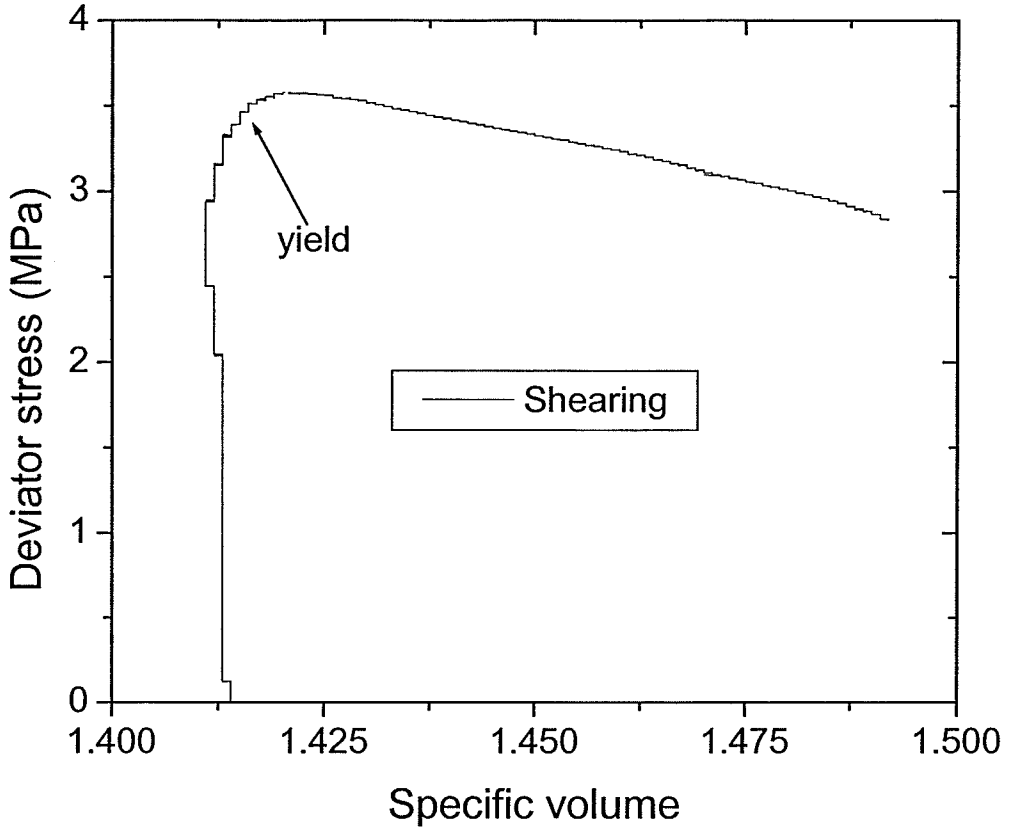

Figure 6.55 Deviator stress versus specific volume during triaxial shearing of DA-016 at 20 MPa target suction

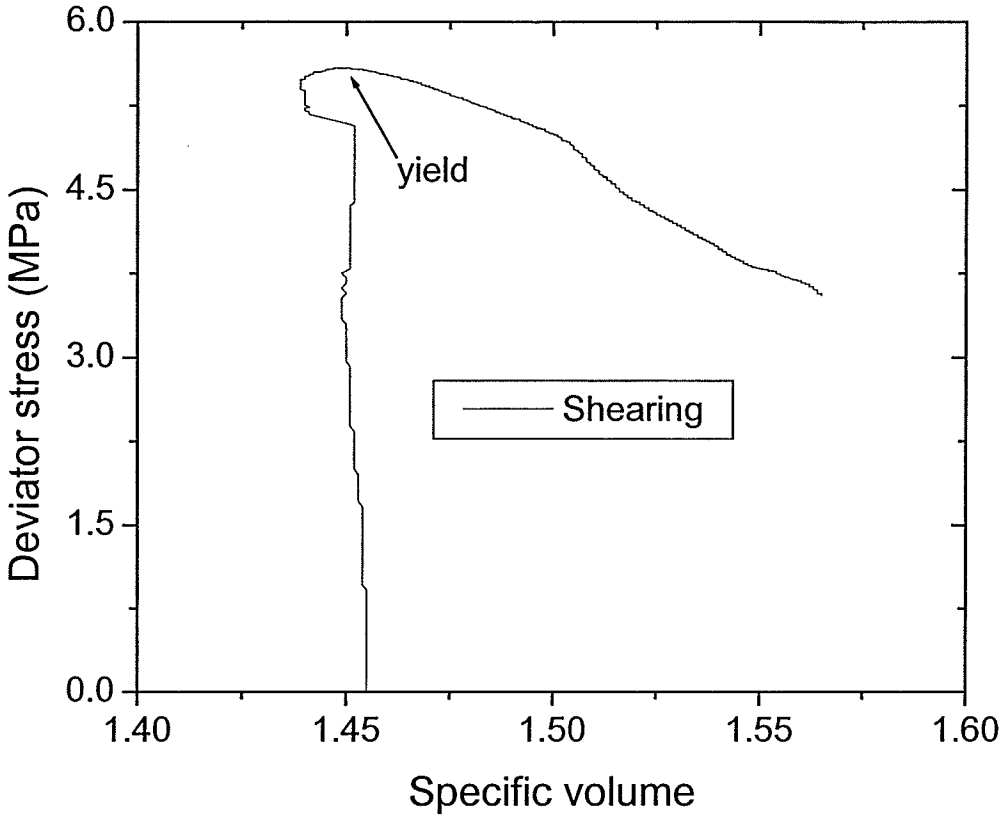

Figure 6.56 Deviator stress versus specific volume during triaxial shearing of DA-030 at 40 MPa target suction

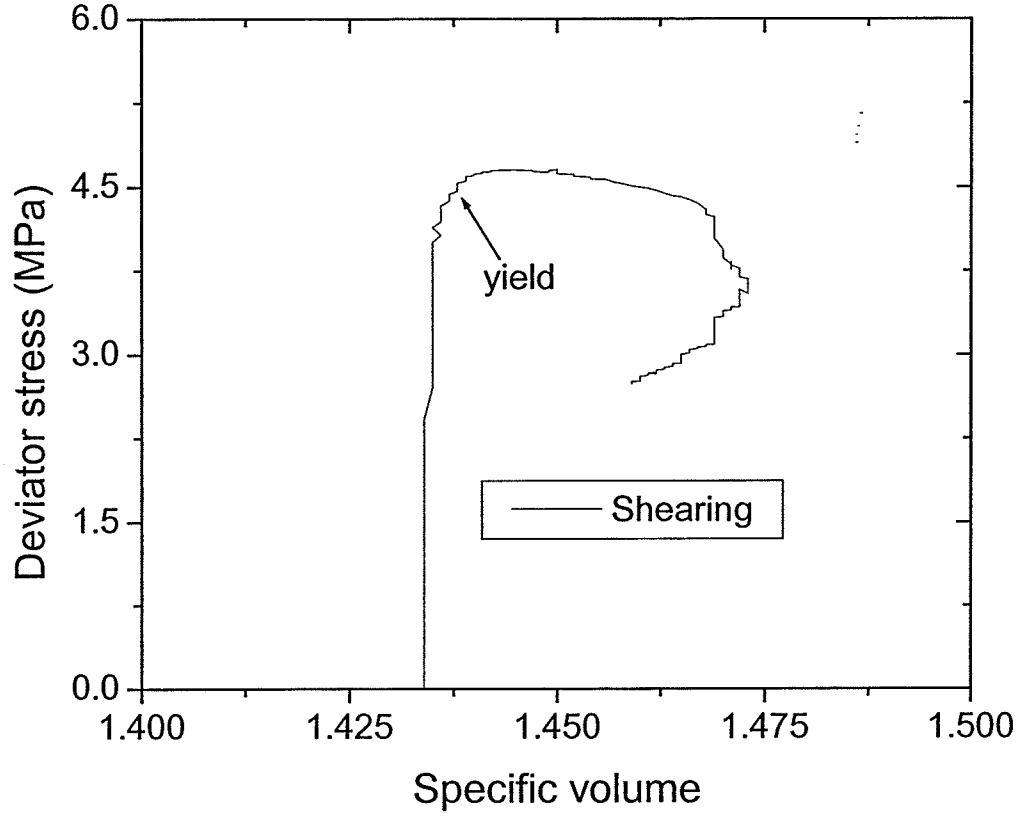

Figure 6.57 Deviator stress versus specific volume during triaxial shearing of DA-013 at 40 MPa target suction

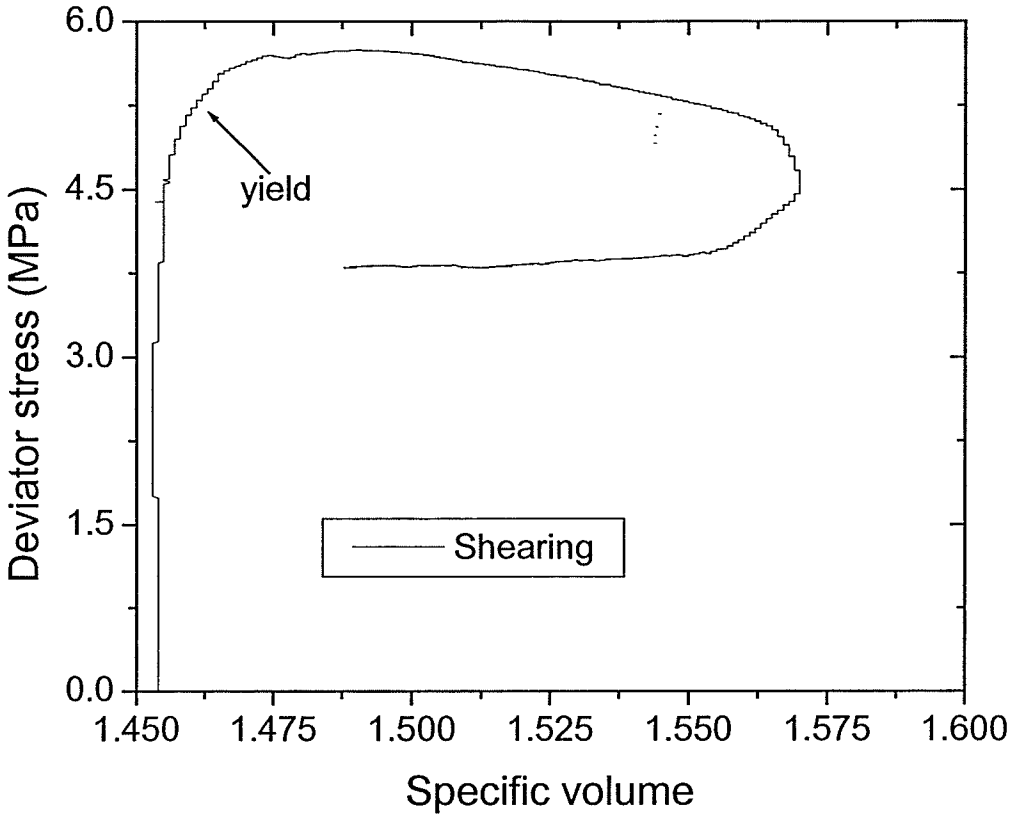

Figure 6.58 Deviator stress versus specific volume during triaxial shearing of DA-036 at 80 MPa target suction

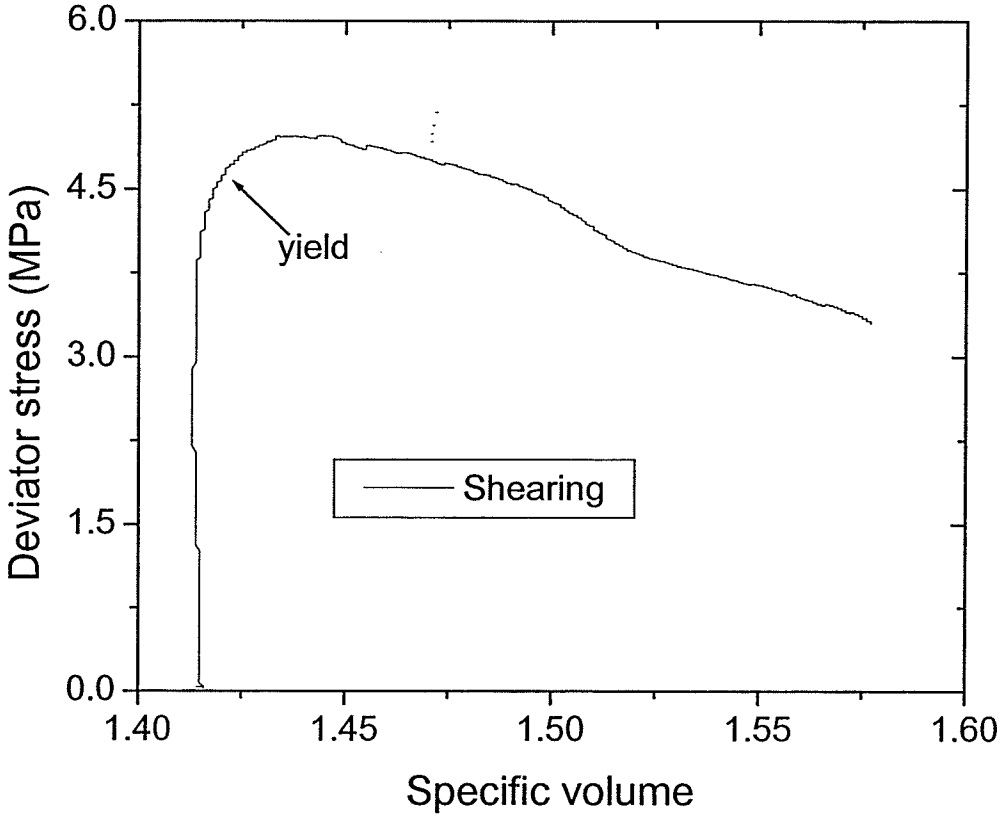

Figure 6.59 Deviator stress versus specific volume during triaxial shearing of DA-019 at 80 MPa target suction

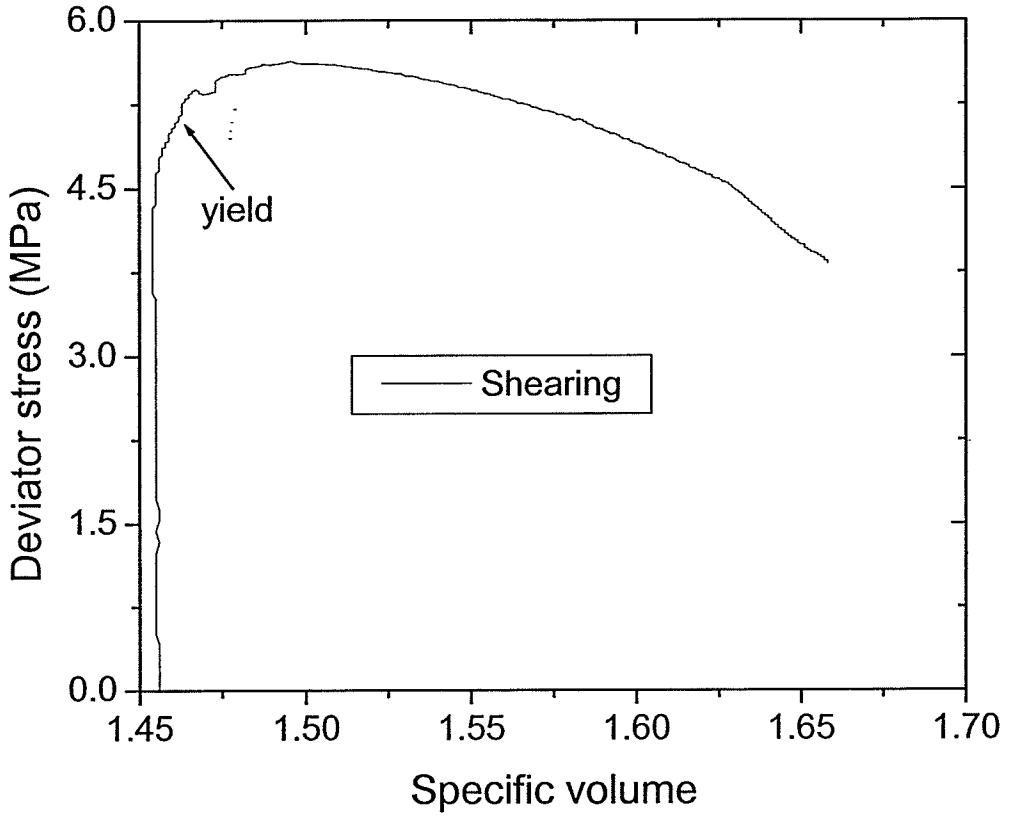

Figure 6.60 Deviator stress versus specific volume during triaxial shearing of DA-027 at 160 MPa target suction

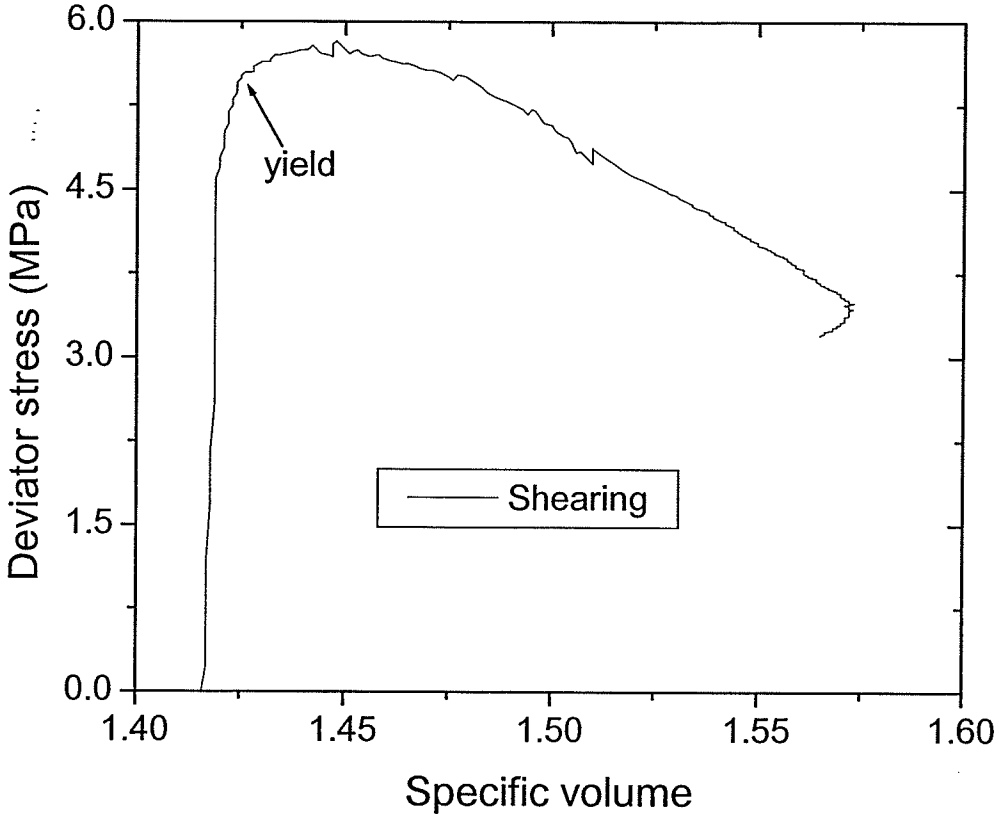

Figure 6.61 Deviator stress versus specific volume during triaxial shearing of DA-010 at 160 MPa target suction

7.0 HYDRAULIC CHARACTERISTICS OF BUFFER

7.1 Introduction

In unsaturated soil, the permeability is significantly affected by combined changes in void ratio and degree of saturation (as reflected for example by water content) of the soil (Fredlund and Rahardjo, 1993). Because pore spaces in unsaturated soil de-saturate as suctions increase, the path available for liquid water flow reduces, thus reducing the permeability. There are many models used to predict permeability of unsaturated soil, including those presented by Brooks and Corey (1964), van Genuchten (1980), and Fredlund and Xing (1994). The common bond between these models is the use of the SWCC for the predictions. The pore size distribution of the soil forms the foundation of the prediction of the permeability. Before models can be used for prediction purposes, the initial state of the soil must be defined. The initial state of the specimens in this program was presented in Chapter 5.

In the deep geologic repository concept, buffer will be expected to transmit heat from waste containers to the surrounding rock. Buffer will also form a barrier to inhibit the transport of potential contaminants in groundwater. Since heat and moisture flow are coupled processes, the temperature gradient that is expected to develop in the buffer will cause drying near the container and wetting near the rock. In the field application, the buffer will be placed in an unsaturated state. Since the processes of wetting and drying affect the hydro-mechanical characteristics of the buffer material significantly (Graham *et al.* 1997), an

understanding of the unsaturated flow characteristics of the buffer is needed if the behaviour of the proposed sealing system is to be understood.

This chapter examines the hydraulic characteristics of buffer. The experimental program includes measurement of the water content distribution in buffer as a function of suction level and time after being subjected to selected suctions above the as compacted condition. The results provide new measurements of the hydraulic properties of unsaturated buffer.

7.2 Suction Environments

As in the shrinkage and triaxial testing, suctions were applied using relative humidity environments. For this testing program suctions of 40, 80, and 160 MPa were chosen to be applied to the specimens. The specimens were removed from the desiccators after 5, 15, and 30 days. Table 7.1 summarizes the suctions in each desiccator after the removal of each specimen from each desiccator.

7.3 Quality Control

Specimens in this program were larger than any previous specimens compacted to RBM parameters (100 mm high by 100 mm diameter). As mentioned earlier, this required modification to the existing static compaction ram and development of a new static compaction mould. Verification of the compaction process had to be carried out to ensure that specimens met RBM parameters. To do this, two specimens (HC-001 and HC-002) were used to verify and potentially modify the compaction process. Figure 7.1 shows the water content distribution of both of the specimens. This figure shows that the

process provides a relatively uniform distribution of water content for each lift of the specimen and it closely matched the target water content of 19.4%.

7.4 Results

Specimens were measured and weighed before being placed in the desiccators and again following removal from the desiccators. After the measurements were taken, specimens were cut into pre-defined regions and the water content distribution was measured. Results of the water content distributions are shown in Figures 7.2 through 7.4 for 40, 80, and 160 MPa target suctions respectively.

As shown by the figures of water content distribution, water contents decrease with time as expected. Bearing in mind the imposed boundary conditions, the water content distribution is fairly uniform throughout each layer, with only a small decrease in water content with distance from the centre to the edge of the specimens. Another important feature is that equilibrium has not been reached by any of the specimens after 30 days in the desiccator. When comparing water contents from the SWCC for Saskatchewan buffer presented in Chapter 5 after equilibration, to the water contents after 30 days for the large specimens, the water contents are still higher than the equilibrium water content at the same suction level. This lack of equilibrium may be due to the larger specimen size. Tang (1999) showed that 30 days should produce equilibrium between smaller 50 mm specimens and the headspace in the desiccator. Further work must be undertaken to examine this apparent discrepancy. Figure 7.5 shows the water content of each specimen versus time

for all three target suction levels. This figure shows that as time increases the water content in the specimen decreases at each suction level.

Darcy's Law was used ($Q = k \times i \times A$) to calculate the permeability of the buffer at each suction level. Since this research into the hydraulic characteristics of buffer is very preliminary, Darcy's Law was used to simplify the description of the hydraulic behaviour of buffer so to provide future research efforts into investigating buffer hydraulic behaviour with a starting point. This was completed by converting the mass of water that was lost while in the desiccator to a volume of water and dividing by the length of time in the desiccator, to calculate the flow (Q). The gradient (i) was calculated based on the initial head in the specimen (4 MPa) and the final head in each desiccator at the end of the time interval. It is realized that this is a simplification of the gradient, since the gradient changes with time as moisture content changes, which is a transient problem, and is being investigated as a steady state problem. The area (A) was calculated using the measured dimensions of each specimen. Table 7.2 summarizes the calculated permeabilities over each time interval.

As shown by the results in the table, permeability decreases with increasing suction. It must be pointed out that the decrease in permeability is relatively small and could be considered within experimental error of the testing program. Also, the calculated permeabilities are greater than the saturated permeability found by Dixon *et al.* (1999) for compacted buffer material (10^{-13} m/s). The difference in permeabilities is associated with the fact that

Dixon *et al.* (1999) used fluid to find the permeability. In these tests, the mass transfer is postulated to be associated with vapour flow and not liquid flow.

Kirkham (1995) and Hume (1998) showed that at degrees of saturation from 80 to 90%, there was little resistance to gas breakthrough in compacted bentonite materials. This suggests there are continuous air passages in unsaturated specimens with S_r < 90%. Existence of a continuous air phase results in there being little to no resistance to movement of vapour through the macropores. Specimens used in this testing program were compacted to a degree of saturation of approximately 85%. Therefore, continuous air phases would be expected to occur in these specimens. With a continuous air phase, once specimens were placed in the desiccators, the lower water potential of the partial vapour pressure would cause vapour to migrate into the macropores very quickly. This would result in the uniform water content distributions that were observed throughout the specimens after each of the drying periods. Once the water potential of the desiccator solution was present in the macropores, the time dependent drying of the micropores would occur at a slower rate as has been shown in the data.

The validity of this mechanism can be confirmed using specimens compacted to 100% saturation. In fully saturated specimens the water fills the voids and there is no air phase. In saturated specimens it was expected that water content distributions would remain saturated near the centre and then decrease towards the outer edge as time spent in the desiccator increased. This would resemble a gradient or flow of water from high head (low suction, the

centre of the specimen) to low head (high suction, applied at the edge of the specimen).

This hypothesis was tested using two additional specimens. Figure 7.6 shows the results of drying for two compacted saturated specimens after defined time intervals. These specimens were compacted to a target water content of 22.8%, which produced a 100% degree of saturation. The initial dimensions were 100 mm in height by 100 mm in diameter. Figure 7.6 shows a radial water content distribution that suggests a gradient of potential in the specimens. As time progresses, the distribution becomes more uniform and reflects the change of the specimen from a saturated state to an unsaturated state.

Initial planning included numerical modeling of the time dependent movement of moisture in unsaturated specimens. Since the results indicated that the lower water potentials were reaching the macropores almost instantaneously, this problem can be characterized as a dual flow application in both the macropores and micropores. The numerical modeling tools initially planned to undertake this work are not capable of modeling this type of application and as such the modeling was not conducted. Also, it must be remembered that the molding water content determines the micropore distribution and hence the development of suctions in these materials. Therefore using saturated specimens to represent unsaturated materials must be done very thoughtfully since the macropore and micropore distributions will be different.

7.5 Summary of Results

The previous sections presented an introductory investigation into the hydraulic behaviour of buffer for the purpose of serving as a starting point for future research efforts at the University of Manitoba into the hydraulic behaviour of buffer. Also presented was the drying behaviour of buffer compacted to RBM parameters and then subjected to increased suction. Water contents were found to decrease with time as expected. However, the distribution of water contents did not appear to vary appreciably with spatial distribution in the radial direction. This was not consistent with results of thermally-induced drying where a water content gradient was measured during the tests (Graham *et al.* 1997). The tests confirm that a continuous air phase exists in specimens with $S_r < 85\%$ resulting in the vapour pressure being transmitted throughout the specimen immediately following placement in the relative humidity environment. (Work by Graham *et al.* (2002) shows that continuous air passages can be found when $S_r < 92\%$.)

With further evidence of a continuous air phase in unsaturated buffer, this would impact its performance in a deep geologic repository for the storage of waste materials. A continuous air phase in the buffer would present a preferential path for vapour flow of contaminants. This could potentially allow contaminants to escape the repository and enter the groundwater should a container rupture during the lifetime of the repository.

Sample	S_i (MPa)	Δt (days)	S_f (MPa)
HC-005	40	5	39.1
HC-003	80	5	75.9
HC-004	160	5	147.7
HC-006	40	15	36.6
HC-007	80	15	69.8
HC-008	160	15	135.2
HC-009	40	30	34.9
HC-010	80	30	66.6
HC-011	160	30	128.8

Table 7.1 Suction in desiccators after removal of specimens

Time Interval (days)	40 MPa (m/s)	80 MPa (m/s)	160 MPa (m/s)
0 – 5	8×10^{-11}	8×10^{-11}	7×10^{-11}
5 – 15	9×10^{-11}	7×10^{-11}	5×10^{-11}
15 – 30	6×10^{-11}	4×10^{-11}	3×10^{-11}

Table 7.2 Calculated permeabilities

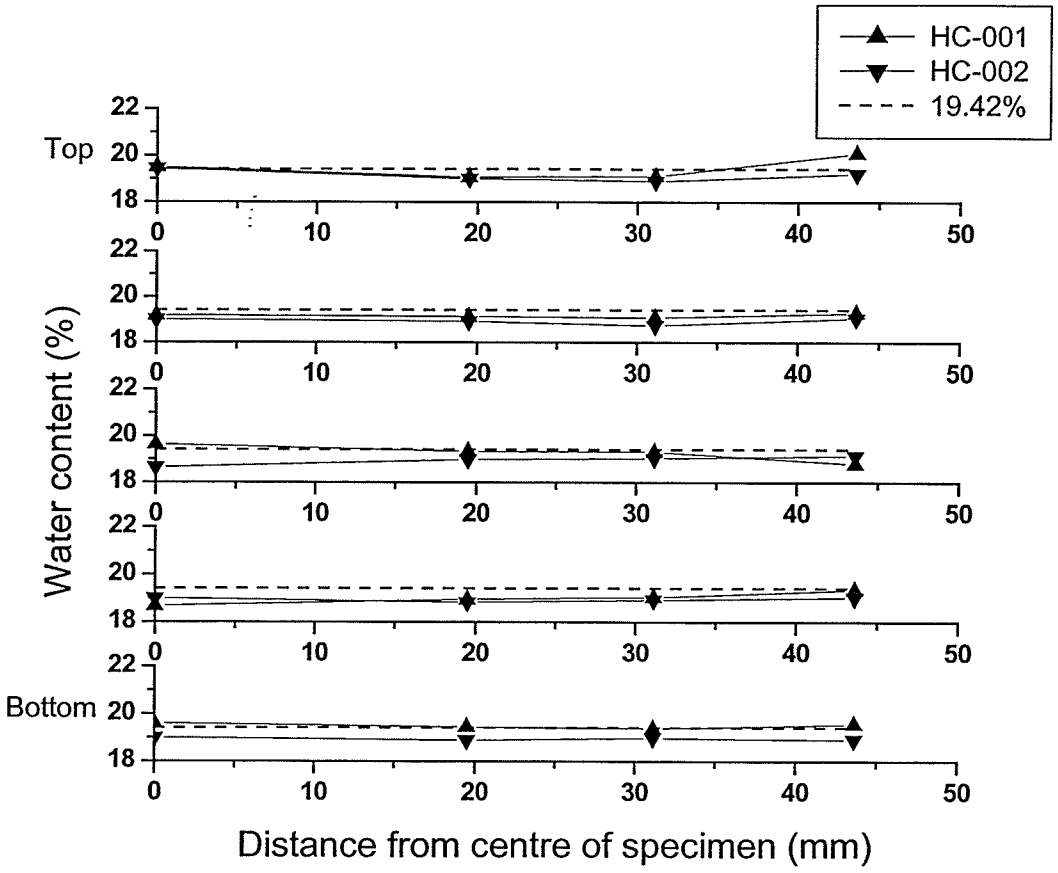

Figure 7.1 Quality control specimens for large specimen compaction procedure

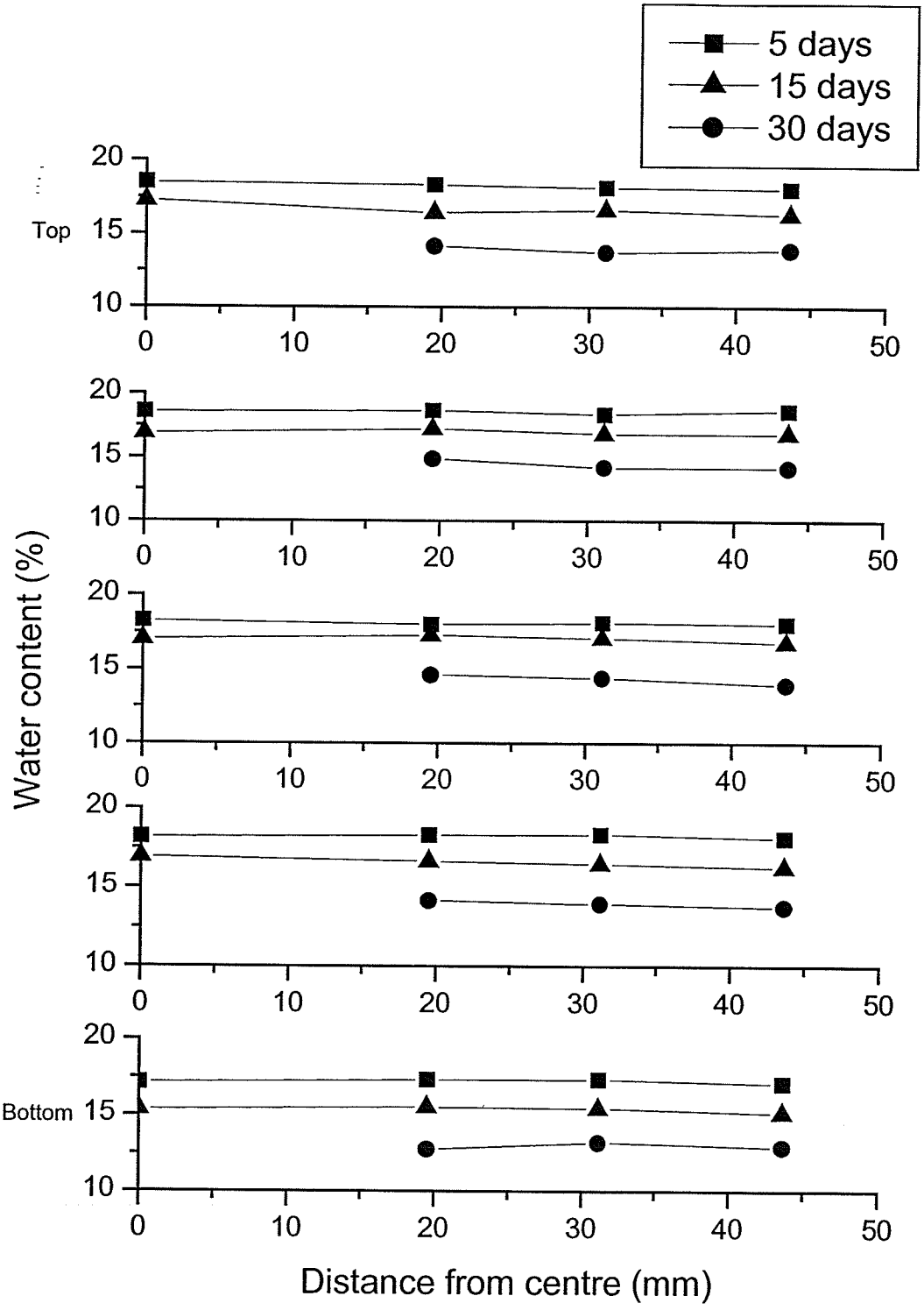

Figure 7.2 Water content distributions for 40 MPa target suction

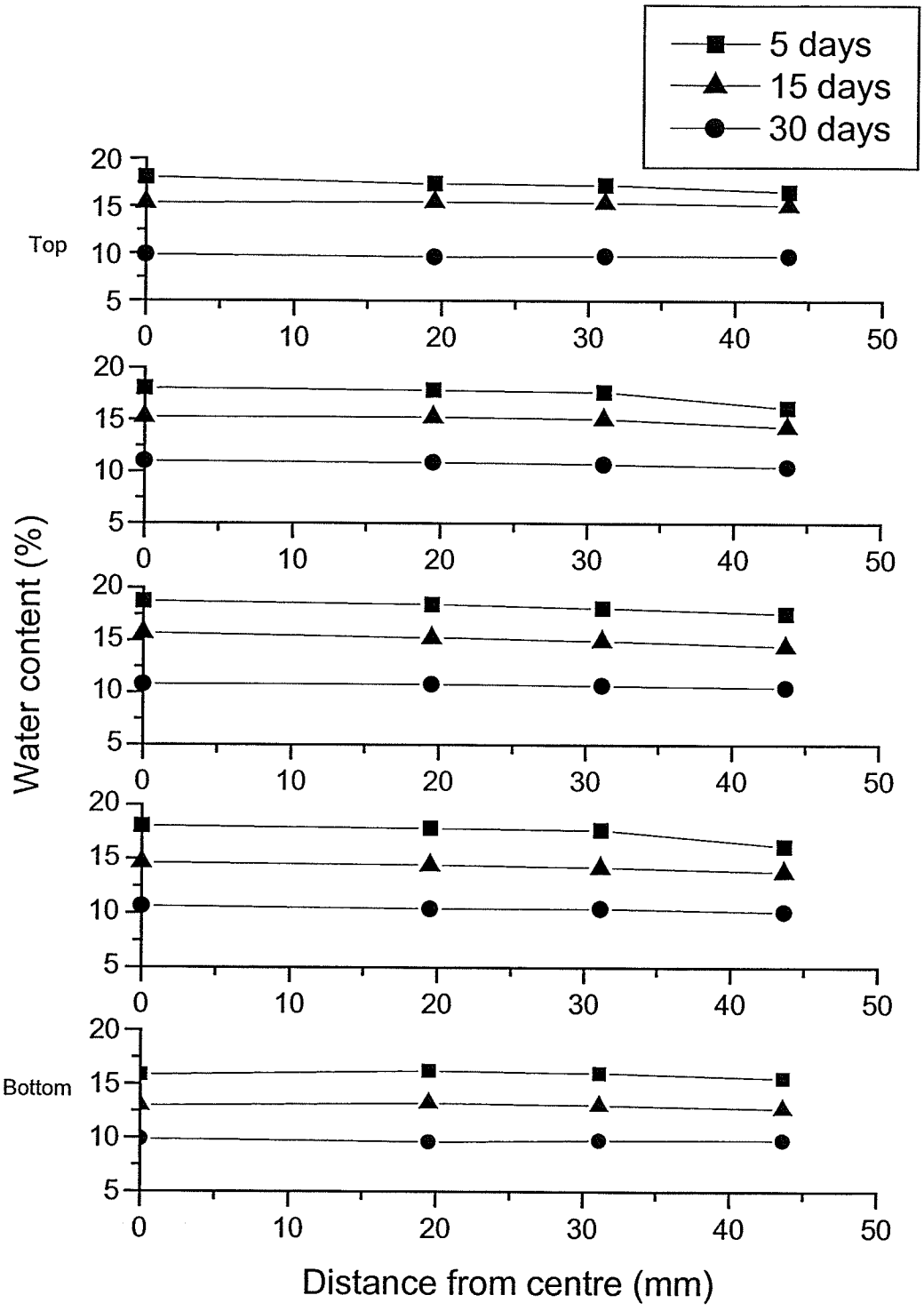

Figure 7.3 Water content distributions for 80 MPa target suction

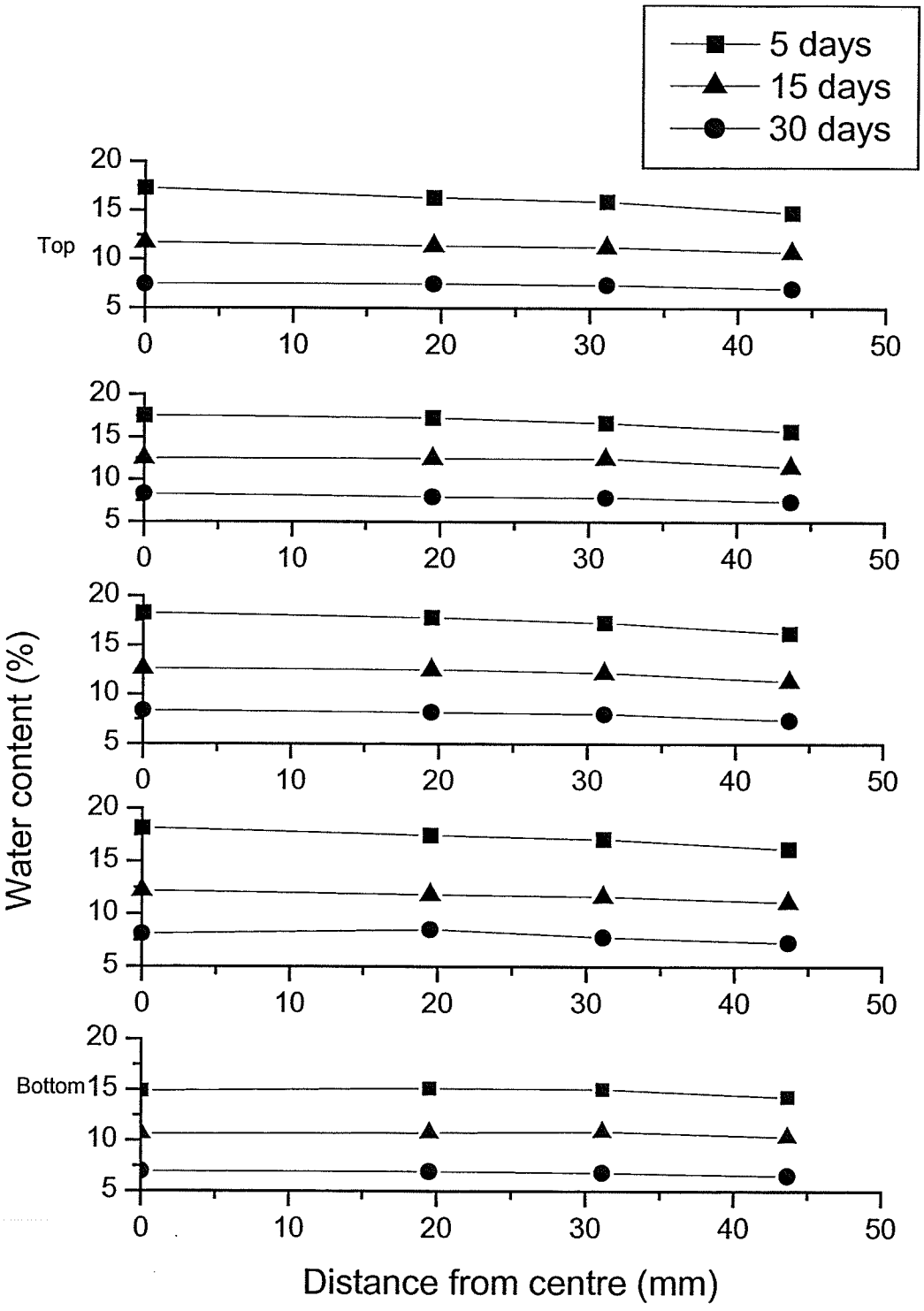

Figure 7.4 Water content distributions for 160 MPa target suction

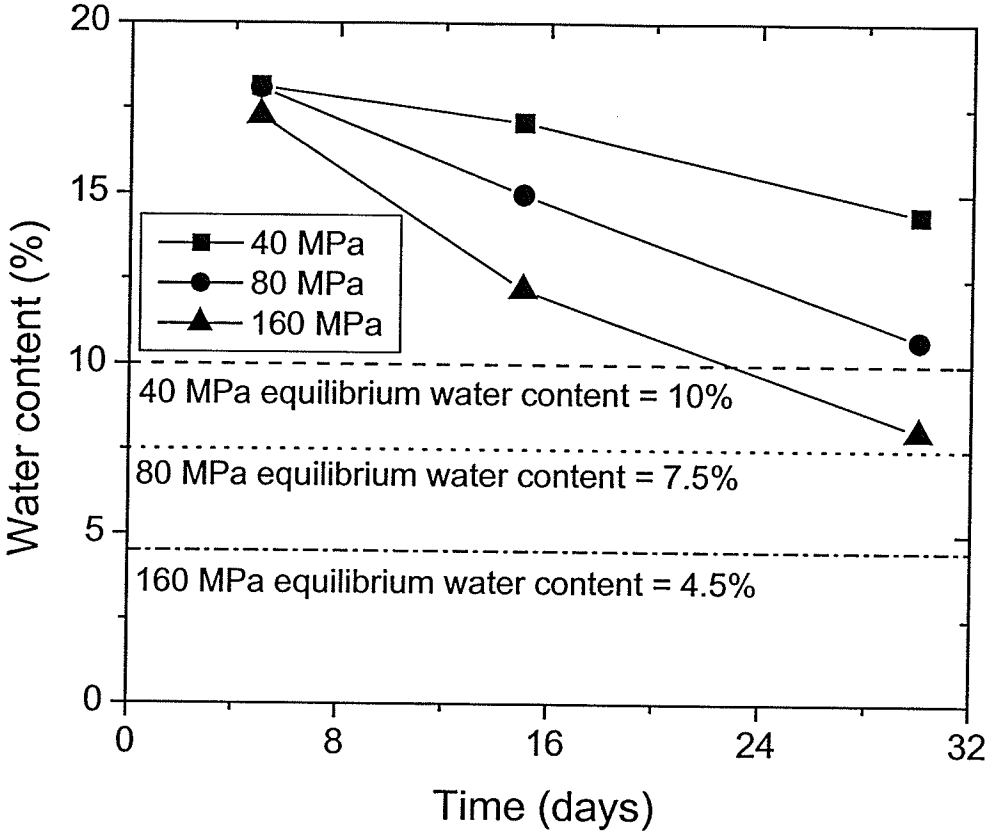

Figure 7.5 Water content versus time for all target suction levels

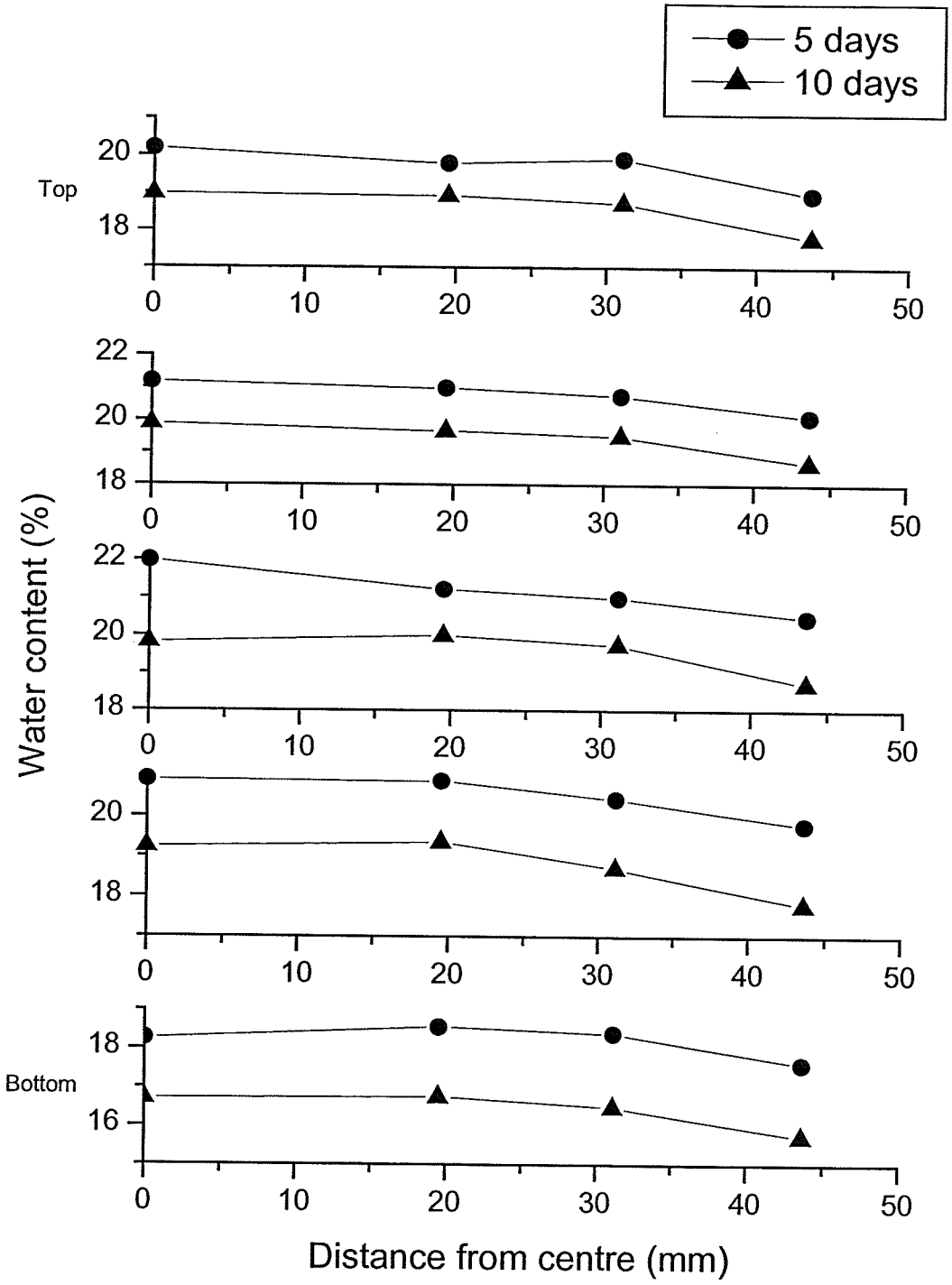

Figure 7.6 Water content distributions for saturated specimens at 80 MPa target suction

8.0 DISCUSSION

8.1 Introduction

Chapters 5, 6, and 7 present new data that describe the mechanical and hydraulic characteristics of two sand-bentonite buffers subjected to varying stress conditions. The two buffers vary only in the constituent bentonite material mixed with the sand, each of which was prepared to RBM parameters. This chapter summarizes the mechanical behaviour interpretations of the preceding chapters and discusses them with respect to existing elastic-plastic models for unsaturated soils and also presents introductory hydraulic characteristics of buffer.

8.2 Shrinkage Characteristics

Results of shrinkage tests have shown that the two buffers show only slightly different behaviour even though the Atterberg limits would indicate large differences in the mineralogical properties. It should be noted that the Atterberg limits do not only depend on the mineralogical properties but also the pore fluid, exchangeable cations, specific surface area, and montmorillonite content of the material. The similar shrinkage characteristics have been attributed to the low water contents (below the plastic limit) that result from high suction levels used in the tests. At higher water contents, larger differences in the mineral activity reflected in the liquid limits would be expected to play a greater role in the mechanical behaviour of the two materials. The soil water characteristic curve and the shrinkage curves showed consistent behaviour over the suction ranges examined. Both materials show a clear limiting volumetric shrinkage associated

with volume strains that are believed to result in stress transfer from the clay to the sand component of the mixture. The transition from clay-dominated behaviour to sand-dominated behaviour during the drying phase has a considerable impact on the mechanical response when specimens are subsequently subjected to external stress conditions.

8.3 Isotropic Compression and Triaxial Shear

Figures 8.1(a) and (b) show idealized graphical descriptions of the testing in p-S-V and p-q-S spaces respectively. These two figures provide a visual representation of stress paths in both p-S-V and p-q-S space. Compaction of the buffer to RBM parameters produces a known initial state (A). Increasing suctions in a relative humidity environment at atmospheric pressure (no confinement, p=0) in each specimen produces the next known state (B) prior to isotropic compression and triaxial shearing. A line connecting these two points (A and B) in p-S-V space (Figure 8.1 (a)) lies in the S-V plane (p=0) and is inclined due to a decrease in volume associated with compression during drying. In p-q-S space (Figure 8.1 (b)) the line is horizontal and lies along the S axis. This shows the need for the two three-dimensional regions to fully describe the behaviour of the buffer.

Under isotropic compression, the specimen continues along a line with slope of κ_i (in log p-S-V space), this line does not lie along a constant suction trace, but one assumed at a slope of $\Delta S/\Delta p = -0.83$ (Tang *et al.* 1997 and Blatz and Graham 2003). The specimen continues until initial load yield (C) is reached. As mentioned earlier, this point (C) lies on the load yield (LY) line and

defines the initial yield state of the material. The yield state is developed by the initial compaction process of buffer materials and is related to the microstructure of the compacted material. In p-q-S space this line (BC) lies in the p-S plane with a slope of $\Delta S/\Delta p = -0.83$. At this point (C), plastic deformations begin to accumulate with further loading, which is represented by movement along a line with slope λ in log p-S-V space to the point of maximum mean stress during isotropic compression (D). This line (CD) represents a boundary in p-S-V space of the volume state surface. In p-q-S space, point (D) lies along the same line as B and C since there has been no application of deviator stress q throughout isotropic compression even though the material may still be anisotropic in nature due to the compaction process. Movement from C to D represents an expansion of the elastic region. Point (D) in p-q-S space also represents a known extent of the stress state surface. The specimen then undergoes isotropic unloading, which brings the specimen back into the elastic region (E) of both state boundary surfaces. This line has a slope of κ_u in log p-S-V space and lies along the same line as (C) and (D) in p-q-S space.

Examination of triaxial shear stress paths allows for a better description of the state boundary surfaces in the p-q-S space. With the commencement of triaxial shearing, the specimen follows one of three stress paths starting from (E). Corresponding to q/p ratio of 1:1 (path 1), constant-p (path 2), or q/p ratio of 3:-1 (path 3). The 1:1 stress path lies along $EF_1G_1H_1$, the constant-p stress path lies along $EF_2G_2H_2$, and the 3:-1 stress path lies along $EF_3G_3H_3$. In either space, point F_1, F_2, or F_3 (depending on path taken) is reached first during triaxial

shearing, which corresponds to yield. Next, the specimen reaches peak, denoted by G_1, G_2, or G_3 depending on the path taken during triaxial shear. Points G_1, G_2, and G_3 are also associated with a further expansion of the elastic region in p-q-S space. After peak, the specimen continues to point H_1, H_2, or H_3, the end-of-test value (critical state).

During triaxial shearing, specimens always progress from yield to peak to end-of-test in either p-S-V or p-q-S space. In p-q-S space, the triaxial shear paths are straight lines at the slope of the q/p ratio and suction is a function of mean stress, p. In p-S-V space, the triaxial shear paths do not lie along a straight line in all cases as in the 1:1 and 3:-1 stress paths. It must be remembered, that even though the rate of shearing kept suction constant, increases or decreases in mean stress, p, (associated with maintaining the stress path) would still result in an assumed decrease or increase in suction ($\Delta S/\Delta p = -0.83$). Therefore yield loci defined by points D, F_1, F_2, and F_3 do not lie along a constant suction plane, but rather a plane with an assumed slope of $\Delta S/\Delta p = -0.83$.

Testing has shown the initial elastic behaviour of the buffer followed by plastic deformations after a well-defined yield point. This fact implies that the material should be examined in an elastic-plastic framework. After examining all the results during all phases of testing, the data support the general shape of the state boundary surface as described by Alonso *et al.* (1990) and later Blatz and Graham (2003) for the volume state space and the general shape of the stress state boundary surface as presented by Wheeler and Sivakumar (1995).

The responses of the materials to mechanical loading of both isotropic and shear stress conditions are again only slightly different. The Wyoming buffer generally showed more compressible behaviour at comparable suction levels. Both materials clearly showed a transition of the material behaviour from low suctions to high suctions. This is consistent with the concept that at low suctions (before limit of shrinkage) the material behaves as a clay-dominated material while after the limit of volumetric shrinkage the material behaves as a sand-dominated material.

The experimental program has shown that although there are slight differences, the Wyoming buffer behaves in a similar fashion to the Saskatchewan buffer under the stress conditions examined in this program. This is important for evaluating which bentonite to use in the design of engineering seals. In addition to the comparison of the two buffers, the mechanical properties of the two buffers have been reported (Chapter 6). The properties will be required for both materials for modeling exercises. Although Saskatchewan bentonite may not ultimately be selected in the final design concept put forward, understanding the properties of the Saskatchewan buffer is important for calibrating and examining the validity of proposed numerical models which can use results from past full-scale experiments (Isothermal and Buffer/Container) where the Saskatchewan bentonite was used. The properties of the Wyoming bentonite will be useful for future predictive modeling and for current model development.

8.3.1 Yield Loci

In order to use models to predict elastic-plastic behaviour of materials, some form of yield loci must be included, which separates elastic behaviour from plastic behaviour. Potential yield loci for the buffers are generated using two different strengths interpreted from the triaxial shearing data. The first locus use the yield values of p and q, which are normalized with respect to the maximum mean stress achieved during isotropic compression, p_c. The second locus examined use peak values of p and q during triaxial shear, which are normalized with respect to p_c. In the case of the specimens sheared along the 1:1 stress path, the modified p_c is used to normalize the peak values of p and q (modified p_c is described in section 6.4.3).

Figure 8.2 and Figure 8.3 show normalized peak and yield values of q and p for specimens of both Saskatchewan and Wyoming buffer at target suctions of 10 and 20 MPa, respectively with the interpreted loci being drawn by hand. Figure 8.4 shows normalized peak and yield values of q and p for specimens of both Saskatchewan and Wyoming buffer at target suctions of 40, 80, and 160 MPa and the interpreted loci were drawn by hand. These specimens have been grouped together because as shown in the figure when normalizing the yield and peak values they tend to cluster together. Again this similar behaviour of specimens above 30 MPa under shear loading is attributed to the transition from a clay-dominated material to a sand-dominated material through the shrinkage occurring during the initial suction stress application. The similar size and shape of the loci generated using either yield or peak values at the different

target suction levels is of particular interest. This is of interest because obtaining peak values from triaxial shear data is much simpler than the interpretation of yield stresses. The figures suggest that the use of the peak strength values for the generation of yield loci would produce similar loci as using yield stress values. The verification of the use of peak strength values instead of yield stress values should be further investigated to ensure that the same loci are produced and also to better define the shape of the yield loci.

Figure 8.5 shows the normalized peak values of q and p data for both Saskatchewan and Wyoming buffers at all suction levels with the loci being drawn by hand. Again this shows the similarity between the peak strengths for the two distinctly different bentonite buffers. As shown there is a transition from a small yield locus at "low" suctions (approximately 10 MPa), which then grows to a larger yield locus for "high" suctions (30 MPa and up). This transition (from small to large locus) is attributed to the location of the buffers with respect to their limit of volumetric shrinkage. Since at "low" suctions the applied suction has not been able to remove enough water to shrink the specimens to the point where the sand particles come into contact, this allows the bentonite clay to dominate the strength of the buffer resulting in a lower strength and yield point. At "high" suctions, enough water has been removed to shrink the specimens to bring the sand particles into contact with each other, thus resulting in higher observed strengths. It should also be remembered that the yield loci are not in constant suction planes, but rather planes with an assumed slope of $\Delta S/\Delta p = -0.83$.

8.3.2 Critical State

Critical state in soils is a key soil parameter as it represents a steady-state shear strength condition that is reached at large strains. Critical state for saturated soils has been defined in Chapter 2. In the case of unsaturated soil, suction affects critical state strength of the material and therefore it must also be included in the expression for critical state, (i.e. $\partial S/\partial \varepsilon_s = 0$) (Wiebe *et al.* 1998). In saturated soils, critical state failure is described by a line with the slope, M, of a line through a series of critical state values in q-p space. Unsaturated soil mechanics uses an additional property to account for the suction present called M^b. This value of M^b has been shown to be non-linear and decreasing with increasing suction (Fredlund and Rahardjo 1993). To help describe critical state along constant suction planes **Blatz (2000)** and later Blatz and Graham (2003) introduced a new parameter called the N parameter. It is defined as:

$$N = \frac{q_{cs}}{p_{cs} + T}$$

where q_{cs} is the deviator stress at critical state, p_{cs} is the mean stress at critical state and T is the tensile strength and is taken as positive. This N parameter gives the slope of the line through the "tops" of the yield loci for buffer, as would M for saturated soil and M and M^b for unsaturated soil. This parameter was chosen to avoid confusion between saturated and unsaturated models. The tensile strength for buffer was taken from Tang (1999). In that research the tensile strength was only found up to a suction of 10 MPa. For the calculation of N it has been assumed here that beyond 10 MPa suction, the tensile strength remains constant, with a value of 0.31 MPa.

In Figure 8.6 the N values for both buffers from this testing program are plotted *versus* suction (adjusted by $\Delta S/\Delta p$ = -0.83) with lines fitted to the data drawn by hand. Included in the figure are the results from Blatz (2000) for quick undrained tests and the critical state value of q/p from Ferris (2000) for tests on "Frac" sand. Saskatchewan and Wyoming buffers show the same trend. Suction increases produce an increase in N, and at approximately 30 MPa the values remain constant or increase at a decreasing rate. This is due to the fact that at approximately 30 MPa the buffers have reached the limit of volumetric shrinkage, where upon they have become a sand-dominated material. The limits on N appear to be approximately 1.4 for Saskatchewan buffer and approximately 1.2 for Wyoming buffer. The differences in N value are related to the higher strengths that were observed in the Saskatchewan buffer as compared to the Wyoming buffer sheared along the same stress path.

Above 30 MPa the calculated N values compare very well with the critical state value ($(q/p)_{cs}$ = 1.28) from Ferris (2000) for "Frac" sand. This is once again related to the transition of the buffers from a clay-dominated material at suctions below 30 MPa to a sand-dominated material at suctions higher than 30 MPa.

The higher N values found by Blatz (2000) as compared to the N values from this testing may be a result of the rate of shear. Results from Blatz (2000) are for quick undrained tests, which had a shear rate of 3.2 mm/min while shear loading in this testing program was applied at a rate of 0.0139 mm/min. Graham, Crooks and Bell (1983) showed that the rate of loading affected the size of the yield envelope. The rapid loading yield envelope was found to be larger

than the observed slow loading yield envelope. This possibility would result in the higher N values that are being calculated by Blatz (2000), as the shear rate was much faster than the one used in this program thus producing larger yield envelopes and larger N values.

The dependency of shear strength on strain rate has only been examined for saturated soils. Additional studies are needed to extend this idea to unsaturated soils. A further possibility might involve consideration of using suction alone as a measure of the effects of unsaturation on critical state strength. Other approaches may produce additional understanding of N varying with suction. These include the thermodynamics approach by Murray (2002), and the coupled p-S approach proposed by Tang and Graham (2002).

8.3.2.1 A Simple Mathematical Model for End-of-Test Strength

A key soil strength parameter in engineering is the critical state strength as it represents large strain steady state strength. In the case of the data presented here for the end-of-test it is debatable as to whether or not they represent critical state as previously mentioned. For this reason the term end-of-test is used instead of critical state as not all sheared specimens have reached an apparent steady state condition at the end of the test according to the formal definition.

Figure 8.7 shows all the end of test data along with corresponding lines statistically fitted to the data at three levels of suction, low (<10 MPa), mid (~20 MPa), and high (>30 MPa) for both buffers. The deviator and mean stress

values at the end of testing have been normalized with respect to p_c, the maximum mean stress reached during isotropic compression or the modified value of p_c for specimens sheared along 1:1 stress paths. Fits to the data are represented by linear equations as follows,

Low suction (<10 MPa): $q_{eot}/p_c = 0.1756\, p_{eot}/p_c + 0.2183$ [8.1]

Mid suction (~20 MPa): $q_{eot}/p_c = 0.5819\, p_{eot}/p_c + 0.2533$ [8.2]

High suction (>30 MPa): $q_{eot}/p_c = 0.9451 p_{eot}/p_c + 0.1757$ [8.3]

Of note in the figure are the increasing slopes of the lines fit to the end-of-test data as suction increases. This is once again believed to be evidence of the buffer transitioning from a clay-dominated material at "low" suctions to a sand-dominated material at "high" suctions.

8.4 Hydraulic Characteristics

The experimental program to examine hydraulic characteristics provided some important new information regarding moisture flow in unsaturated buffer but the experiments did not provide the specific information of interest due to the experimental design of this program. The existence of a continuous air phase was confirmed as has been shown in the gas breakthrough testing (Kirkham 1995 and Hume 1998). This is indicated by the fact that specimens compacted to a degree of saturation of 85% showed little to no gradient in radial distribution of water content and specimens compacted to 100% saturation showed a distinct gradient to movement of water radially.

8.5 Significance of Research

This research has shown the broad similarity in behaviour between these two different buffers. This was a surprising fact because both buffers consist of two different bentonite materials having different predominant exchangeable cations, specific surface area, and pore fluid chemistry, which all affect the behaviour of both bentonite materials. The observed behaviour of these two buffers suggest that either one could be used as the buffer for the storage of waste materials in deep geologic repositories as proposed by AECL when the containers are initially placed in the repository. However, it should be remembered that the similarity in behaviour that was observed between these two buffers was at low water contents ($w < 19\%$).

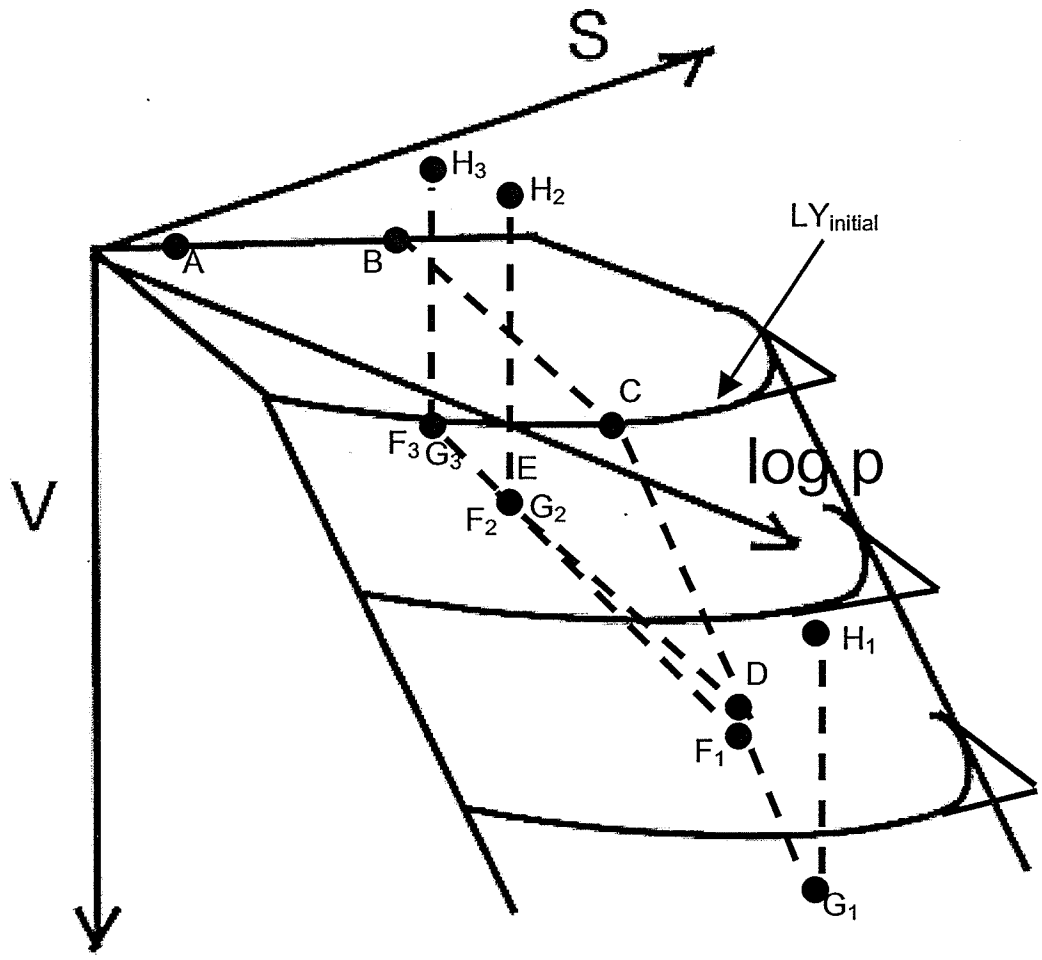

Figure 8.1(a) Idealized p-S-V space stress paths

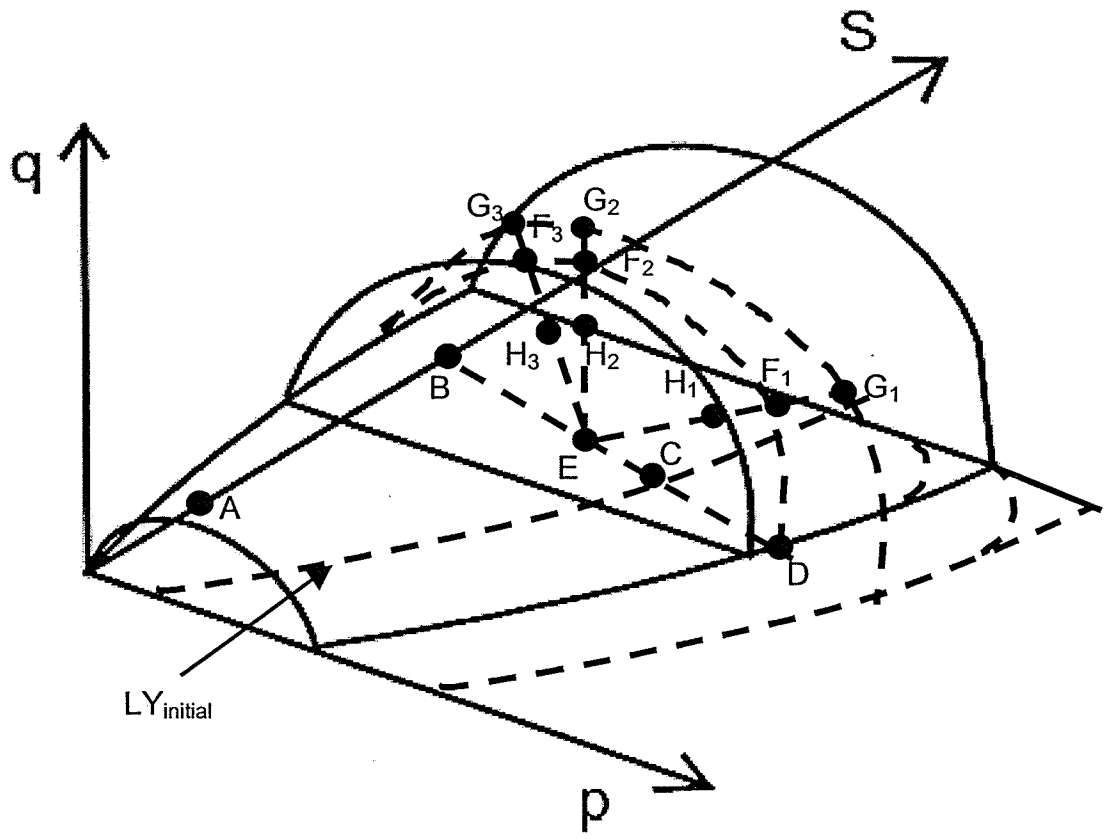

Figure 8.1(b) Idealized p-q-S space stress paths

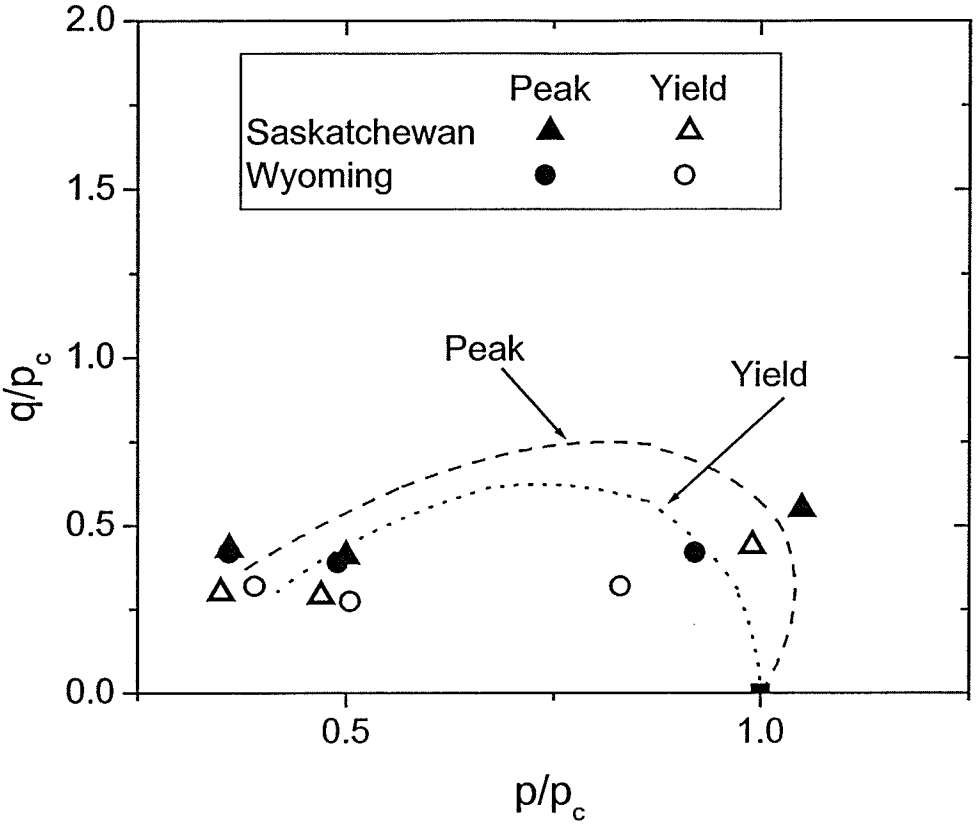

Figure 8.2 Normalized shear strengths for Saskatchewan and Wyoming buffers at 10 MPa target suction

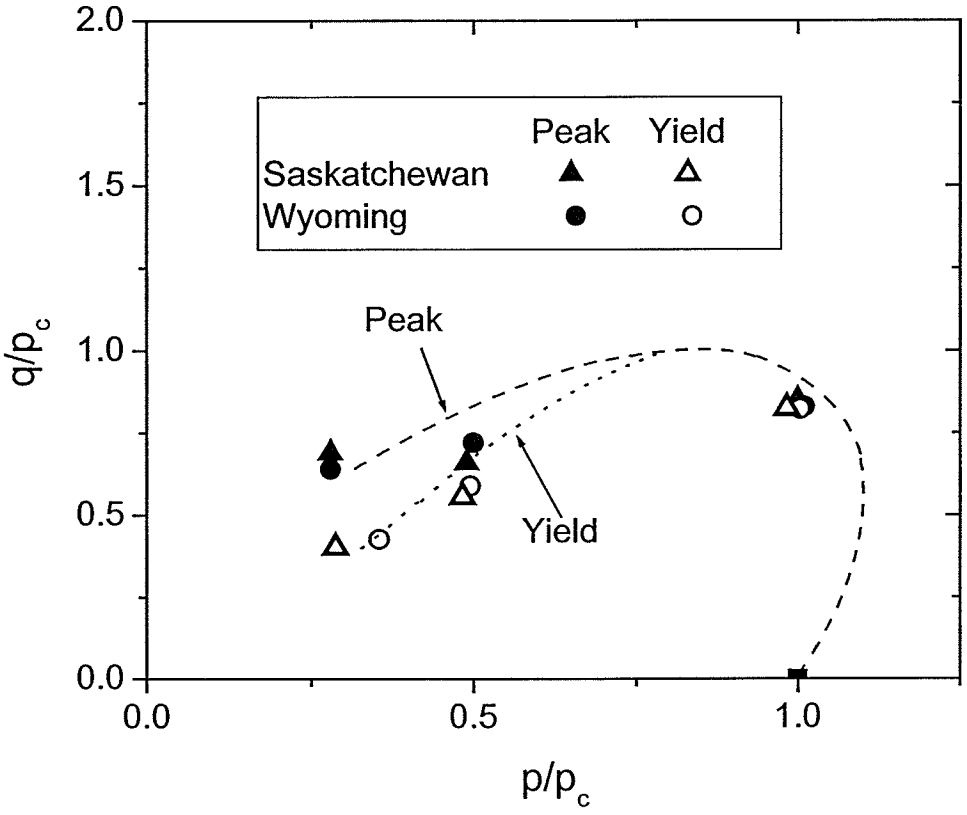

Figure 8.3 Normalized shear strengths for Saskatchewan and Wyoming buffers at 20 MPa target suction

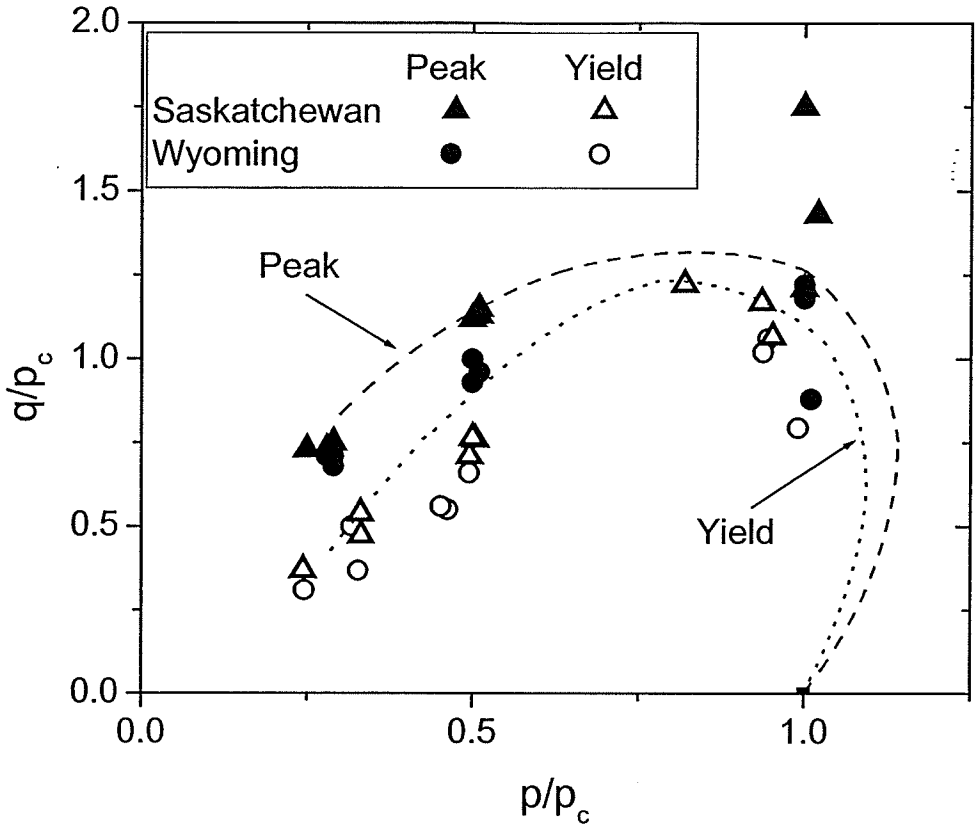

Figure 8.4 Normalized shear strengths for Saskatchewan and Wyoming buffers at 40, 80, and 160 MPa target suctions

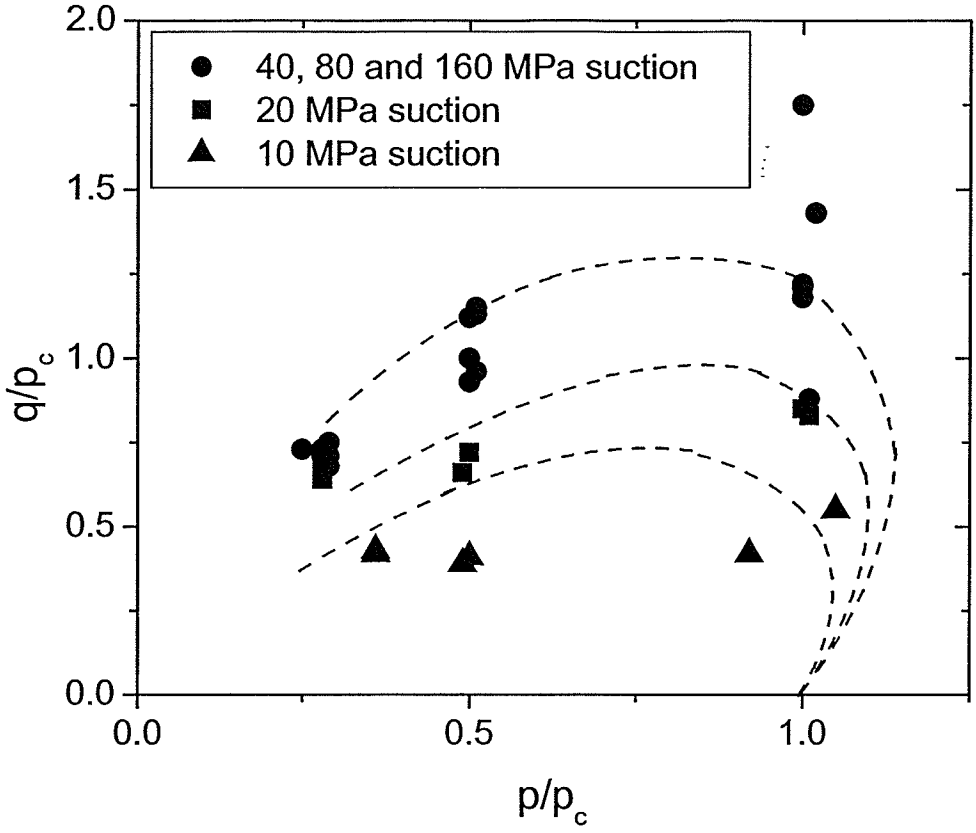

Figure 8.5 Summary of normalized peak strengths for Saskatchewan and Wyoming buffers at all target suctions

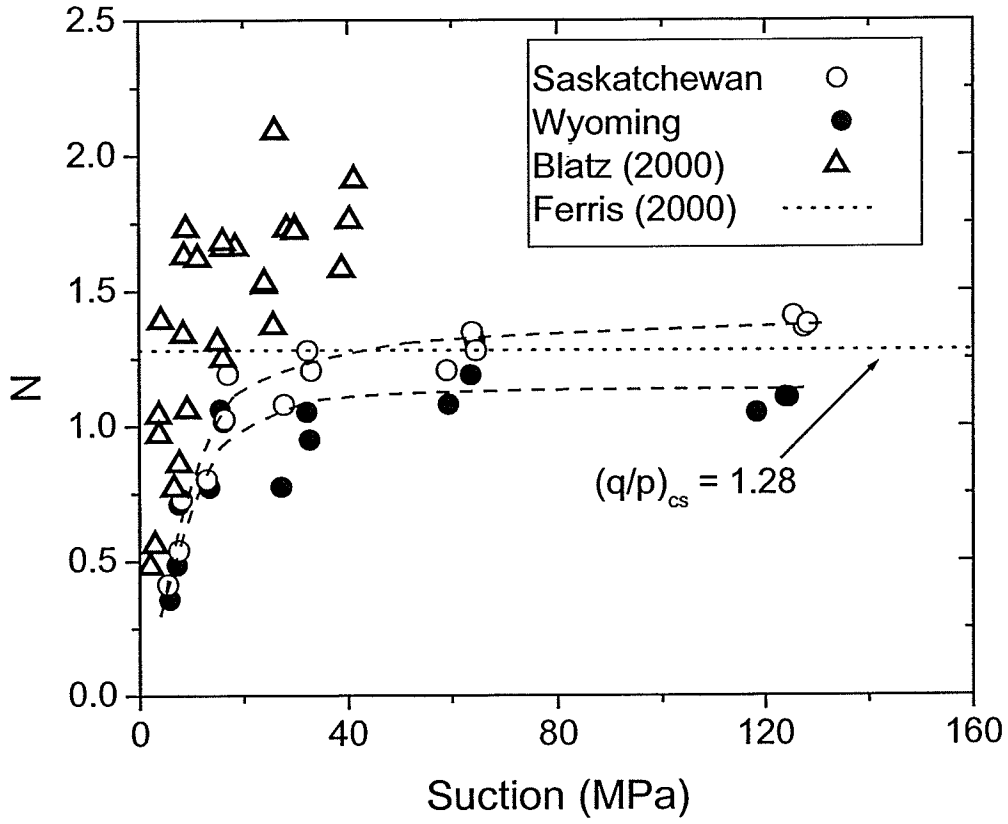

Figure 8.6 Calculated N values for Saskatchewan and Wyoming buffers at varying suctions

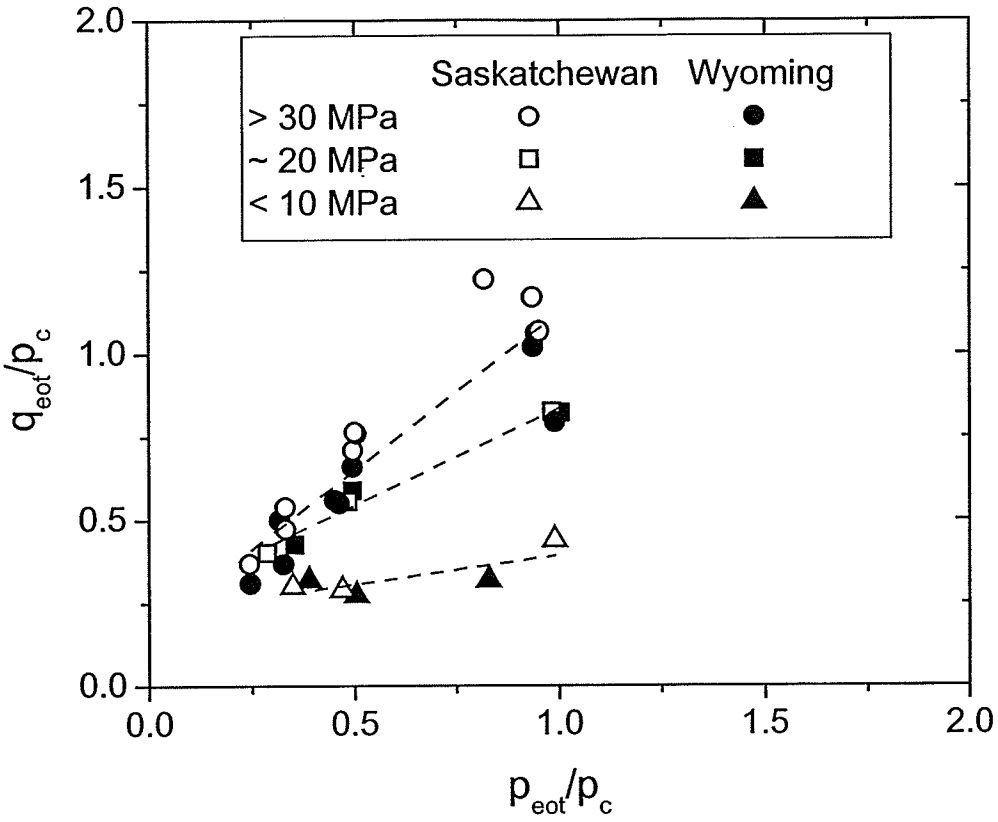

Figure 8.7 Normalized end-of-test shear strengths for Saskatchewan and Wyoming buffers

9.0 CONCLUSIONS AND RECOMMENDATIONS FOR FUTURE WORK

9.1 Principal Hypothesis and Conclusions

The principle hypothesis examined by this research was:

Hypothesis: The different physical properties of Wyoming buffer as compared to Saskatchewan buffer will result in different mechanical behaviour at similar suction levels (see Chapter 1).

A series of experiments were completed to examine shrinkage behaviour under suction stresses and stiffness, strength and yielding under triaxial conditions. Results from tests on Saskatchewan and Wyoming buffer supported the hypothesis but the differences in behaviour were not as large as expected. Larger differences in behaviour were expected because of the differences in physical properties between the two constituent bentonites.

In the testing, yielding was observed under both isotropic compression and triaxial shear conditions. Suction measurements were not performed during testing but were calculated from a relationship developed at relatively low suctions up to 10 MPa. This raises the important question of the actual suctions in both materials during both isotropic compression and triaxial shear tests. It was shown by Tang et al. 1997 and Blatz and Graham 2003 that changes in mean stress resulted in changes in suction. Since, during both isotropic compression and triaxial shear testing the mean stress changed, it can be expected that there would be changes in suction as well.

The following principal conclusions have been drawn from the research:

1. Under increasing suctions, the soil water characteristic curve for Saskatchewan and Wyoming buffers are only slightly different. Shrinkage of both buffers showed a clear limiting volume strain under increased suction stress. The Wyoming buffer limit of volumetric shrinkage (~10%) was higher than Saskatchewan buffer (~8%). The limit of volumetric shrinkage indicates a transition from clay-dominated behaviour at low suctions (< 30 MPa) to sand-dominated behaviour at high suctions (> 30 MPa).

2. Saskatchewan and Wyoming buffers exhibit broadly similar behaviour under isotropic compression. Interpreted isotropic compression yield stresses are slightly higher in Saskatchewan buffer and the Wyoming buffer experienced greater compression under similar stress conditions at similar target suction levels. Further development of the initial load yield (LY) curve was done, extending the work previously done by Blatz (2000). The normally consolidated (plastic hardening) isotropic compression index (λ) was consistent with compression testing of "Frac" sand (Ferris 2000) values at suctions greater than 30 MPa for the Saskatchewan buffer.

3. Increased suctions produced higher strengths and stiffness in both buffers. Normalized yield loci under triaxial shear conditions increased in size with increasing suction and showed an apparent transition from clay-dominated behaviour at low suctions (<10 MPa) to sand-dominated behaviour at high suctions (> 30 MPa). Yielding under triaxial stress conditions can be seen using

p-V plots. The end of test strength parameter N is slightly lower than the N parameter predicted for quick undrained shear tests (Blatz 2000). Existing elastic-plastic models are supported by the results of this testing program.

4. Hydraulic characteristic testing supported the existence of continuous void spaces in specimens compacted to a degree of saturation less than 90%. These continuous void spaces provide little resistance to the movement of gas, in this case, water vapour with low partial vapour pressure.

5. The results of the mechanical testing of both buffers would suggest that either buffer would be suitable for use in the storage of waste materials in a deep geologic repository as proposed by AECL.

9.2 Recommendations for Future Work

A major development during this research was the design and implementation of a new, fully automated data acquisition and control system. This new system allows for generalized stress paths under triaxial conditions to be accurately examined in q/p space. The following points outline further research that needs to be undertaken to extend current understanding of the elastic-plastic behaviour of unsaturated soils and provide required experimental evidence to add further confidence to numerical modeling activities.

1. The addition of suction control and measurement at suctions higher than 8 MPa during isotropic compression and triaxial shearing. This would allow for more general stress paths to be examined and also allow verification of the

$\Delta S/\Delta p$ = -0.83 relationship (Tang et al. 1997 and Blatz and Graham 2003) at suctions higher than 8 MPa.

2. Identification of suction yielding should be undertaken. This will permit examination of the coupling between mean stress and suction that was proposed by Delage and Graham (1995). This would provide further development of yielding under triaxial shear conditions to better define the state boundary surface in volume state space.

3. Measurement of suction distribution with time during constant suction application in desiccators and under triaxial stress conditions. This would allow for the determination of diffusion coefficients of vapour and air for buffer.

4. While evidence has been shown for a transition between clay and sand dominated behaviour in buffer, this transition is still difficult to model. Testing of pure unsaturated clay materials would allow for a better understanding of the effects of suction on unsaturated soils and eliminate the inherent complexities that are introduced with the use of buffer materials.

REFERENCES

Alonso, E.E, Gens, A., and Josa, A. 1990. A constitutive model for partially saturated soils. Geotechnique, **40**: 405-430.

Alonso, E.E, Gens, A., and Hight, D.W. 1987. General Report. Special problem soils. Proc. 9th Eur. Conf. Soil Mech. Found. Eng. **3**: 1087-1146.

Baumgartner, P. 2000. Elemental composition of disposal vault sealing materials, Ontario Power Generation, Nuclear Fuel Waste Management Division, Supporting Technical Report, 06819-REP-01300-10015-R00.

Bishop, A.W. 1959. The principle of effective stress. Lecture delivered in Oslo, Norway, in 1955; published in Teknisk Ukeblad, **106**(39):33-52.

Blatz, J., Tang, G.X., Graham, J., Wan, A. 1999. Psychrometer techniques for measuring suction in the triaxial test. 52nd Canadian Geotechnical Conference, Regina, Saskatchewan, Oct. 1999, pp. 237-245.

Blatz, J.A. 2000. Elastic-plastic modeling of unsaturated high-plastic clay using results from a new triaxial test with controlled suction. Ph.D. Thesis, Department of Civil Engineering, University of Manitoba, (Winnipeg, Manitoba).

Blatz, J.A., and Graham, J. 2003. Elastic plastic modelling of unsaturated high plastic clay using results from a new triaxial test with controlled suction. Géotechnique Special Symposium in Print on Unsaturated Soils, **53**(1):113-122.

Brooks, R.H., and Corey, A.T. 1964. Hydraulic properties of porous media. Colorado State University, Hydrology paper **3**.

Coleman, J.D. 1962. Stress/strain relations for partly saturated soils. Geotechnique, (Correspondence) **12**(4):348-350.

Cui, Y.J. and Delage, P. 1996. Yielding and plastic behaviour of an unsaturated silt. Geotechnique, **46**(2): 291-312.

Delage, P. and Graham, J. 1995. Understanding the behavior of unsaturated soils requires reliable conceptual model. State of the Art Report, Proceedings, 1st Int. Conf. on Unsaturated Soils, Paris, France, 1995, 1223-1256.

Dixon, D.A. and Gray, M.N. 1985. The engineering properties of buffer material. Technical report TR-350, Fuel Waste Technology Branch, Whiteshell Laboratories, Pinawa MB, Canada.

Dixon, D.A., Campbell, S.L., and Hnatiw, D.S.J. 1994. Preplacement quality control and as-placed properties of the buffer materials used in the URL isothermal buffer experiment, AECL Technical Record, TR-612, COG-94-35.

Dixon, D.A. 1994. Sodium bentonites of Canada, the United States and Mexico: sources, reserves and properties. Engineering Materials for Waste Isolation, CSCE-Engineering Material Division-Special Publication. pp 37-65.

Dixon, D.A. 1995. Towards an understanding of water structure and water movement through dense clays. Ph.D. thesis, University of Manitoba, May 1995.

Dixon, D.A. and Miller, S.H. 1995. Comparison of the mineralogical composition, physical, swelling and hydraulic properties of bentonites from Canada, the United States and Japan. Atomic Energy of Canada Limited Report AECL-11303, COG-95-156.

Dixon D.A., Graham, J. and Gray, M.N. 1999. Hydraulic conductivity of clays in confined tests under low hydraulic gradients. Canadian Geotechnical Journal **36**: 815-825.

Ferreira, N.J., Blatz, J.A., Graham, J., and Kenyon, R.M. 2001. Examination of instability in an unsaturated highway cut. 54th Canadian Geotechnical Conference, Calgary, Alberta, Sept. 2001, pp. 984-901.

Ferris, G.W. 2000. An elastic-plastic approach: Modeling deformation of dense sand. M.Sc. Thesis, Department of Civil Engineering, University of Manitoba, (Winnipeg, Manitoba).

Fredlund, D.G. and Morgenstern, N.R. 1977. Stress strain variables for unsaturated soils. Proc. American Society of Civil Engineers. **103**, GT5, 447-466.

Fredlund, D.G., Morgenstern, N.R. and Widger, R.A. 1978. The shear strength of unsaturated soils. Can. Geotechnical Journal, **15**(3):313-321.

Fredlund, D.G., Rahardjo, H. and Gan, J.K.M. 1987. Non-linearity of strength envelope for unsaturated soils. In Proceedings of the 6th International Conference on Expansive Soils, 1-4 Dec. 1987, New Delhi. Central Board of Irrigation and Power, **1**:49-54.

Fredlund, D.G. and Rahardjo, H. 1993. Soil Mechanics for Unsaturated Soil. A Wiley-Interscience Publication. John Wiley & Sons, Inc., New York, NY.

Fredlund, D.G. and Xing, A. 1994. Equations for the soil-water characteristic curve. Canadian Geotechnical Journal. **31**: 521-532.

Garinger, B.D. 2002. Instability of dykes at seven sisters generating station. M.Sc. Thesis, Department of Civil Engineering, University of Manitoba, (Winnipeg, Manitoba)

Gens, A. and Alons, E.E. 1992. A framework for the behaviour of unsaturated expansive clays. Canadian Geotechnical Journal, **29**: 1013-1032.

Graham, J., Crooks, J.H., and Bell, A.L. 1983. Time effects on the stress-strain behaviour of natural soft clays. Geotechnique, **33**(3):327-340.

Graham, J. and Houlsby, G.T. 1983. Anisotropic elasticity of a natural clay. Geotechnique, **33**(2):165-180.

Graham, J., Tang, X., Wiebe, B., Rajapakse, R.K.N.D., and Zhou, Y. 1995. Progress report on second year of contract no. WS102679: Modelling of Sand-bentonite Buffer for use in the Canadian Nuclear Fuel Waste Management Program. AECL-Research., July 1995. 170 pp.

Graham, J., Chandler, N.A., Dixon, D.A., Roach, P.J., To., T., Wan, A.W.L. 1997. The Buffer/Container Experiment: results, synthesis, issues. AECL Whiteshell laboratories, Pinawa, Manitoba. AECL-11746.

Graham, J., Halayko, K.G., Hume, H., Kirkham, T., Gray, M., and Oscarson, D. 2002. A capillarity-advective model for gas break-through in clay. Engineering Geology **64**: 273-286.

Ho, D.Y., Fredlund, D.G., and Rahardjo, H. 1992. Volume change indices during loading and unloading of an unsaturated soil. Geotechnique, **12**(2):195-207.

Hume, H.B. 1998. Gas breakthrough in compacted Avonlea bentonite. M.Sc. Thesis, Department of Civil Engineering, University of Manitoba, (Winnipeg, Manitoba).

Jennings, J.E. and Burland, J.B. 1962. Limitations of the use of effective stress in partly saturated soils. Geotechnique, **12**(2):125-144.

Josa, A., Alono, E.E., Gens, A., and Lloret, A. 1987. Stress-strain behaviour of partially saturated soils. Proc. 9th Eur. Conf. Soil Mech. Found. Eng. **2**: 561-564.

Karnland, O. 1997. Long Term Test of Buffer Material. Construction and Emplacement of the two Pilot Test Parcels, SKB HRL Progress Report, HRL-97-30.

Kirkham, T.L. 1995. Development of test equipment and procedures for determination of the gas-breakthrough pressure of compacted clay materials with preliminary results. M.Sc. Thesis, Department of Civil Engineering, University of Manitoba, (Winnipeg, Manitoba).

Lambe, T.W. 1958 The structure of compacted clay. Journal of soil mechanics and foundation engineering. American Society of Civil Engineers. **84.**

Lingnau, B.E. 1993. Consolidated undrained triaxial behaviour of a sand-bentonite mixture at elevated temperature. Ph.D. Thesis, Department of Civil Engineering, University of Manitoba, (Winnipeg, Manitoba).

Lingnau, B.E., Graham, J., Yarechewski, D., Tanaka, N., and Gray, M.N. 1996. Effects of temperature on strength and compressibility of sand-bentonite buffer. Engineering Geology **41**:103-115.

Michel, C.W. 1961. The International Dictionary of Physics and Electronics, 2nd ed. Toronto: Van Norstrand.

Murray, E.J. 2002. An equation of state for unsaturated soils. Canadian Geotechnical Journal **39**: 125-140.

Oscarson, D.W. and D.A. Dixon. 1989. Elemental, mineralogical and pore solution compositions of selected Canadian clays. Atomic Energy of Canada Limited Report, AECL-9891.

Pusch, R. 1994. Waste disposal in rock. Elsevier Science B.V. Amsterdam, The Netherlands.

Richards, B.G. 1974. Behaviour of unsaturated soils, in soil mechanics—new horizons, I.K. Lee ed. New York: American Elsevier, 112-157.

Roscoe, K.H. and Burland, J.B. 1968. On the generalised stress-strain behaviour of 'wet' clay. Engineering Plasticity, Cambridge: Cambridge University Press, 535-609.

Russell, S.B. and G.R. Simmons. 2003. Engineered barrier system for a deep geologic repository. To be presented at the 2003 International High-Level Radioactive Waste Management Conference, March 30-April 2, 2003, Las Vegas, NV.

Saadat, F. 1989. Constitutive modeling of the behaviour of a sand-bentonite mixture. Ph.D. Thesis, Department of Civil Engineering, University of Manitoba, (Winnipeg, Manitoba).

Stokes, R.H. and Robinson, R.A. 1948. Standard solutions for humidity control at 25°C. Journal of phys. chem. 36.

Tanaka, N. 1995. Thermal elastic plastic behaviour and modelling of saturated clay. Ph.D. Thesis, Department of Civil Engineering, University of Manitoba, (Winnipeg, Manitoba).

Tang, G.X., Graham, J. and Wan, A. 1997. Measuring total suctions by psychrometers in traixial tests. Proc. XIVth International Conference on Soil Mechanics and Foundation Engineering, Hamburg, Germany, 1997. 1:213-216.

Tang, G.X., Graham, J., Blatz, J., Rajapakse, R. and Gray, M.N. 1998. Suction characteristics of unsaturated sand-bentonite. In preparation for publication on International Journal of Engineering Geology.

Tang, G.X. 1999. Suction characteristics and elastic-plastic modeling of unsaturated sand-bentonite mixture. Ph.D. Thesis, Department of Civil Engineering, University of Manitoba, (Winnipeg, Manitoba).

Tang, G.X. and Graham, J. 2000. A method for testing tensile strength on unsaturated soils. Geotechnical Testing Journal GTJODJ 23, 377-382.

Tang, G.X. and Graham, J. 2002. A possible elastic-plastic framework for unsaturated soils with high-plasticity. Canadian Geotechnical Journal, **39**: 894-907.

Terzaghi, K. 1936. The shearing resistance of saturated soils and the angle between the planes of shear. Proc. First. Int. Conf. Soil Mech., **1**:54-56.

Toll, D.G. 1990. A framework for unsaturated soils behaviour (discussion). Geotechnique, **41**(1):159-161.

van Genuchten, M. Th. 1980. A close form equation for predicting the hydraulic conductivity of unsaturated soils. Soil Science Society of American Journal 44: 892-898

Wan, A.W.-L., Graham, J., and Gray, M.N. 1990. Influence of soil structure on the stress-strain behaviour of sand-bentonite mixtures. Geotechnical Testing Journal, GTJODJ, **13**(3):179-187.

Wan, A.W.-L., Gray, M.N., and Graham, J. 1995 On the relations of suction, moisture content, and soil structure in compacted clays. Proc. of 1st. Int. Conf. on Unsaturated Soils, Paris, (1995), 215-222, eds. E.E.Alonso and P.Delage, publ. Balkema, Rotterdam.

Wan, A.W.-L. 1996. The use of thermocouple psychrometer to measure in-situ suctions and water contents in compacted clays. Ph.D. Thesis, Department of Civil and Geological Engineering, University of Manitoba, (Winnipeg, Manitoba)

Wheeler, S.J. and Sivakumar, V. 1993. Development and application of a critical state model for unsaturated soil. Predictive Soil Mechanics. Proceedings of the Wroth Memorial Symposium. Thomas Telford, London 1993, 709-728.

Wheeler, S.J. and Sivakumar, V. 1995. An-elasto-plastic critical state framework for unsaturated soil. Geotechnique, **45**(1):35-53.

Wiebe, B.J. 1996. The effect of confining pressure, temperature, and suction on the strength and stiffness of unsaturated buffer. M.Sc. Thesis, Department of Civil and Geological Engineering, University of Manitoba, (Winnipeg, Manitoba).

Wiebe, B., Graham, J., Tang, G.X., and Dixon, D. 1998. Influence of pressure, saturation and temperature on unsaturated buffer materials. Canadian Geotechnical Journal, **35**(2):194-205.

Wood, D.M. 1990. Soil behaviour and critical state soil mechanics. Cambridge University Press, Cambridge.

Yarechewski, D.S. 1993. Constant mean effective stress tests on sand - bentonite specimens at elevated temperature. M.Sc. Thesis, University of Manitoba, Department of Civil and Geological Engineering, Winnipeg, MB.

Yin, J-H. and Graham, J. 1999. Elastic viscoplastic modeling of the time-dependant stress-strain behaviour of soils. Canadian Geotechnical Journal, **36**: 736-745.

Young, J.F. 1967. Humidity control in the laboratory using salt solutions – a review. J. of applied chemistry. **17**.